Copy No. 15

DEFENCE R&D DÉFENSE

COMPUTATIONAL EVALUATION OF DAMPING AND DECOUPLING MATERIALS – PHASE III

O. Foin – A. Berry

DEFENCE RESEARCH ESTABLISHMENT ATLANTIC

Contractor Report

DREA CR 2000-016

February 2000

National Defence Défense nationale

Canada

National Defence
Research and Development Branch

Défense nationale
Bureau de recherche et développement

DREA CR 2000-016

COMPUTATIONAL EVALUATION OF DAMPING AND DECOUPLING MATERIALS – PHASE III

by

O. Foin and A. Berry

Acoustics and Vibration Group
University of Sherbrooke
Sherbrooke, Quebec, Canada
J1K 2R1

Scientific Authority J.P. Szabo

W7707-8-5839/001/HAL
Contract Number

February 2000

CONTRACTOR REPORT

Prepared for

Defence Research Establishment Atlantic

Centre de Recherches pour la Défense Atlantique

Canada

Abstract

This report presents theoretical models and numerical results of the vibroacoustic behaviour of plane structures covered by damping or decoupling materials and immersed in water. A novel theoretical model that accounts for the three-dimensional theory of elasticity for decoupling coatings is proposed. This model allows all components of stress and strain to be taken into account in the coating layer. The three-dimensional model points out the existence of two types of waves in the coating : longitudinal (or compressional) waves and shear (or transverse) waves. Numerical results show that the shear waves are almost negligible in comparison to the compressional waves, so that a simplified model that neglects shear waves can be derived from the complete 3D model.

The 3D model is compared to a previous model developed for DREA, based on the locally reacting assumption (DREA CR/96/427). It is also compared to models proposed in the literature for infinite structures (Ko 1997, House 1991). A complete parametric study of the 3D model allows its interest to be highlighted.

A model that accounts for partial constrained damping treatment is also proposed. This model is able to evaluate the vibration and acoustic response of a plate partially covered by a viscoelastic layer and a constraining layer. The influence of the surface of the coverage on the global noise reduction is investigated.

Résumé

Ce rapport présente un modèle théorique et des résultats numériques du comportement vibroacoutisque d'une structure plane, couverte par un matériau amortissant ou un matériau de masquage et immergée dans l'eau. Un nouveau modèle utilisant l'élasticité tridimensionnelle pour le matériau de masquage est proposé. Ce modèle permet de prendre en compte les contraintes et les déformations dans toutes les directions dans le matériau de masquage. Ce modèle met en évidence l'existence de deux types d'ondes dans le matériau de masquage : des ondes longitudinales (compression) et des ondes transversales (cisaillement). Les résultats numériques montrent que les ondes transversales ont une influence très faible en comparaison des ondes longitudinales, de sorte qu'un modèle simplifié qui les néglige est dérivé du modèle complet.

Le modèle tridimensionnel est comparé au modèle à réaction localisée précédemment développé pour DREA (DREA CR/96/427), il est aussi comparé à des modèles de plaques infinies (Ko 1997, House 1991). Une étude paramétrique complète du modèle tridimensionnel permet de mettre en évidence son intérêt face aux modèles plus simples.

Un modèle théorique qui prend en compte une couverture viscoélastique contrainte partielle est également proposé. Ce modèle évalue la réponse vibratoire et acoustique d'une plaque partiellement couverte par une couche viscoélastique et une couche contraignante rigide. L'influence de la surface de couverture sur l'atténuation acoustique globale est étudiée.

DREA CR 2000-016

Computational Evaluation of Damping and Decoupling Materials - Phase III

O. Foin and A. Berry

EXECUTIVE SUMMARY

Background

This report has presented the theoretical formulation and numerical results of a new 3D model to describe the vibroacoustic behaviour of a finite elastic plate covered by a decoupling coating and immersed in water. This 3D model (VIBRO3D) uses the three-dimensional theory of elasticity to describe stress and strain within the decoupling material, and is therefore more complete than the locally-reacting model implemented in a previous version of the software (VIBRO).

Principle Results

- Good agreement was found between the locally reacting model and the 3D model in the case of relatively stiff , lightly damped and low mass density coating materials. In the other cases the locally reacting model overestimates the decoupling effectiveness in comparison to the 3D model.
- House's 1D model for infinite plates was found to be in good agreement with the 3D model in terms of the insertion loss of a plate covered by a decoupling coating. An attractive aspect of House's model is its simplicity.
- Good agreement was observed between the model of Ko for infinite plates and the 3D model in terms of the mean square velocity ratio.
- The calculation of the absolute intensity through a mapping plane at a distance d (called *near field acoustic power* in this report) was found to be a valuable indicator to evaluate the transmission loss of a plate/coating system.
- The velocity ratio at a single point (base plate vs. coating surface at driving point) was found to be similar to the geometrically averaged mean square velocity ratio, and is thus an appropriate indicator of the properties of the coating material.
- The approximate (hybrid) method proposed to evaluate the influence of partial decoupling on the acoustic response shows that small uncovered areas rapidly reduce the global decoupling effectiveness.
- Finally, a model that considers a simply supported base plate partially covered by a constrained damping treatment was proposed. The parametric study shows that efficient global damping can be achieved without covering the whole structure. In general, a 50% coverage is sufficient to obtain

significant vibration / sound attenuation, and additional coverage above this value has a low impact on the attenuation obtained.

Significance of Results

The close agreement that was found between VIBRO3D and House's 1D infinite plate model for the insertion loss of a decoupling coating is significant. The amplification of radiated sound power below a critical "cut-off" frequency as a result of the decoupling coating is predicted by both of these models, and has been attributed to the mass-spring behaviour of the plate/coating/water system at low frequencies. It was not observed using the less accurate locally reacting version of the VIBRO code. The more accurate VIBRO3D results also showed that the mean square velocity ratio is not necessarily in agreement with the insertion loss spectrum in 1/3 octave bands, especially below the cut-off frequency. The latter indicator is perhaps the most appropriate indicator of decoupling performance. The study also found that the insertion loss calculated from the near field acoustic power, which is a convenient experimental parameter to measure when acoustic intensity methods are employed, gives identical results to the insertion loss calculated from the far field acoustic power. The studies of partial covering showed that it is important to completely cover a structure with decoupling material, while complete covering with a damping material is not as critical.

Future Work

Validation of the VIBRO code will be carried out using laser doppler velocimetry to measure the vibration response of the coating surface in contact with water, and the substrate surface in contact with air. A collaborative program of work on decoupling materials evaluation and modelling with TNO/ TPD in the Netherlands is underway, and will continue over the next year. This work will involve a comparative study of modelling approaches used by both participants on a number of "generic" coatings with realistic properties. The decoupling behaviour of a reduced scale model of a floating ship-like structure coated with neoprene foam has been evaluated using near field acoustic holography. The results from this experiment will be interpreted by a number of models, using material properties of the foam determined from a range of experiments. Experimental characterization of the foam will include dilatational modulus measurements using a shaker apparatus, dynamic mechanical thermal analysis, impedance tube experiments, and Oberst beam measurements.

J. Szabo, Scientific Authority
February 2000

Table of contents

ABSTRACT i

EXECUTIVE SUMMARY ii

1 THREE-DIMENSIONAL MODEL FOR DECOUPLING COATING 1

1.1 HYPOTHESES 1

1.2 PROPAGATION OF WAVES IN AN ELASTIC SOLID 2

1.3 CONSTITUTIVE EQUATIONS OF THE VIBROACOUSTIC PROBLEM 5

1.3.1 Equation of motion of the base plate 5

1.3.2 Equation of motion of the coating 6

1.3.3 Fluid-structure interaction 7

1.3.4 Boundary conditions 8

1.3.5 Solving the problem 9

1.3.6 Summary of the vibroacoustic problem 17

1.4 VIBROACOUSTIC INDICATORS 18

1.4.1 Expression of the various vibroacoustic indicators 19

1.4.2 "Near field" acoustic power 23

2 NUMERICAL RESULTS OF THE NEW 3D MODEL 27

2.1 INTRODUCTION 27

2.2 INFLUENCE OF THE SHEAR WAVES IN THE THREE-DIMENSIONAL MODEL 27

2.3 COMPARISON BETWEEN VIBRO AND THE NEW 3D MODEL 31

2.3.1 Vibration and acoustic response 32

2.3.2 Vibration isolation 38

2.3.3 Realistic decoupling material, influence of the coating density 41

2.4 COMPARISON BETWEEN THE MODEL OF KO AND VIBRO3D 44

2.5 COMPARISON BETWEEN THE MODEL OF HOUSE AND VIBRO3D 48

2.6 "NEAR-FIELD" ACOUSTIC POWER 51

3 PARTIAL COVERAGE FOR DECOUPLING COATING 55

3.1 PRESENTATION OF THE HYBRID METHOD 55

3.2 PARTIAL COATING WITH THE HYBRID METHOD 56

3.3 VALIDATION OF THE HYBRID METHOD 60

3.4 PARTIAL COVERAGE ANALYSIS 61

4 ANALYSIS OF DRIVING POINT MOBILITY 67

5 PARTIAL COVERAGE FOR DAMPING MATERIAL 71

5.1 INTRODUCTION 71
5.2 THEORETICAL MODEL 72
5.2.1 Hypotheses 72
5.2.2 Displacement field 73
5.2.3 Strain field 74
5.2.4 Stress field 75
5.2.5 Rayleigh-Ritz method 76
5.2.6 Hamilton functional 77
5.2.7 Kinetic energy 77
5.2.8 Strain energy 78
5.2.9 Work of external forces 80
5.2.10 Integral formulation 81
5.2.11 Equation of motion of the plate 82
5.3 NUMERICAL RESULTS 83

6 CONCLUSION 88

7 APPENDIX A SOME USEFUL VECTORIAL ANALYSIS DEFINITIONS 90

8 BIBLIOGRAPHY 92

1 Three-dimensional model for decoupling coating

1.1 Hypotheses

The structure under study is a rectangular plate fully covered by a decoupling coating and immersed in water. The outer surface of the coating immersed in water is inserted in an infinite rigid baffle. The excitation is a point force or an acoustic plane wave exerted on the base plate (Figure 1.1).

The base plate is described with the classical Love-Kirchhoff theory for bending motion, whereas an exact model based on the 3-dimensional elasticity is used for the decoupling coating. The model for the coating accounts for compressional (longitudinal) waves and shear (transverse) waves. The main difference between the locally reacting model previously presented in the DREA report (CR/96/427) lies in the fact that the locally reacting model only accounts for thickness deformation of the coating, whereas the 3D model accounts for all types of deformations. To our knowledge, all previous modelling of decoupling coatings using the 3-dimensional theory of elasticity considered only infinite geometry; in this work, the 3-dimensional theory of elasticity is extended to finite plates. The sound radiation in the fluid is accurately evaluated using the integral formulation.

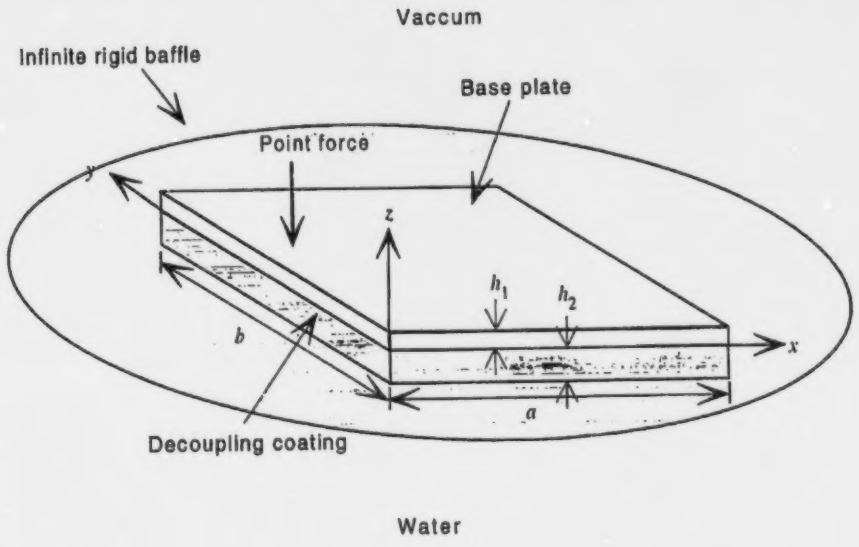

Figure 1.1 : Base plate with the coating layer immersed in water.

1.2 *Propagation of waves in an elastic so'id*

This section presents the basic theory to describe the propagation of waves in an elastic solid. The following results are borrowed from classical references such as Koslky (1963), Achenbach (1973) or Davies (1988). These results will be used to model the propagation of elastic waves in the decoupling layer. The strain-displacement relation in an elastic solid is given by :

$$\begin{cases} \varepsilon_x = \dfrac{\partial u_x}{\partial x} \\ \varepsilon_y = \dfrac{\partial u_y}{\partial y} \\ \varepsilon_z = \dfrac{\partial u_z}{\partial z} \\ \gamma_{xy} = \dfrac{\partial u_x}{\partial y} + \dfrac{\partial u_y}{\partial x} \\ \gamma_{xz} = \dfrac{\partial u_x}{\partial z} + \dfrac{\partial u_z}{\partial x} \\ \gamma_{yz} = \dfrac{\partial u_y}{\partial z} + \dfrac{\partial u_z}{\partial y} \end{cases} \tag{1.1}$$

where u_x, u_y, u_z are the components of the displacement vector $\vec{u}$ at a point M (x,y,z) in the solid, ε_x, ε_y, ε_z, γ_{xy}, γ_{xz}, γ_{yz} are the components of the strain tensor.

For three-dimensional, homogeneous elastic media, the stress-strain relation can be written :

$$\begin{Bmatrix} \sigma_x \\ \sigma_y \\ \sigma_z \\ \sigma_{xy} \\ \sigma_{xz} \\ \sigma_{yz} \end{Bmatrix} = \begin{bmatrix} \lambda+2\mu & \lambda & \lambda & 0 & 0 & 0 \\ \lambda & \lambda+2\mu & \lambda & 0 & 0 & 0 \\ \lambda & \lambda & \lambda+2\mu & 0 & 0 & 0 \\ 0 & 0 & 0 & \mu & 0 & 0 \\ 0 & 0 & 0 & 0 & \mu & 0 \\ 0 & 0 & 0 & 0 & 0 & \mu \end{bmatrix} \begin{Bmatrix} \varepsilon_x \\ \varepsilon_y \\ \varepsilon_z \\ \gamma_{xy} \\ \gamma_{xz} \\ \gamma_{yz} \end{Bmatrix} \tag{1.2}$$

where , σ_x, σ_y, σ_z, σ_{xy}, σ_{xz}, σ_{yz} are the components of the stress tensor and, λ and μ are the Lamé constants which can be expressed as a function of the Young's modulus E, the shear modulus G and the Poisson's ratio ν, by :

$$\begin{cases} \lambda = \dfrac{E\nu}{(1+\nu)(1-2\nu)} \\ \mu = G = \dfrac{E}{2(1+\nu)} \end{cases} \tag{1.3}$$

If body forces (such as gravity) are neglected, the equation of motion of an elastic solid can be written (Kolsky 1963) :

$$\begin{cases} \rho \dfrac{\partial^2 u_x}{\partial t^2} = \dfrac{\partial \sigma_x}{\partial x} + \dfrac{\partial \sigma_{xy}}{\partial y} + \dfrac{\partial \sigma_{xz}}{\partial z} \\ \rho \dfrac{\partial^2 u_y}{\partial t^2} = \dfrac{\partial \sigma_{xy}}{\partial x} + \dfrac{\partial \sigma_y}{\partial y} + \dfrac{\partial \sigma_{yz}}{\partial z} \\ \rho \dfrac{\partial^2 u_z}{\partial t^2} = \dfrac{\partial \sigma_{xz}}{\partial x} + \dfrac{\partial \sigma_{yz}}{\partial y} + \dfrac{\partial \sigma_z}{\partial z} \end{cases} \tag{1.4}$$

where ρ is the density of the medium. These equations do not depend on the stress-strain relation. Upon substitution of equations 1.1 and 1.2, it is possible to express the equation of motion in a condensed form (Davies 1988) :

$$\mu\nabla^2\vec{u} + (\lambda+\mu)\nabla\Theta = \rho\frac{\partial^2\vec{u}}{\partial t^2} \tag{1.5}$$

where $\Theta = \varepsilon_x + \varepsilon_y + \varepsilon_z$. The definition of the nabla operator (∇) is presented in appendix A.

In general, the elastic displacement can be written in the form: $\vec{u} = \vec{u}_L + \vec{u}_T$. The term $\vec{u}_L$ corresponds to a longitudinal (or compressional) wave (the displacement of the solid is in the direction of the wave propagation). The term $\vec{u}_T$ corresponds to a transverse (or shear) wave (the displacement of the solid is orthogonal to the direction of the wave propagation). These two types of waves can be expressed as a function of scalar and vector potentials by the following relations :

$$\vec{u}_L = \nabla\phi, \tag{1.6}$$

where ϕ is called the scalar potential ($\Theta = \nabla^2\phi$) and :

$$\vec{u}_T = \nabla\times\vec{\psi}, \tag{1.7}$$

where $\vec{\psi}$ is called the potential vector with components ψ_x, ψ_y, ψ_z, $\times$ is the vector product. The displacement in the solid can therefore be expressed as :

$$\vec{u} = \nabla\phi + \nabla\times\vec{\psi}. \tag{1.8}$$

Invoking the mathematical identity $\nabla^2\vec{u} = \nabla(\nabla\cdot\vec{u}) - \nabla\times(\nabla\times\vec{u})$, which in our case gives $\nabla^2\vec{u} = \nabla(\nabla\cdot\vec{u}) - \nabla\times\vec{\psi}$, allows the equation of motion to be expressed in terms of ϕ (or Θ) and $\vec{\psi}$:

$$-\mu\nabla\times\vec{\psi} + (\lambda+2\mu)\nabla\Theta = \rho\frac{\partial^2\vec{u}}{\partial t^2} \tag{1.9}$$

This equation will be used to derive the longitudinal and transverse wave equations.

Multiplying equation 1.9 by $\nabla\cdot$ and using the fact that $\nabla.(\nabla\vec{\psi}) = 0$, one obtains a wave equation governing longitudinal propagation in the elastic medium:

$$\nabla^2\phi - \frac{\rho}{\lambda+2\mu}\frac{\partial^2\phi}{\partial t^2} = 0, \tag{1.10}$$

where the longitudinal wave speed is $c_L = \left(\frac{\lambda+2\mu}{\rho}\right)^{1/2}$.

On the other hand, multiplying equation 1.9 by $\nabla\times$ and using $\nabla\times(\nabla\Theta)=0$, one obtains a similar wave equation for shear wave propagation:

$$\nabla^2\vec{\psi}-\frac{\rho}{\mu}\frac{\partial^2\vec{\psi}}{\partial t^2}=0, \tag{1.11}$$

where the shear wave speed is $c_T=\left(\frac{\lambda}{\rho}\right)^{1/2}$.

Since the three components of the displacement u_x, u_y, u_z depend on four potential components ϕ, ψ_x, ψ_y, ψ_z, (equation 1.8), it is necessary to specify an additional relation on the potentials. Aschenbach (1973) assumes an additional relation of the form :

$$\nabla\cdot\vec{\psi}=\frac{\partial\psi_x}{\partial x}+\frac{\partial\psi_y}{\partial y}+\frac{\partial\psi_z}{\partial z}=0. \tag{1.12}$$

In addition to the above equations, boundary conditions on the surface of the elastic domain need to be specified in order to completely solve the scalar potential and potential vector. These boundary conditions will be later detailed in the case of the system considered in this study.

1.3 Constitutive equations of the vibroacoustic problem

The problem considered in this report is a rectangular elastic base plate, fully covered by a decoupling coating which is immersed in water on one side. The base plate is simply supported on the four edges, and the decoupling coating is assumed to be inserted in an infinite rigid baffle. The excitation is applied on the base plate and consists either of a point force or an acoustic plane wave. The fluid loading on the free side of the base plate is neglected in the theoretical formulation of the problem (light fluid assumption). The system is depicted in the Figure 1.1. In this document subscript 1 is dedicated to the base plate while subscript 2 is dedicated to the coating.

1.3.1 Equation of motion of the base plate

The equation of motion of the base plate is :

$$\rho_1 h_1\frac{\partial^2 w}{\partial t^2}+D_1\nabla^4 w=-f(x,y)-\sigma_z(x,y,0), \tag{1.13}$$

where ρ_1 is the density and h_1 is the thickness of the plate, w is the transverse displacement, $f(x,y)$ is the force acting on the plate (point force or acoustic plane wave) and $\sigma_z(x,y,0)$ is the normal stress exerted by the coating on the plate. Also, D_1 is the bending stiffness of the plate :

$$D_1 = \frac{E_1 (h_1)^3}{12\left(1-(\nu_1)^2\right)}, \tag{1.14}$$

where E_1, and ν_1 are respectively the Young's modulus and the Poisson's ratio of the plate.

1.3.2 *Equation of motion of the coating*

Using the results of section 1.2, a wave equation is used to describe the propagation of longitudinal wave in the coating :

$$\nabla^2 \phi - \frac{1}{c_L^2}\frac{\partial^2 \phi}{\partial t^2} = 0, \tag{1.15}$$

where ϕ is the scalar potential and c_L the longitudinal wave speed in the coating, $c_L = \left(\frac{\lambda_2 + 2\mu_2}{\rho_2}\right)^{1/2}$, λ_2 and μ_2 are the Lamé coefficients of the coati..g.

Similarly, three wave equations are written for the three components of the potential vector $\vec{\psi}$ describing the shear wave in the coating:

$$\begin{cases} \nabla^2 \psi_x - \frac{1}{c_T^2}\frac{\partial^2 \psi_x}{\partial t^2} = 0 \\ \nabla^2 \psi_y - \frac{1}{c_T^2}\frac{\partial^2 \psi_y}{\partial t^2} = 0 \\ \nabla^2 \psi_z - \frac{1}{c_T^2}\frac{\partial^2 \psi_z}{\partial t^2} = 0 \end{cases} \tag{1.16}$$

where c_T is the shear wave speed in the coating, $c_T = (\mu_2/\rho_2)^{1/2}$, and ψ_x, ψ_y, ψ_z are the three components of the potential vector $\vec{\psi}$.

The displacement of the coating $\vec{u}$ is expressed in terms of the potentials ϕ and $\vec{\psi}$ by the following relation :

$$\vec{u} = \nabla\phi + \nabla \times \vec{\psi}, \tag{1.17}$$

1.3.3 *Fluid-structure interaction*

In this section the interaction between the surrounding fluid (water) and the decoupling coating is presented. In the fluid, the usual acoustic wave equation applies :

$$\nabla^2 p - \frac{1}{c_0^2}\frac{\partial^2 p}{\partial t^2} = 0, \tag{1.18}$$

where c_0 is the speed of acoustic waves in the fluid, and $p(x,y,z)$ is the acoustic pressure in the fluid.

At the fluid-coating interface the continuity of normal mechanical and acoustic velocities allows the Euler's equation to be written in the form :

$$\left.\frac{\partial^2 u_z}{\partial t^2}\right|_{z=-h_2} = \frac{1}{\rho_0}\left.\frac{\partial p}{\partial z}\right|_{z=-h_2}, \tag{1.19}$$

where ρ_0 is the density of the fluid.

To solve the acoustic problem, the integral formulation is used. In all the following developments, a complex time-harmonic dependence is assumed ($e^{j\omega t}$). The rigid baffle condition allows the Green function satisfying a Neumann's condition on the baffle to be used, so that the relation between the acoustic pressure in the fluid space and the normal displacement at the coating surface, takes the form of the usual Rayleigh integral:

$$p(x,y,z) = -\rho_0\omega^2 \iint_S u_z(x',y',-h_2)G(x,y,z/x',y',-h_2)dx'dy', \tag{1.20}$$

where G is the acoustic Green's function defined by :

$$G = \frac{e^{-jk_0\left((x-x')^2+(y-y')^2+(z+h_2)^2\right)^{1/2}}}{2\pi\left((x-x')^2+(y-y')^2+(z+h_2)^2\right)^{1/2}}, \tag{1.21}$$

where $k_0 = \omega / c_0$. This Green function satisfies a Neumann's condition on the baffle surface: $\left.\frac{\partial G}{\partial z}\right|_{z=-h_2} = 0$.

Equation 1.20 relates the acoustic pressure in the fluid space to the displacement of the outer surface of the coating. This equation will later be used to solve the sound radiation in the fluid medium.

1.3.4 Boundary conditions

In order to completely solve the problem, boundary conditions of the plate/coating/fluid system need to be specified.

- The boundary conditions at the plate/coating interface are:

$$z=0\begin{cases} w(x,y)=u_z(x,y,0) & (1.22)\\ \dfrac{h_1}{2}\dfrac{\partial w(x,y)}{\partial x}=u_x(x,y,0) & (1.23)\\ \dfrac{h_1}{2}\dfrac{\partial w(x,y)}{\partial y}=u_y(x,y,0) & (1.24)\end{cases}$$

where u_x, u_y, u_z, are the component of the displacement $\vec{u}$ of the coating in the x, y and z directions respectively. These boundary conditions express the continuity of the displacement between the plate and the coating in all three directions.

- The boundary conditions at the coating/fluid interface are:

$$z=-h_2\begin{cases} \sigma_z(x,y,-h_2)=-p(x,y,-h_2) & (1.25)\\ \sigma_{xz}(x,y,-h_2)=0 & (1.26)\\ \sigma_{yz}(x,y,-h_2)=0 & (1.27)\end{cases}$$

These equations express the stress continuity at the coating/fluid interface. Namely, the tangential strain is zero on the coating surface and the normal strain is equal to the surface acoustic pressure $-p(x,y,-h_2)$.

- The boundary conditions on the lateral sides of the coating are:

$$\begin{cases} u_z = 0 \text{ on the four sides } x=0, x=a, y=0, y=b \\ u_x = 0 \text{ on both sides } y=0, y=b \\ u_y = 0 \text{ on both sides } x=0, x=a \\ \sigma_x = 0 \text{ on the four sides } x=0, x=a, y=0, y=b \\ \sigma_y = 0 \text{ on the four sides } x=0, x=a, y=0, y=b \\ \sigma_{xz} = 0 \text{ on both sides } y=0, y=b \\ \sigma_{yz} = 0 \text{ on both sides } x=0, x=a \end{cases} \tag{1.28}$$

The above boundary conditions physically mean that the lateral sides of the coating are fixed in the z direction and in the tangential direction, but are free to move along the direction normal to the side. These boundary conditions will allow the scalar potential ϕ and the potential vector $\vec{\psi}$ to be simply expressed in terms of trigonometric functions, as will be shown later.

- The boundary conditions at the edges of the plate (simply-supported boundary conditions) are:

$$w = 0 \text{ on the four sides of the plate } x=0, x=a, y=0, y=b \tag{1.29}$$

These boundary conditions allow the displacement of the plate w to be expressed in terms of trigonometric functions.

The problem is then entirely defined. In the following a solution is derived in for the four unknown variables w, ϕ, ψ_x, ψ_y, (ψ_z is ultimately expressed in terms of ψ_x, ψ_y using equation 1.12).

1.3.5 Solving the problem

In this section the method used to solve the vibroacoustic problem is presented. The boundary conditions presented in the previous section allow the four unknowns of the problem, w, ϕ, ψ_x, ψ_y to be evaluated.

Equation 1.29 allows the displacement of the base plate w to be written in terms of trigonometric functions :

$$w(x,y) = \sum_{m=1}^{\infty}\sum_{n=1}^{\infty} a_{mn} W_{mn}(x,y), \tag{1.30}$$

where $W_{mn}(x,y)=\sin\left(\frac{m\pi x}{a}\right)\sin\left(\frac{n\pi y}{b}\right)$ are the eigenfunctions of a simply-supported plate *in-vacuo*.

It is proposed that the scalar potential can also be written in terms of the same trigonometric functions :

$$\phi(x,y,z)=\sum_{p=1}^{\infty}\sum_{q=1}^{\infty}\phi_{pq}(z)W_{pq}(x,y). \tag{1.31}$$

The choice of such functions will later be justified by the boundary conditions 1.28. If the above expression is introduced into the wave equation 1.15, one obtains the following second-order differential equation :

$$\left[\frac{\omega^2}{c_L^2}-\left(\frac{p\pi}{a}\right)^2-\left(\frac{q\pi}{b}\right)^2\right]\phi_{pq}(z)+\frac{\partial^2\phi_{pq}(z)}{\partial z^2}=0. \tag{1.32}$$

The general solution of this equation can be written in the form :

$$\phi_{pq}(z)=b_{pq}\cos(\alpha_{pq}z)+c_{pq}\sin(\alpha_{pq}z) \tag{1.33}$$

where b_{pq} and c_{pq} are unknown coefficients related to the longitudinal wave in the decouping layer and α_{pq} is defined by :

$$\alpha_{pq}=\left(\frac{\omega^2}{(c_L)^2}-\left(\frac{p\pi}{a}\right)^2-\left(\frac{q\pi}{b}\right)^2\right)^{1/2}, \tag{1.34}$$

which is a complex quantity in general.

Similarly, it is proposed that ψ_x and ψ_y can be expressed in the following form :

$$\begin{cases} \psi_x(x,y,z) = \sum_{p=1}^{\infty}\sum_{q=0}^{\infty} \psi_{x,pq}(z)\sin\left(\frac{p\pi x}{a}\right)\cos\left(\frac{q\pi y}{b}\right) \\ \psi_y(x,y,z) = \sum_{p=0}^{\infty}\sum_{q=1}^{\infty} \psi_{y,pq}(z)\cos\left(\frac{p\pi x}{a}\right)\sin\left(\frac{q\pi y}{b}\right) \end{cases} \tag{1.35}$$

Again, the choice of sine and cosine functions for the x and y dependence of ψ_x and ψ_y will be later justified by the boundary conditions 1.28. If the above expressions are introduced in the wave equation 1.16, one obtains the following second-order differential equations :

$$\begin{cases} \left[\frac{\omega^2}{c_T^2} - \left(\frac{p\pi}{a}\right)^2 - \left(\frac{q\pi}{b}\right)^2\right]\psi_{x,pq}(z) + \frac{\partial^2\psi_{x,pq}(z)}{\partial z^2} = 0 \\ \left[\frac{\omega^2}{c_T^2} - \left(\frac{p\pi}{a}\right)^2 - \left(\frac{q\pi}{b}\right)^2\right]\psi_{y,pq}(z) + \frac{\partial^2\psi_{y,pq}(z)}{\partial z^2} = 0 \end{cases} \tag{1.36}$$

The general solution of these equations can be written in the form :

$$\begin{cases} \psi_{x,pq}(z) = d_{pq}\cos(\beta_{pq}z) + e_{pq}\sin(\beta_{pq}z) \\ \psi_{y,pq}(z) = f_{pq}\cos(\beta_{pq}z) + g_{pq}\sin(\beta_{pq}z) \end{cases} \tag{1.37}$$

where d_{pq}, e_{pq}, f_{pq} and g_{pq} are unknown coefficients related to the shear wave in the decoupling layer and β_{pq} is defined by :

$$\beta_{pq} = \left(\frac{\omega^2}{(c_T)^2} - \left(\frac{p\pi}{a}\right)^2 - \left(\frac{q\pi}{b}\right)^2\right)^{1/2}, \tag{1.38}$$

The three displacements u_x, u_y, u_z, and the six stresses σ_x, σ_y, σ_z, σ_{xy}, σ_{xz}, σ_{yz} in the decoupling layer can later be expressed as a function of the potentials ϕ and $\vec{\psi}$. Ultimately, the displacements and stress depend on the six unknown coefficients b_{pq}, c_{pq}, d_{pq}, e_{pq}, f_{pq} and g_{pq}, as detailed in what follows. Equation 1.17 allows the displacement in the x direction to be written :

$$u_x(x,y,z) = \frac{\partial\phi}{\partial x} + \frac{\partial\psi_z}{\partial y} - \frac{\partial\psi_y}{\partial z}. \tag{1.39}$$

This leads to :

$$u_x(x,y,z)=\sum_{p=0}^{\infty}\sum_{q=1}^{\infty}\cos\left(\frac{p\pi x}{a}\right)\sin\left(\frac{q\pi y}{b}\right)u_{x,pq}(z), \tag{1.40}$$

where $u_{x,pq}$ is defined by :

$$u_{x,pq}(z)=\frac{p\pi}{a}\phi_{pq}(z)-\frac{q\pi}{b}\psi_{z,pq}(z)-\frac{\partial\psi_{y,pq}(z)}{\partial z}. \tag{1.41}$$

It can be noted that u_x automatically satisfies the second boundary condition in 1.28.
It is possible to proceed similarly for the other displacement and stress components. Equation 1.17 allows the displacement in the y direction to be written :

$$u_y(x,y,z)=\frac{\partial\phi}{\partial y}-\frac{\partial\psi_z}{\partial x}+\frac{\partial\psi_x}{\partial z}. \tag{1.42}$$

This leads to :

$$u_y(x,y,z)=\sum_{p=1}^{\infty}\sum_{q=0}^{\infty}\sin\left(\frac{p\pi x}{a}\right)\cos\left(\frac{q\pi y}{b}\right)u_{y,pq}(z), \tag{1.43}$$

where $u_{y,pq}$ is defined by :

$$u_{y,pq}(z)=\frac{q\pi}{b}\phi_{pq}(z)+\frac{p\pi}{a}\psi_{z,pq}(z)+\frac{\partial\psi_{x,pq}(z)}{\partial z}. \tag{1.44}$$

Again u_y automatically satisfies the third boundary condition in 1.28. The displacement in the z direction is :

$$u_z(x,y,z)=\frac{\partial\phi}{\partial z}+\frac{\partial\psi_y}{\partial x}-\frac{\partial\psi_x}{\partial y}. \tag{1.45}$$

which leads to :

$$u_z(x,y,z)=\sum_{p=1}^{\infty}\sum_{q=0}^{\infty}\sin\left(\frac{p\pi x}{a}\right)\sin\left(\frac{q\pi y}{b}\right)u_{z,pq}(z), \tag{1.46}$$

where $u_{z,pq}$ is defined by :

$$u_{z,pq}(z)=\frac{\partial\phi_{pq}(z)}{\partial z}-\frac{p\pi}{a}\psi_{y,pq}(z)+\frac{q\pi}{b}\psi_{x,pq}(z), \tag{1.47}$$

and u_z automatically satisfies the first boundary condition in 1.28

The stress components in the coating are also derived. Equations 1.1 and 1.2 allow the stress components in the coating to be expressed in terms of the displacement. The stress σ_x is defined by :

$$\sigma_x=(\lambda_2+2\mu_2)\frac{\partial u_x}{\partial x}+\lambda_2\frac{\partial u_y}{\partial y}+\lambda_2\frac{\partial u_z}{\partial z}, \tag{1.48}$$

which can be written in the form :

$$\sigma_x(x,y,z)=\sum_{p=1}^{\infty}\sum_{q=1}^{\infty}\sin\left(\frac{p\pi x}{a}\right)\sin\left(\frac{q\pi y}{b}\right)\sigma_{x,pq}(z), \tag{1.49}$$

where $\sigma_{x,pq}$ is defined by :

$$\sigma_{x,pq}(z)=-\frac{p\pi}{a}(\lambda_2+2\mu_2)u_{x,pq}(z)-\frac{q\pi}{b}\lambda_2 u_{y,pq}(z)+\lambda_2\frac{\partial u_{z,pq}(z)}{\partial z}. \tag{1.50}$$

Again, the stress σ_x in Equation 1.49 automatically satisfies the related boundary condition in 1.28. The other stress components are given by

$$\sigma_y=\lambda_2\frac{\partial u_x}{\partial x}+(\lambda_2+2\mu_2)\frac{\partial u_y}{\partial y}+\lambda_2\frac{\partial u_z}{\partial z}, \tag{1.51}$$

$$\sigma_z=\lambda_2\frac{\partial u_x}{\partial x}+\lambda_2\frac{\partial u_y}{\partial y}+(\lambda_2+2\mu_2)\frac{\partial u_z}{\partial z}, \tag{1.52}$$

$$\sigma_{xy}=\mu_2\left(\frac{\partial u_x}{\partial y}+\frac{\partial u_y}{\partial x}\right), \tag{1.53}$$

$$\sigma_{xz} = \mu_2\left(\frac{\partial u_x}{\partial z} + \frac{\partial u_z}{\partial x}\right), \tag{1.54}$$

$$\sigma_{yz} = \mu_2\left(\frac{\partial u_y}{\partial z} + \frac{\partial u_z}{\partial x}\right), \tag{1.55}$$

which gives:

$$\sigma_y(x,y,z) = \sum_{p=1}^{\infty}\sum_{q=1}^{\infty}\sin\left(\frac{p\pi x}{a}\right)\sin\left(\frac{q\pi y}{b}\right)\sigma_{y,pq}(z), \tag{1.56}$$

$$\sigma_z(x,y,z) = \sum_{p=1}^{\infty}\sum_{q=1}^{\infty}\sin\left(\frac{p\pi x}{a}\right)\sin\left(\frac{q\pi y}{b}\right)\sigma_{z,pq}(z), \tag{1.57}$$

$$\sigma_{xy}(x,y,z) = \sum_{p=0}^{\infty}\sum_{q=0}^{\infty}\cos\left(\frac{p\pi x}{a}\right)\cos\left(\frac{q\pi y}{b}\right)\sigma_{xy,pq}(z), \tag{1.58}$$

$$\sigma_{xz}(x,y,z) = \sum_{p=0}^{\infty}\sum_{q=1}^{\infty}\cos\left(\frac{p\pi x}{a}\right)\sin\left(\frac{q\pi y}{b}\right)\sigma_{xz,pq}(z), \tag{1.59}$$

$$\sigma_{yz}(x,y,z) = \sum_{p=1}^{\infty}\sum_{q=0}^{\infty}\sin\left(\frac{p\pi x}{a}\right)\cos\left(\frac{q\pi y}{b}\right)\sigma_{yz,pq}(z), \tag{1.60}$$

where

$$\sigma_{y,pq}(z) = -\frac{p\pi}{a}\lambda_2 u_{x,pq}(z) - \frac{q\pi}{b}(\lambda_2 + 2\mu_2)u_{y,pq}(z) + \lambda_2\frac{\partial u_{z,pq}(z)}{\partial z}. \tag{1.61}$$

$$\sigma_{z,pq}(z) = -\frac{p\pi}{a}\lambda_2 u_{x,pq}(z) - \frac{q\pi}{b}\lambda_2 u_{y,pq}(z) + (\lambda_2 + 2\mu_2)\frac{\partial u_{z,pq}(z)}{\partial z}. \tag{1.62}$$

$$\sigma_{xy,pq}(z) = \mu_2 \frac{q\pi}{b} u_{x,pq}(z) + \mu_2 \frac{p\pi}{a} u_{y,pq}(z). \tag{1.63}$$

$$\sigma_{xz,pq}(z) = \mu_2 \frac{\partial u_{x,pq}(z)}{\partial z} + \mu_2 \frac{p\pi}{a} u_{z,pq}(z). \tag{1.64}$$

$$\sigma_{yz,pq}(z) = \mu_2 \frac{\partial u_{y,pq}(z)}{\partial z} + \mu_2 \frac{q\pi}{b} u_{z,pq}(z). \tag{1.65}$$

The stress components in Equations 1.56 to 1.60 satisfy the boundary conditions 1.28

It is now necessary to rewrite the equations of the problem in terms of the series of unknown coefficients a_{mn}, b_{pq}, c_{pq}, d_{pq}, e_{pq}, f_{pq} and g_{pq}. Using the orthogonal properties of the eigenfunctions $W_{mn}(x,y)$, the equation of motion of the base plate can be written :

$$\rho_1 h_1 \left(\omega_{mn}^2 - \omega^2\right) a_{mn} N_{mn} = -\int_0^a \int_0^b f(x,y) W_{mn}(x,y)\,dx\,dy - \int_0^a \int_0^b \sigma_z(x,y,0) W_{mn}(x,y)\,dx\,dy \tag{1.66}$$

where the natural angular frequencies of the base plate *in-vacuo* are defined by :

$$\omega_{mn} = \sqrt{\frac{D_1}{\rho_1 h_1}}\left(\left(\frac{m\pi}{a}\right)^2 + \left(\frac{n\pi}{b}\right)^2\right), \tag{1.67}$$

and

$$N_{mn} = \int_0^a \int_0^b W_{mn}^2(x,y)\,dx\,dy = \frac{ab}{4}. \tag{1.68}$$

The other equations are provided by the plate/coating and coating/fluid interface conditions. The boundary condition 1.22 becomes :

$$\sum_{m=1}^{\infty}\sum_{n=1}^{\infty} a_{mn} W_{mn}(x,y) = \sum_{p=1}^{\infty}\sum_{q=1}^{\infty} u_{z,pq}(0) W_{pq}(x,y), \text{ for all } x, y \tag{1.69}$$

which leads to :

$$a_{mn} = u_{z,mn}(0) \tag{1.70}$$

The boundary condition 1.23 becomes :

$$\frac{h_1}{2}\sum_{m=1}^{\infty}\sum_{n=1}^{\infty} a_{mn}\frac{m\pi}{a}\cos\left(\frac{m\pi x}{a}\right)\sin\left(\frac{n\pi y}{b}\right) = \sum_{p=0}^{\infty}\sum_{q=1}^{\infty} u_{x,pq}(0)\cos\left(\frac{m\pi x}{a}\right)\sin\left(\frac{n\pi y}{b}\right), \tag{1.71}$$

which leads to :

$$\begin{cases} \frac{h_1}{2}\frac{m\pi}{a} a_{mn} = u_{x,mn}(0) \text{ if } m > 0 \\ u_{x,mn}(0) = 0 \text{ if } m = 0 \end{cases} \tag{1.72}$$

The boundary condition 1.24 becomes :

$$\frac{h_1}{2}\sum_{m=1}^{\infty}\sum_{n=1}^{\infty} a_{mn}\frac{n\pi}{b}\sin\left(\frac{m\pi x}{a}\right)\cos\left(\frac{n\pi y}{b}\right) = \sum_{p=1}^{\infty}\sum_{q=0}^{\infty} u_{y,pq}(0)\sin\left(\frac{m\pi x}{a}\right)\cos\left(\frac{n\pi y}{b}\right), \tag{1.73}$$

which leads to :

$$\begin{cases} \frac{h_1}{2}\frac{n\pi}{b} a_{mn} = u_{y,mn}(0) \text{ if } n > 0 \\ u_{y,mn}(0) = 0 \text{ if } n = 0 \end{cases} \tag{1.74}$$

Equations (1.20) and (1.25) lead a plate/coating interface condition of the form :

$$\sum_{p=1}^{\infty}\sum_{q=1}^{\infty} \sigma_{z,pq}(-h_2) W_{mn}(x,y) = \rho_0 \omega^2 \int_0^a \int_0^b \sum_{m=1}^{\infty}\sum_{n=1}^{\infty} u_{z,mn}(-h_2) W_{mn}(x,y) G(x,y,-h_2 / x', y', -h2) dx' dy' \tag{1.75}$$

The orthogonal properties of $W_{mn}(x,y)$ simplify the above relation:

$$N_{pq}\sigma_{z,pq}(-h_2) = j\omega \sum_{m=1}^{\infty}\sum_{n=1}^{\infty} u_{z,mn}(-h_2) Z_{mnpq}, \tag{1.76}$$

where Z_{mnpq} are the radiation impedance terms defined by :

$$Z_{mnpq} = j\rho_0\omega \int_0^a \int_0^b \int_0^a \int_0^b W_{mn}(x',y') G(x,y,-h_2,x',y',-h_2) W_{pq}(x,y) dx dy dx' dy' \tag{1.77}$$

It should be noted here that these radiation terms take the same form as in the locally reacting model of the decoupling material (DREA reports 97/423, 96/427 and 96/422); therefore, the same numerical procedures are used to evaluate these terms.

Equations 1.26 and 1.27 can be rewritten in the following form :

$$\begin{cases} \sigma_{xz,pq}(-h_2) = 0 & (1.78) \\ \sigma_{yz,pq}(-h_2) = 0 & (1.79) \end{cases}$$

Equations 1.66, 1.70, 1.72, 1.74, 1.76, 1.78 and 1.79 form the equations of the problem in terms of the unknowns a_{mn}, b_{pq}, c_{pq}, d_{pq}, e_{pq}, f_{pq} and g_{pq}. Solving the corresponding linear system allows the unknowns of the problem to be obtained.

1.3.6 Summary of the vibroacoustic problem

The following table summarizes the constitutive equations of the problem

Table 1.1 : The equations of the vibroacoustic problem : simply supported plate (Love-Kirchhoff theory) covered by a decoupling coating (three-dimensional theory of elasticity) and immersed in water.

$\rho_1 h_1 \frac{\partial^2 w}{\partial t^2} + D_1 \nabla^4 w = -f(x,y) - \sigma_z(x,y,0)$	Equation of motion of the base plate
$w(x,y) = u_z(x,y,0)$	Continuity of the transverse displacement at the plate / coating interface
$\frac{h_1}{2}\frac{\partial w(x,y)}{\partial x} = u_x(x,y,0)$	Continuity of the tangential displacement in the x direction at the plate / coating interface
$\frac{h_1}{2}\frac{\partial w(x,y)}{\partial y} = u_y(x,y,0)$	Continuity of the tangential displacement in the y direction at the plate / coating interface
$\sigma_z(x,y,-h_2) = -p(x,y,-h_2)$	Continuity of the transverse stress at the coating / fluid interface
$\sigma_{xz}(x,y,-h_2) = 0$	Zero shear stress at the coating / fluid interface
$\sigma_{yz}(x,y,-h_2) = 0$	Zero shear stress at the coating / fluid interface

1.4 *Vibroacoustic indicators*

In this section several local / global vibroacoustic indicators are derived from the previous theoretical study. The vibroacoustic indicators calculated are :

- The mean square velocity of the base structure;
- The mean square velocity of the outer surface of the decoupling layer;

- The sound power radiated by the system in water;
- The radiation efficiency;
- The transmission loss;
- The insertion loss;
- The input power imparted by the excitation;
- The acceleration at the driving point;
- The acceleration at a user specified point on the air side of the base plate and on the coating surface;
- The "near field" acoustic power defined in terms of the absolute intensity trough a mapping plane located at a distance *d* from the plate;

1.4.1 Expression of the various vibroacoustic indicators

- **Vibration indicators**

The mean square velocity of the base plate is defined by :

$$\left\langle V_1^2 \right\rangle = \frac{\omega^2}{2ab} \int_0^a \int_0^b w(x,y) w^*(x,y) dx dy = \frac{\omega^2}{8} \sum_{m=1}^{\infty} \sum_{n=1}^{\infty} |a_{mn}|^2 . \tag{1.80}$$

The transverse mean square velocity of the outer surface of the decoupling layer is :

$$\left\langle V_2^2 \right\rangle = \frac{\omega^2}{2ab} \int_0^a \int_0^b u_z(x,y,-h_2) u_z^*(x,y,-h_2) dx dy = \frac{\omega^2}{8} \sum_{p=1}^{\infty} \sum_{q=1}^{\infty} |u_{z,pq}(-h_2)|^2 . \tag{1.81}$$

The mean square velocity ratio is expressed as the ratio of the mean square velocity of the base plate to the mean square velocity of the outer surface of the decoupling layer :

$$V_R = \frac{\left\langle V_1^2 \right\rangle}{\left\langle V_2^2 \right\rangle} . \tag{1.82}$$

The quantities defined in Equations (1.80), (1.81) and (1.82) can be calculated after the linear system formed by equations 1.66, 1.70, 1.72, 1.74, 1.76, 1.78 and 1.79 is solved.

- **Acoustic indicators**

The sound power radiated by the system in the fluid is given by :

$$W = \frac{1}{2} Re\left[\int_0^a \int_0^b p(x, y, -h_2)(-j\omega) u_z^*(x, y, -h_2) dx dy \right] = \frac{\omega^2}{2} \sum_{mnpq} u_{z,pq}(-h_2) Re\left[Z_{mnpq}\right] u_{z,mn}^*(-h_2) . \quad (1.83)$$

Again, the calculation of the sound power involves the solution of the linear system formed by equations 1.66, 1.70, 1.72, 1.74, 1.76, 1.78 and 1.79, as well as the radiation impedance coefficients Z_{mnpq} which are similar to those used in the locally reacting model, DREA report (CR/96/427). The radiation efficiency of the coating / water system is given by :

$$\sigma = \frac{W}{\rho_0 c_0 ab \left\langle V_2^2 \right\rangle} . \quad (1.84)$$

The transmission loss τ is useful in the context of an *acoustic* excitation of the system : it is expressed by the ratio of the transmitted acoustic power to the incident power :

$$\tau = \frac{W}{W_i^0} , \quad (1.85)$$

where W is the sound power radiated by the structure in the fluid (equation 1.83) and W_i^0 is the incident power due to the acoustic plane wave exciting the structure. It is expressed by :

$$W_i = \frac{1}{2} Re\left[\int_0^a \int_0^b p_i(x, y, 0) V_n^*(x, y, 0) dx dy \right] , \quad (1.86)$$

where p_i is the acoustic pressure of the incident plane wave in the $z = 0$ plane and V_n^* is the complex conjugate of the acoustic velocity in the same plane $z = 0$ due to the incident plane wave. The sound pressure of the incident plane wave is of the form :

$$p_i(x, y, z) = P_0 e^{-jk_i(x \cos\varphi \sin\theta + y \sin\varphi \sin\theta + z \cos\theta)} e^{j\omega t} , \quad (1.87)$$

where P_0 is the magnitude of the plane wave, k_i is the wave number in the incident fluid : $k_i = \omega / c_i$, c_i is the acoustic velocity in the fluid on the side of the incident wave, θ and φ are the angles of incidence of the plane wave (Figure 1.2). The Euler's equation provides a relation between the acoustic pressure and the acoustic velocity :

$$\frac{\partial p_i(x,y,z)}{\partial z} = j\rho_0\omega V_n(x,y,z). \tag{1.88}$$

Using equation 1.88 the input power can be written :

$$W_i^0 = \frac{ab\cos\theta}{2\rho_0 c_0}(P_0)^2. \tag{1.89}$$

Note

The previous section gives the definition of the transmission loss as commonly used in problems of acoustic transmission through structures or partitions. However, it should be kept in mind that W_i^0 is not the *input* power imparted by the excitation on the structure. The expression of the input power is given in the following. In the computer code the transmission loss is defined by : $10\log_{10}(1/\tau)$.

The insertion loss is defined by the ratio of the radiated power with damping or decoupling treatment to the radiated power of the base structure without treatment :

$$IL = \frac{W_{with}}{W_{without}} \tag{1.90}$$

This indicator is not equivalent to the transmission loss. In the computer code it is evaluated by : $10\log_{10}(W_{without}/W_{with})$.

- **Input power**

The input power imparted in the system by a point force excitation is :

$$W_i = \frac{1}{2}Re\left[\int_0^a\int_0^b F(x_0,y_0)(-j\omega)w^*(x,y)dxdy\right] = -\frac{\omega}{2}F_0\sum_{m=1}^{\infty}\sum_{n=1}^{\infty}\sin\left(\frac{m\pi x_0}{a}\right)\sin\left(\frac{n\pi y_0}{b}\right)\mathrm{Im}[a_{mn}], \tag{1.91}$$

where Im[] denotes the imaginary part of a complex, and F_0 is the magnitude of the point force located at (x_0, y_0).

The input power of an incident plane wave on the structure is expressed by :

$$W_i = \frac{1}{2} Re\left[\int_0^a \int_0^b p_{total}(x,y,0)(-j\omega) w^*(x,y) dxdy \right], \tag{1.92}$$

where p_{total} is the *total* acoustic pressure acting on the base plate, which can be written :

$$p_{total}(x,y,0) = p_i(x,y,0) + p_r(x,y,0), \tag{1.93}$$

where p_i is the pressure of the incident plane wave :

$$p_i(x,y,z) = P_0 e^{-jk_i(x\cos\varphi\sin\theta + y\sin\varphi\sin\theta + z\cos\theta)} e^{j\omega t}, \tag{1.94}$$

and p_r is the pressure of the reflected plane wave. Assuming the blocked pressure hypothesis (total reflection) :

$$p_r(x,y,z) = P_0 e^{-jk_i(x\cos\varphi\sin\theta + y\sin\varphi\sin\theta - z\cos\theta)} e^{j\omega t}, \tag{1.95}$$

where P_0 is the magnitude of the reflected plane wave, k_i is the wave number in the incident fluid : $k_i = \omega / c_i$, c_i is the acoustic velocity in the incident fluid, θ and φ are angle of incidence of the plane wave (Figure 1.2). The input power can then be written :

$$W_i = \frac{1}{2} Re\left[(-j\omega) \sum_{mn} a_{mn}^* \int_0^a \int_0^b 2P_0 e^{-jk_i(x\cos\varphi\sin\theta + y\sin\varphi\sin\theta)} \sin\left(\frac{m\pi x}{a}\right) \sin\left(\frac{n\pi y}{b}\right) dxdy \right] \tag{1.96}$$

An equivalent form is :

$$W_i = \frac{1}{2} Re\left[(-j\omega) \sum_{mn} a_{mn}^* \int_0^a \int_0^b f(x,y) W_{mn}(x,y) dxdy \right] \tag{1.97}$$

where $f(x,y) = 2P_0 e^{-jk_i(x\cos\varphi\sin\theta + y\sin\varphi\sin\theta)}$. The surface integral of equation 1.97 was already evaluated in the second term of equation 1.66. The detail of the calculation of this integral in the case of a

plane wave is presented in the Appendix 1 of the DREA report "Computational Evaluation of Damping and Decoupling Material - Phase I" CR/96/427.

- **Acceleration on the base plate**

The mean square acceleration at a user defined point (x_d, y_d) (possibly including the driving point) on the base plate is expressed by :

$$\begin{cases} A_{cc}(x_d, y_d) = \frac{1}{2}\omega^4 w(x_d, y_d) w^*(x_d, y_d) \\ = \frac{\omega^4}{2} \sum_{mnpq} a_{mn} a^*_{pq} \sin\left(\frac{m\pi x_d}{a}\right) \sin\left(\frac{n\pi y_d}{b}\right) \sin\left(\frac{p\pi x_d}{a}\right) \sin\left(\frac{q\pi y_d}{b}\right) \end{cases} \quad (1.98)$$

The mean square acceleration at a user defined point (x_d, y_d) on the coating surface is expressed by :

$$A_{cc\_coating}(x_d, y_d) = \frac{1}{2}\omega^4 u_z(x_d, y_d) u_z^*(x_d, y_d) \quad (1.99)$$

Note

In the computer code all vibroacoustic indicators are expressed in decibels :

$$Indicator(dB) = 10\log_{10}(Indicator), \quad (1.1100)$$

and a reference of 10^{-12} Watt is used for the acoustic power.

1.4.2 "Near field" acoustic power

This section presents the calculation of the near field acoustic power which is defined in terms of the absolute intensity trough a rectangular mapping plane parallel to the plate and located at a distance d from the plate (Figure 1.2) :

$$N_F(d) = \iint_{S_i} I_z(M) dS_M , \quad (1.101)$$

where S_i is the surface of the mapping plane, M is a point in the fluid on the mapping plane. The acoustic normal intensity (direction z) is given by :

$$I_z(M) = \frac{1}{2} Re\left[p(M) V_z^*(M)\right], \tag{1.102}$$

where $p(M)$ is the acoustic pressure, $V_z^*(M)$ the complex conjugate of the acoustic velocity in the z direction (Figure 1.2). Using the notation of Figure 1.2 the Kirchhoff-Helmholtz equation allows the acoustic pressure at point M to be written in the form :

$$p(M) = -\iint_S \left[\frac{\partial G(M,Q)}{\partial z'} p(Q) - \frac{\partial p(Q)}{\partial z'} G(M,Q)\right] dS_Q, \tag{1.103}$$

where S is the surface of the plate, Q is a point on the coating surface with co-ordinates (x', y', $z' = -h_2$) (Figure 1.2) and G is the Green's function defined in equation 1.21. The Green's function satisfies :

$$\left.\frac{\partial G}{\partial z'}\right|_{z'=-h_2} = 0, \tag{1.104}$$

so that equation 1.103 simplified to the Rayleigh's integral :

$$p(M) = \iint_S \left[\frac{\partial p(Q)}{\partial z'} G(M,Q)\right] dS_Q. \tag{1.105}$$

The continuity of mechanical and acoustic velocities on the coating allows the Euler's equation to be written in the form :

$$\frac{\partial p(Q)}{\partial z'} = -\rho_0 \omega^2 u_z(Q). \tag{1.106}$$

At point M the Euler's equation is :

$$\frac{\partial p(M)}{\partial z} = j\omega\rho_0 V_z(M). \tag{1.107}$$

Equation 1.106 allows the acoustic pressure to be written :

$$p(M) = -\rho_0 \omega^2 \iint_S G(M,Q) u_z(Q) dS_Q. \tag{1.108}$$

The derivative of 1.108 in terms of z is given by :

$$\frac{\partial p(M)}{\partial z} = -\rho_0 \omega^2 \iint_S \frac{\partial G(M,Q)}{\partial z} u_z(Q) dS_Q , \tag{1.109}$$

Equations 1.107 and 1.97 allows the acoustic velocity $V_z(M)$ to be expressed in terms of the Green function G and of the displacement u_z by :

$$V_z(M) = j\omega \iint_S \frac{\partial G(M,Q)}{\partial z} u_z(Q) dS_Q \tag{1.110}$$

Equations 1.108 and 1.97 allow the acoustic intensity to be written in terms of the Green's function and in terms of the transverse displacement of the structure :

$$I_z(M) = \frac{1}{2}\rho_0 \omega^3 Re\left[j \iint_{S_Q} G(M,Q) u_z(Q) dS_Q \iint_{S_{Q'}} \left(\frac{G(M,Q')}{\partial z} \right)^* (u_z(Q'))^* dS_{Q'} \right] \tag{1.111}$$

The acoustic intensity integrated over a surface S_i is thus expressed by :

$$\iint_{S_i} I_z(M) dS_i = \frac{1}{2}\rho_0 \omega^3 Re\left[j \iint_{S_i} \left(\iint_{S_Q} G(M,Q) u_z(Q) dS_Q \iint_{S_{Q'}} \left(\frac{G(M,Q')}{\partial z} \right)^* (u_z(Q'))^* dS_{Q'} \right) dS_i \right] \tag{1.112}$$

These integrals are unable to be evaluated analytically. Hence a Gauss numerical quadrature is used. The complex conjugate of the derivative of the Green function is given by :

$$\left(\frac{\partial G(M,Q)}{\partial z} \right)^* = -\frac{z e^{jk_0 R}}{2\pi R^3} (1 - jk_0 R), \tag{1.113}$$

where $R = \left((x-x')^2 + (y-y')^2 + (z+h_2)^2 \right)^{1/2}$.

The term 1.113 is not defined when z tends toward 0, i.e. when the mapping plane coincides with the plate. To avoid such a problem the mapping plane has to be taken far enough of the plate surface, with respect to the acoustic wavelength. Typically, a distance of 1 cm was sufficient to avoid numerical problems for the frequency range considered.

In the computer code the "near field" acoustic power is expressed by :

$$N_F(z) = 10\log_{10}\left(\frac{\iint_{S_i} |I_z(M)|dS_i}{10^{-12}}\right). \qquad (1.114)$$

Note

The calculation of the near field acoustic power was developed in the previous section considering a decoupling coating, however, the formulation is similar for a bare plate or for plate covered with damping material. In the computer code VIBRO (WinVIBRO2.exe) the calculation of the near field acoustic power is possible for all calculation options.

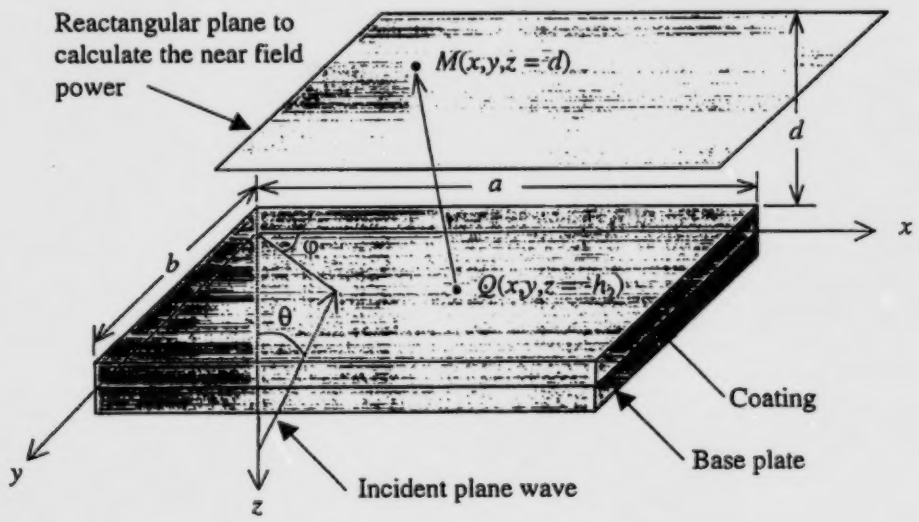

Figure 1.2 : Configuration of the rectangular plane used to calculate the near field power.

2 Numerical results of the new 3D model

2.1 Introduction

This section first investigates the influence of the shear wave component in the theoretical formulation of the 3D model previously presented. Then, results obtained by the 3D model (VIBRO3D) are compared to the locally reacting model (calculated with the numerical code VIBRO). The 3D model is also compared to the model of House (1991) and to the model of Ko (1997) valid for infinite plates. The method based on the "near-field power" to evaluate the insertion loss is presented in the last section.

2.2 Influence of the shear waves in the three-dimensional model

The new theoretical formulation (called VIBRO3D in this report) is implemented in a computer code (WinVIBRO2.exe). This section investigates the effect of neglecting the shear waves in the decoupling coating. Neglecting the shear waves in the formulation implies that only the scalar potential ϕ is considered in the equation of motion of the coating (longitudinal waves), the potential vector $\bar{\psi}$ accounting for the shear waves in the material is neglected. This approximation allows the size of the linear system of the problem to be considerably reduced since in this case only 3 unknowns are remaining: a_{mn}, b_{pq} and c_{pq} instead of the 7 unknowns of the complete 3D model (see section 1.3). In this case the 3 equations which describe the problem are equations 1.66, 1.70 and 1.76. Thus, equations 1.72, 1.74, 1.78 and 1.79 are not considered in this simplified model. Disregarding equations 1.72 and

1.74 physically implies that the continuity of the tangential displacement u_x and u_y between the base plate and the coating is no longer enforced (the coating can slip on the base plate). Disregarding equations 1.78 and 1.79 means that the nullity of the tangential stresses σ_{xz} and σ_{yz} is not enforced at the coating / fluid interface. These simplifications therefore violate some of the physics involved, however, such a model proves to satisfactorily predict the global acoustic behaviour of the system, as the following numerical simulations show. Note that neglecting shear waves in the decoupling layer is not equivalent to the locally reacting model because the propagation of longitudinal waves still allow elastic displacements of the coating in the 3 directions x, y, z, whereas the locally reacting model implies that only a z displacement of the coating is considered.

Figure 2.1, Figure 2.2, Figure 2.3 and Figure 2.4 compare the acoustic response of the complete 3D model and of the 3D model with only the longitudinal waves considered, for various coated plates.

The characteristics of the base plate used in these tests is presented in the Table 2.1. A point force is applied on the base plate at $x = y = 0.06$ m from a corner of the plate. The surrounding fluid is water ($c_0 = 1460$ m/s, $\rho_0 = 1000$ kg/m^3). Figure 2.3 and Figure 2.4 are for a decoupling material with realistic characteristics. In all cases, the simplified 3D model gives correct tendencies except in low frequency in Figure 2.1 and in Figure 2.3. The reason for this discrepancies are not clearly understood but the differences remain small. The conclusion that shear waves in the coating have little influence on the sound radiation is consistent with previous studies in the literature (Ko, 1997).

Table 2.1 : Characteristics of the base plate.

Length (m)	Width (m)	Thickness (mm)	Density (kg/m^3)	Young's modulus (Pa)	Loss factor	Poisson's ratio
a	b	h_1	ρ_1	E_1	η_1	ν_1
0.6	0.6	9	7850	2.1×10^{11}	0.005	0.3

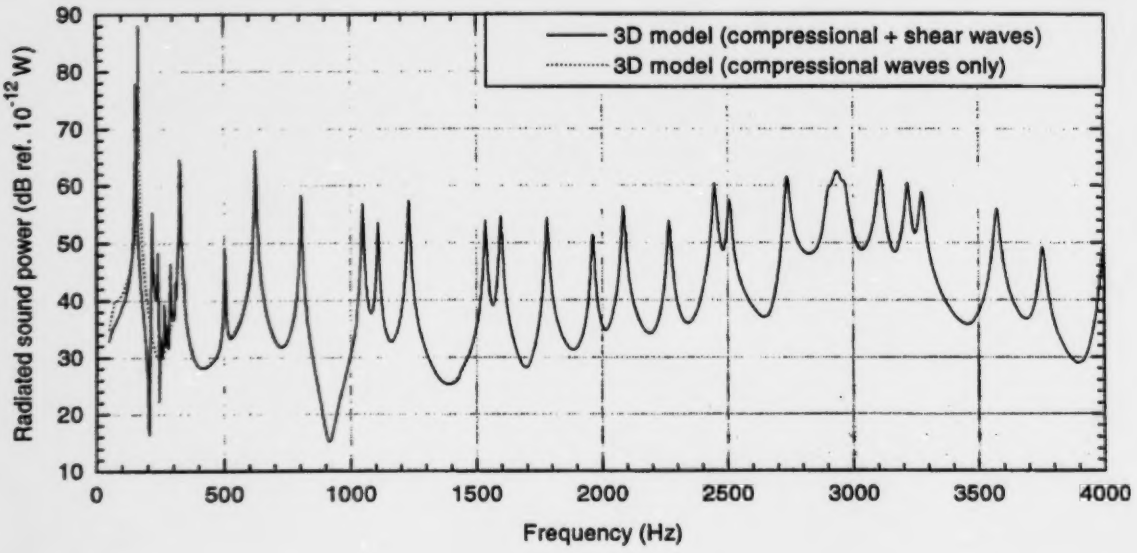

Figure 2.1 : Sound power radiated by the coating calculated with the 3D model with and without the shear waves. The coating has the following characteristics : $h_2 = 0.01$ m, $\rho_2 = 100$ kg/m^3, $E_2 = 2\times10^4$ Pa, $\eta_2 = 0.01$, $\nu_2 = 0.45$.

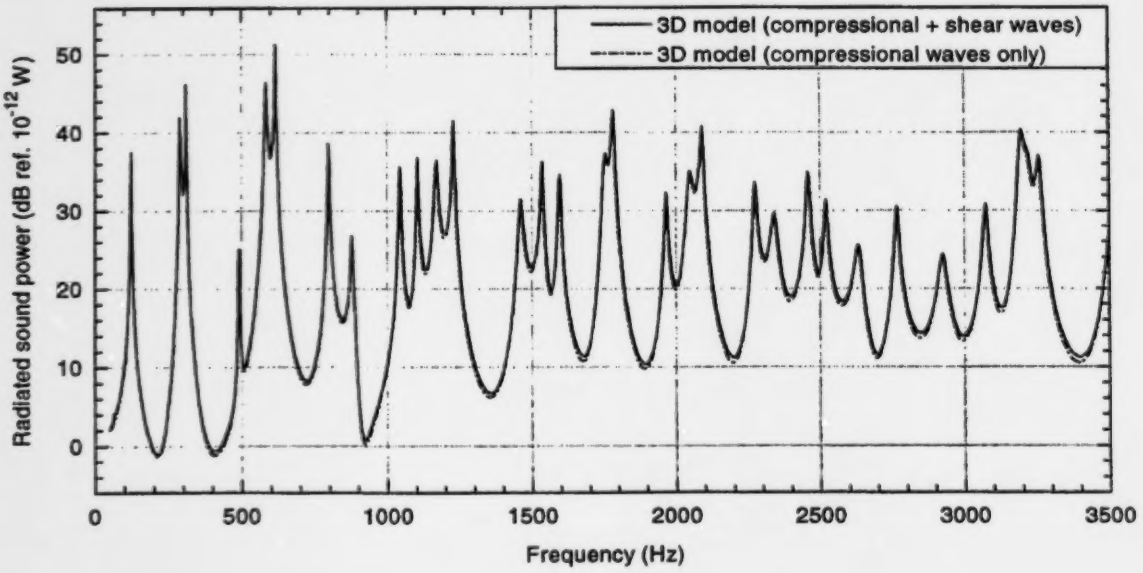

Figure 2.2 : Sound power radiated by the coating calculated with the 3D model with and without the shear waves. The coating has the following characteristics : $h_2 = 0.01$ m, $\rho_2 = 100$ kg/m^3, $E_2 = 2\times10^2$ Pa, $\eta_2 = 0.01$, $\nu_2 = 0.49$.

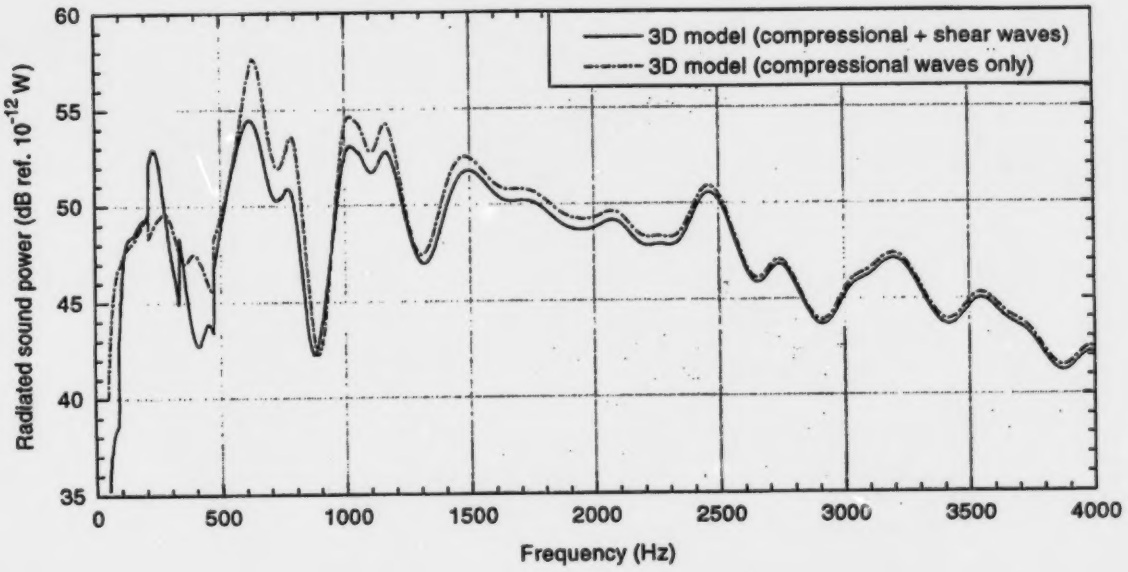

Figure 2.3 : Sound power radiated by the coating calculated with the 3D model with and without the shear waves. The coating has the following characteristics : $h_2 = 0.05$ m, $\rho_2 = 600$ kg/m^3, $E_2 = 7.2\times10^6$ Pa, $\eta_2 = 0.65$, $\nu_2 = 0.38$.

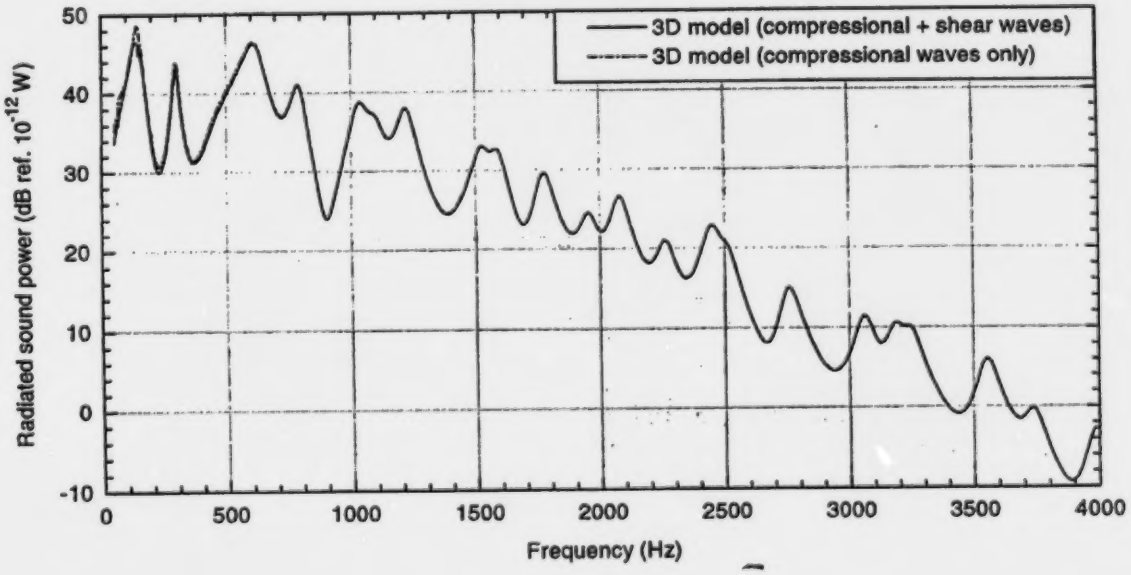

Figure 2.4 : Sound power radiated by the coating calculated with the 3D model with and without the shear waves. The coating has the following characteristics : $h_2 = 0.05$ m, $\rho_2 = 600$ kg/m^3, $E_2 = 7.2\times10^5$ Pa, $\eta_2 = 0.65$, $\nu_2 = 0.38$.

2.3 Comparison between VIBRO and the new 3D model

In this section VIBRO3D is compared to the locally reacting model previously implemented in the computer code VIBRO. For these comparisons only the compressional waves in the coating are accounted for in the 3D model. The characteristics of the base plate used for the parametric study is presented in the Table 2.1 (page 28). A point force is applied on the base plate at $x = y = 0.06$ m from a corner of the plate. The surrounding fluid is water ($c_0 = 1460$ m/s, $\rho_0 = 1000$ kg/m^3).

In the three-dimensional theory of elasticity the transverse stress σ_z is related to the transverse strain ε_z by the following relation (see equation 1.2) :

$$\sigma_z = (\lambda_2 + 2\mu_2)\varepsilon_z = \left(B_2 + \frac{4}{3}\mu_2\right)\varepsilon_z, \tag{2.1}$$

where λ_2 and μ_2 are the Lamé constants and B_2 is the bulk modulus of the coating. The term $L_2 = \lambda_2 + \mu_2$ is often called the plate modulus. In the locally reacting model only the transverse stresses and transverse deformations are considered. Hence, the stress-strain relation should be expressed by the equation 2.1. Applying equation 2.1 to a locally reacting decoupling layer on a base plate yields :

$$P(x, y, -h_2) = L_2\left(\frac{w_2(x,y) - w_1(x,y)}{h_2}\right), \tag{2.2}$$

where $P(x,y,-h_2)$ is the acoustic pressure on the coating surface, w_2 and w_1 are the transverse displacements of the coating surface and of the base structure, respectively. Table 2.2 presents the relation between the plate modulus (used in VIBRO) and the correponding Young's modulus and Poisson's ratio (used in VIBRO3D) for several material characteristics. The others characteristics of the coating are presented in Table 2.3 (the mass density applies only to the 3D model).

Table 2.2 : Coating characteristics used in the comparisons between VIBRO and VIBRO3D (C_L and C_T are the compressional wave speed and the shear wave speed respectively).

	L_2 (Pa)	E_2 (Pa)	ν_2	C_L (m/s)	C_T (m/s)
Case 1	3.793×10^6	10^6	0.45	194.7	58.7
Case 2	3.793×10^5	10^5	0.45	61.6	18.6
Case 3	3.793×10^4	10^4	0.45	19.5	5.9

Case 4	3.793×10^3	10^3	0.45	6.1	1.8

Table 2.3 : Characteristics of the coating.

Thickness (mm)	Density (kg/m^3)	Loss factor
h_2	ρ_2	η_2
10	100	0.01

2.3.1 Vibration and acoustic response

Figure 2.5 shows the mean square velocity of the free surface of the decoupling layer (which is directly related to the sound radiation in the fluid), for case 1 of Table 2.2. The low-frequency modes in VIBRO3D are shifted to higher frequencies as compared to the VIBRO results; this may be attributed to more rigid boundary conditions of the decoupling layer in VIBRO3D (e.g. the edges of the decoupling layer are constrained to have a zero transverse displacement in VIBRO3D, which is not the case in VIBRO). In higher frequency, the resonant frequencies predicted by VIBRO and VIBRO3D are closer. In terms of vibration amplitudes, VIBRO seems to slightly overestimate vibration reductions as compared to the 3D model. This confirms that complex wave propagation in the decoupling material produces larger vibration amplitudes than a simple locally reacting model. Figure 2.6 that presents the radiated sound power for case 1 of Table 2.2 shows similar tendencies.

Figure 2.7 and Figure 2.8 show the results for case 2 of Table 2.2, which corresponds to a softer material. The low-frequency results obtained with the two models are comparable. However, there is a high-frequency (starting at 1500 Hz) deviation of the models; especially VIBRO3D predicts a significant amplification phenomenon around 3000 Hz. The peaks around 3000 Hz are due to coating modes (thickness modes in the coating), which cannot be predicted by the locally reacting model because of the massless assumption of the coating. As a result, the vibration amplitudes in VIBRO3D are much larger than predicted by VIBRO in this frequency range. Further sections of this report show that this amplification phenomenon is present in various forms in other prediction methods for decoupling materials in water.

Figure 2.9 and Figure 2.10 show results for case 3 of Table 2.2, corresponding to an even softer decoupling material. Except in very low-frequency, the results of VIBRO and VIBRO3D are very different. VIBRO shows a continuous decrease of the average vibration amplitude as a function of frequency, whereas VIBRO3D predicts a relatively constant average vibration amplitude in frequency.

This is again due to "coating modes" which contribute to add new resonant modes in the vibration and acoustic spectra, and increase the vibration amplitudes of the coating.

The results of Figure 2.11 and Figure 2.12 show that the above tendencies are accentuated for a very soft decoupling material. Again in these figures many coating modes are visible in the 3D model, and the resulting vibration levels of the coating are much larger than in the locally reacting model.

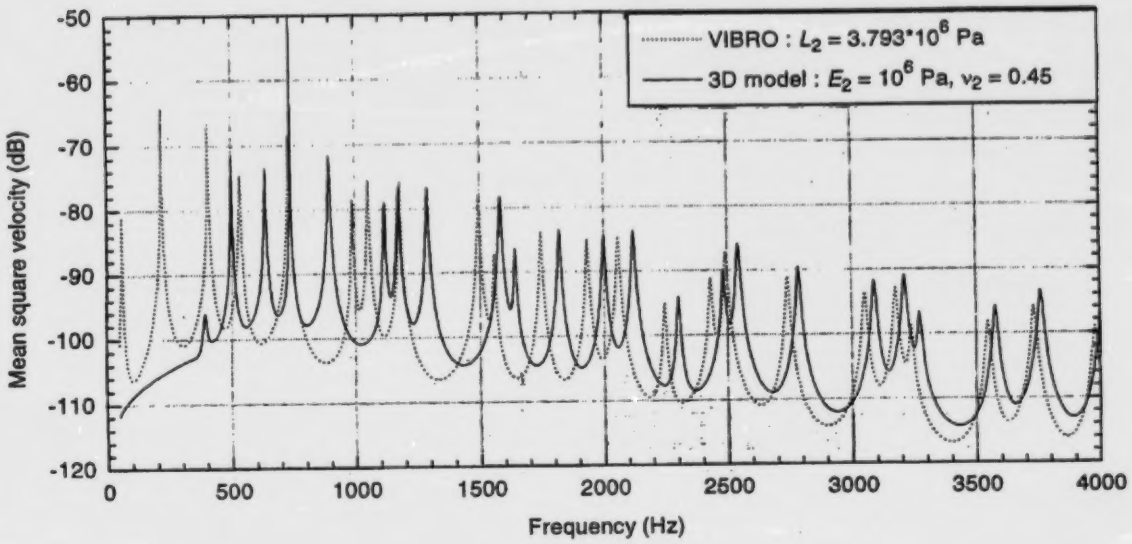

Figure 2.5: Mean square velocity of the outer surface of the coating for case 1 of Table 2.2. Only longitudinal waves are accounted for in the 3D model.

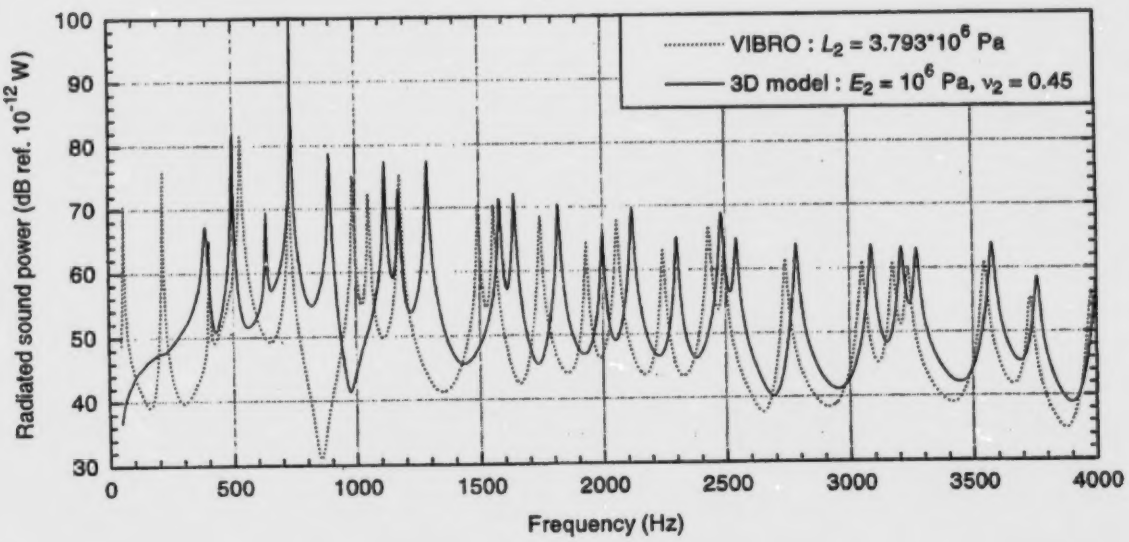

Figure 2.6: Sound power radiated by the coating for case 1 of Table 2.2. Only longitudinal waves are accounted for in the 3D model.

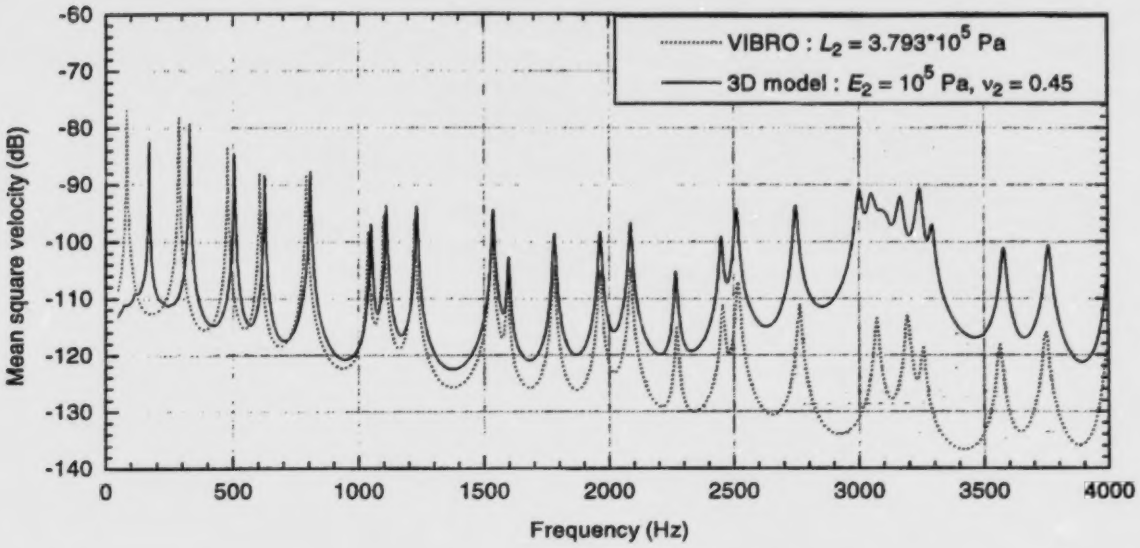

Figure 2.7: Mean square velocity of the outer surface of the coating for case 2 of Table 2.2. Only longitudinal waves are accounted for in the 3D model.

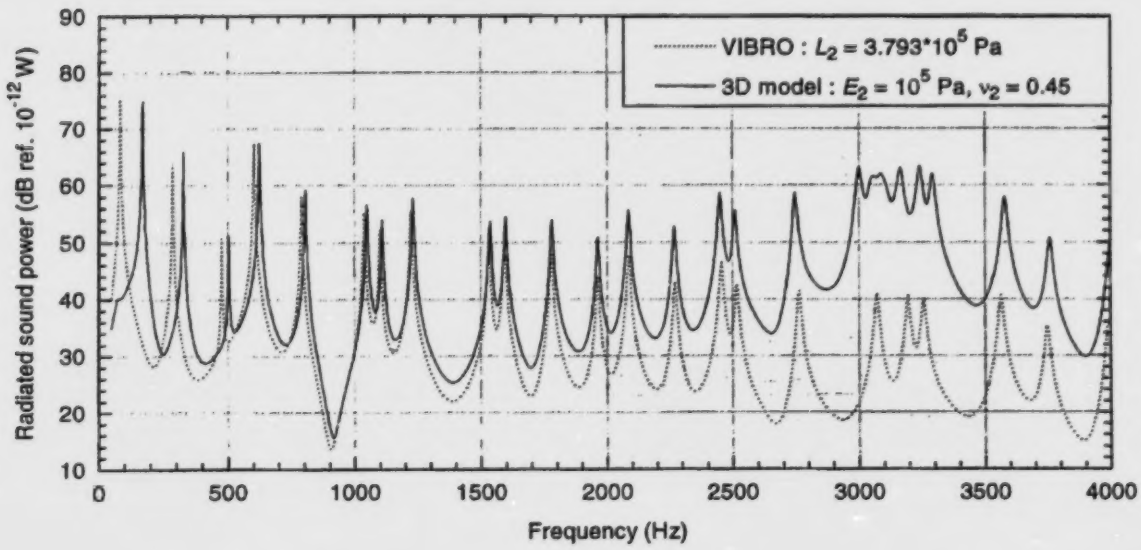

Figure 2.8: Sound power radiated by the coating for case 2 of Table 2.2. Only longitudinal waves are accounted for in the 3D model.

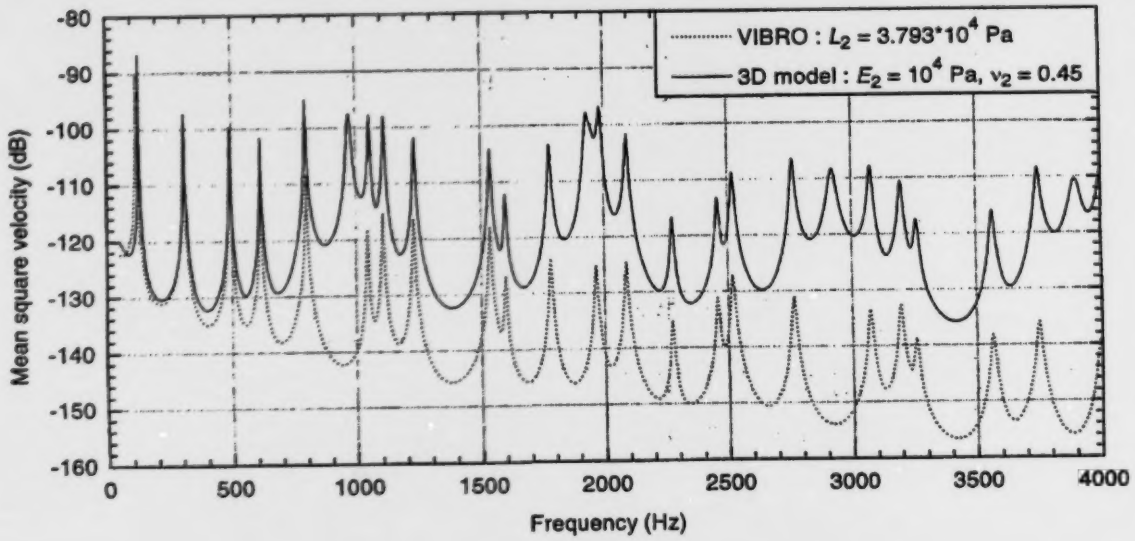

Figure 2.9: Mean square velocity of the outer surface of the coating for case 3 of Table 2.2. Only longitudinal waves are accounted for in the 3D model.

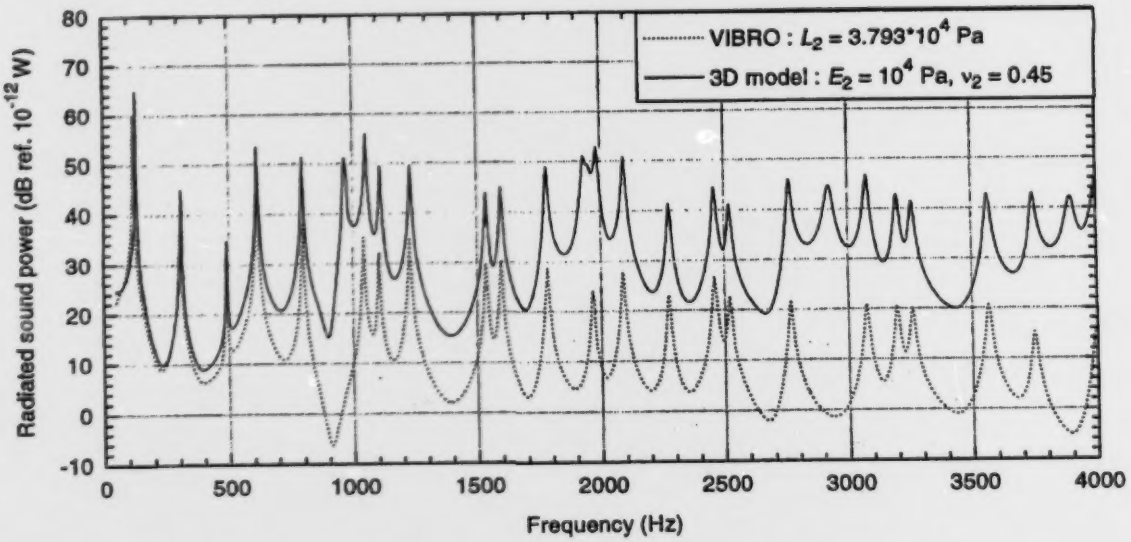

Figure 2.10: Sound power radiated by the coating for case 3 of Table 2.2. Only longitudinal waves are accounted for in the 3D model.

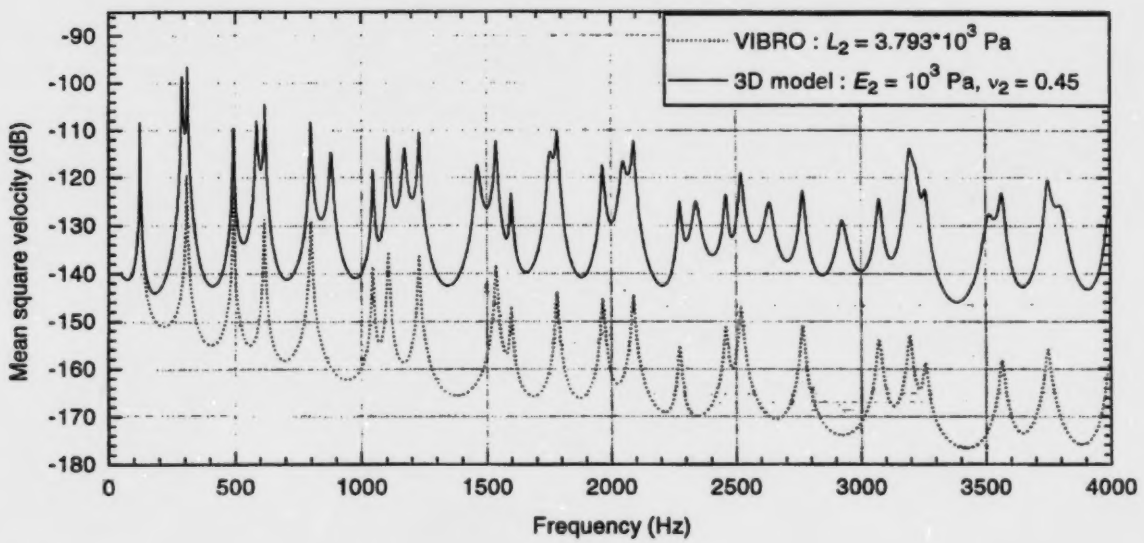

Figure 2.11: Mean square velocity of the outer surface of the coating for case 4 of Table 2.2. Only longitudinal waves are accounted for in the 3D model.

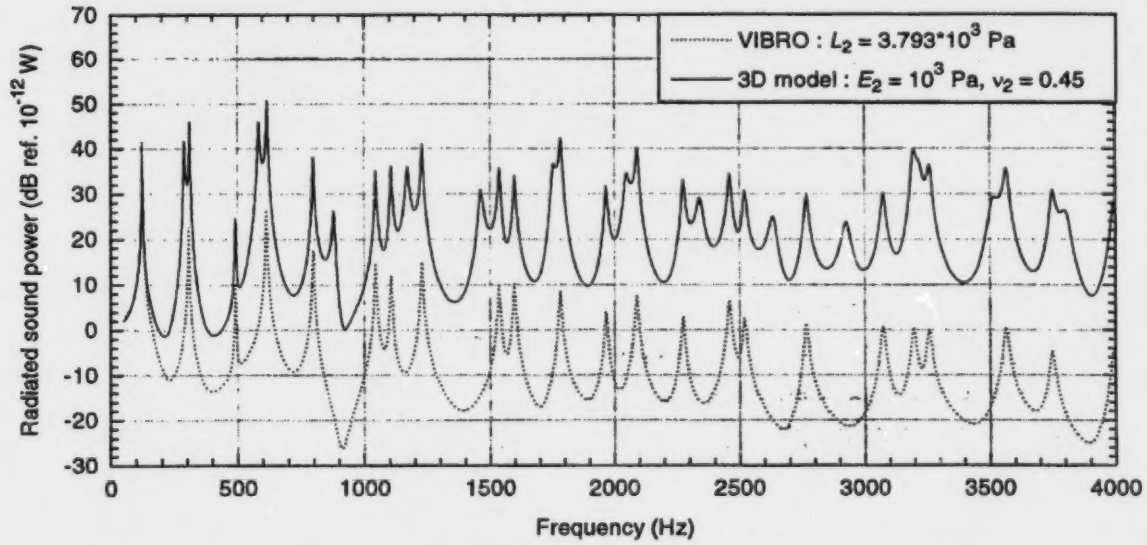

Figure 2.12: Sound power radiated by the coating for case 4 of Table 2.2. Only longitudinal waves are accounted for in the 3D model.

2.3.2 *Vibration isolation*

In this section the mean square velocity ratio (equation 1.82) calculated with VIBRO3D is compared to the mean square velocity ratio calculated with VIBRO. This ratio gives an indication on the vibration isolation provided by the decoupling layer and turns out to be a good indicator of the noise reduction performance of the coating (DREA CR/96/427). The cases studied are the four materials of Table 2.2. The base plate and the excitation are similar to those in the previous sections. In the following figures the same *y*-scale (0-100 dB) is used for the various plots in order to demonstrate the decoupling effect of the coating.

Very good agreement is obtained between VIBRO3D and the locally reacting model in the case of a relatively rigid material, Figure 2.13. In Figure 2.14 (softer material) VIBRO3D shows a frequency region of low vibration isolation, which is not predicted by the locally reacting model. This feature is due to a coating mode (i.e. a standing wave in the thickness of the coating) that appears in the vibration response of the outer surface of the decoupling layer but not in the vibration response of the base plate. These modes are determined by the thickness of the coating and the longitudinal wave velocity in the coating. In an approximate way, the coating modes correspond to cases where the wavelength in the coating γ_2, satisfies the relation:

$$\gamma_2 = \frac{2h_2}{n} \quad \forall n \in [1,...\infty], \tag{2.3}$$

where h_2 is the thickness of the coating. If f is the frequency, then: $\gamma_2 = c_L / f$ (c_L is the longitudinal wave speed). Hence, the frequencies of the coating modes are given by :

$$f_n = \frac{nc_L}{2h_2} \quad \forall n \in [1,...\infty]. \tag{2.4}$$

The locally reacting model cannot predict such modes because of the massless assumption used for the coating.

In Figure 2.15 and Figure 2.16, as the stiffness of the coating decreases, more coating modes appear in the VIBRO3D simulations and the locally reacting model overestimates the vibration isolation predicted by the 3D model. In the present simulations the coating has a small damping factor ($\eta_2 = 0.01$), hence the coating modes are lightly damped and the modes are very sharp. When coatings with a larger loss factor are considered the coating modes dissipate energy so that the decoupling effectiveness in the 3D model can be improved (see next section).

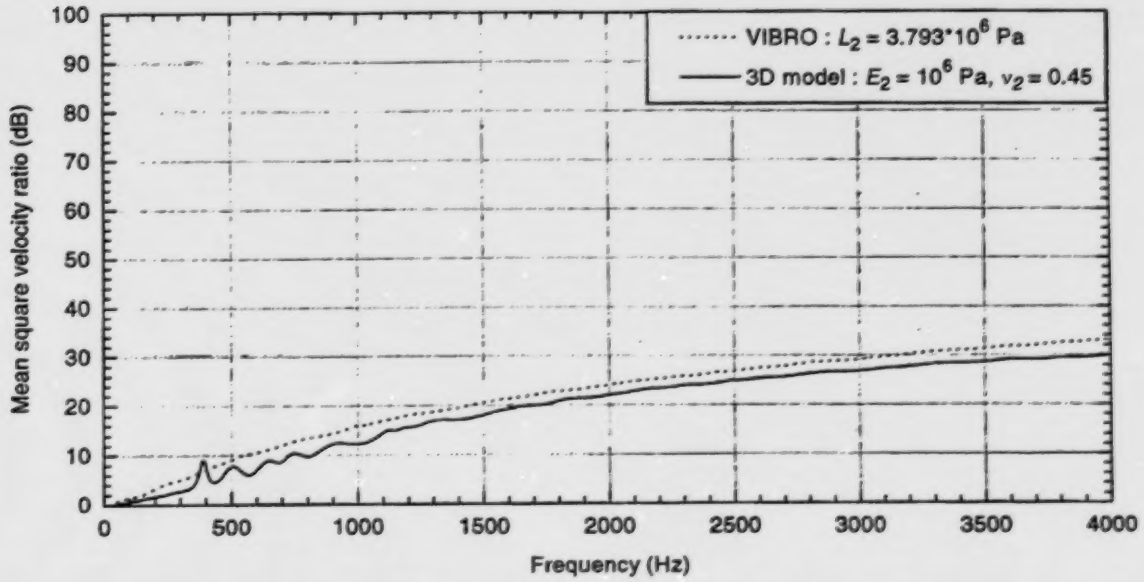

Figure 2.13 : Mean square velocity ratio for case 1 of Table 2.2. Only longitudinal waves are accounted for in the 3D model.

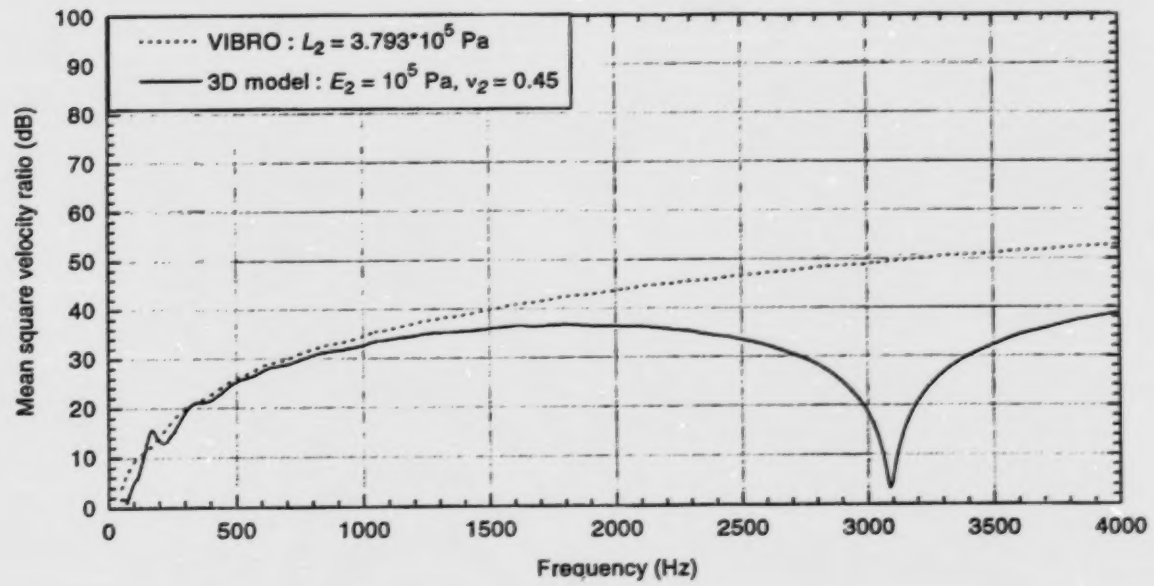

Figure 2.14 : Mean square velocity ratio for case 2 of Table 2.2. Only longitudinal waves are accounted for in the 3D model.

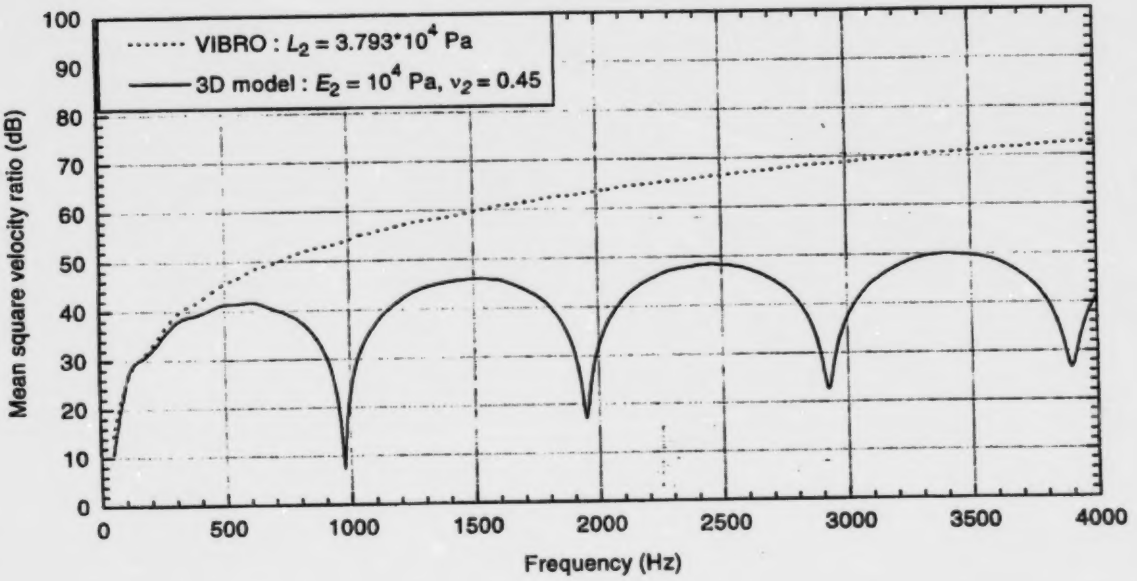

Figure 2.15 : Mean square velocity ratio for case 3 of Table 2.2. Only longitudinal waves are accounted for in the 3D model.

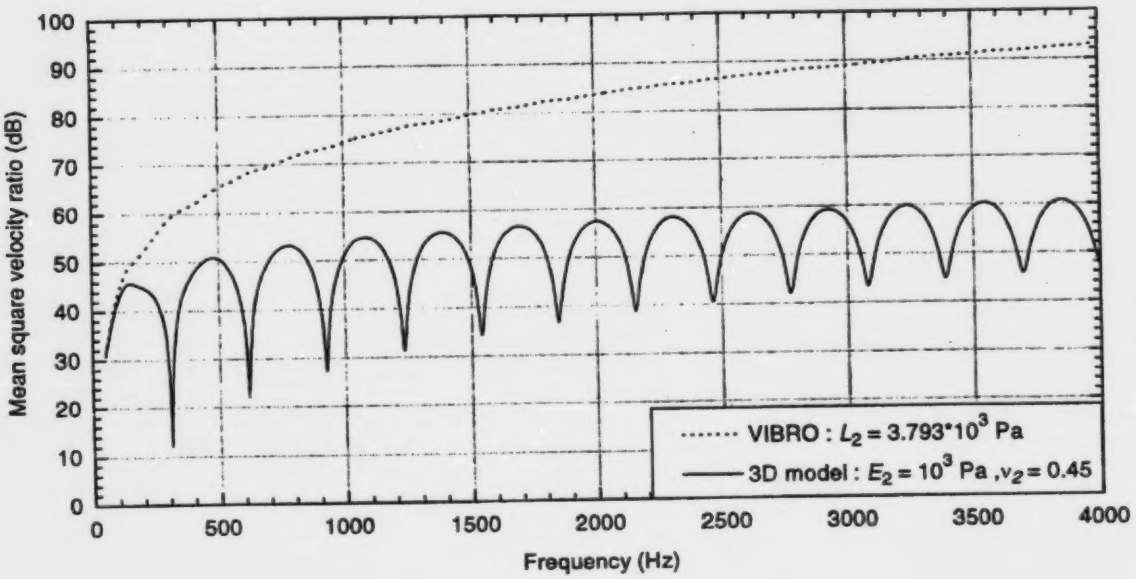

Figure 2.16 : Mean square velocity ratio for case 4 of Table 2.2. Only longitudinal waves are accounted for in the 3D model.

2.3.3 *Realistic decoupling material, influence of the coating density*

In this section simulations are presented based on realistic coating parameters provided by DREA. This material has a relatively high density (ρ_2 = 600 kg/m^3) and it is interesting to compare the locally reacting model to VIBRO3D for such a material. We recall that the density is not taken into account in the locally reacting model (VIBRO) whereas it is accounted for in the 3D model (VIBRO3D).

The base plate used for these tests is described in Table 2.1 (page 28). The characteristics of the coating material provided by DREA are described in Table 2.4. The fluid is water (ρ_0 = 1000 kg/m^3, c_0 = 1460 m/s) and the excitation is a point force located at $x = y = 0.06$ m from a corner of the plate. The locally reacting model is calculated using the plate modulus L_2 shown in Table 2.4.

Table 2.4 : Characteristics of the decoupling coating provided by DREA.

Thickness (mm) h_2	Density (kg/m^3) ρ_2	Young's mod. (Pa) E_2	Plate mod. (Pa) L_2	Loss factor η_2	Poisson's ratio ν_2
50	600	5×10^6	1.87×10^7	0.65	0.38

Figure 2.17 shows the mean square velocity of the base plate and the mean square velocity of the outer surface of the decoupling layer calculated with VIBRO and VIBRO3D. These results clearly show that the response predicted by VIBRO3D is highly damped, whereas the VIBRO results show little damping, especially in higher frequency. These results show that the locally reacting model is unable to predict the vibration damping due to the energy dissipated in the coating. This simulation points out the interest of the 3D model in comparison to the locally reacting model. It is shown in the following section that the discrepancy between VIBRO and VIBRO3D is related to the massless assumption of the locally reacting model.

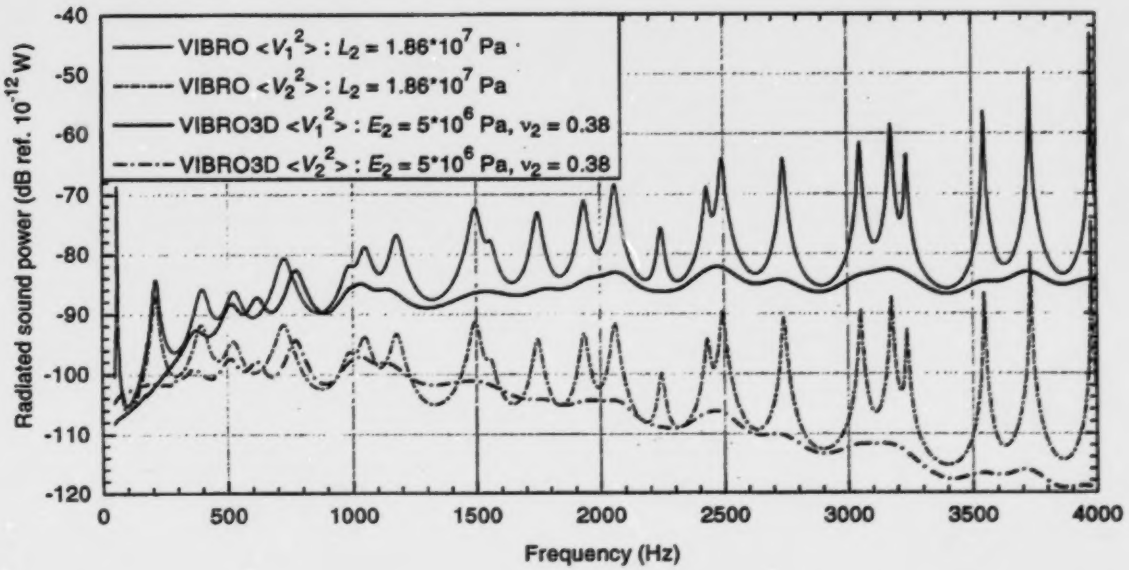

Figure 2.17 : Comparison of the mean square velocity between VIBRO and VIBRO3D (DREA decoupling material, $\langle V_1^2 \rangle$ is the mean square velocity of the base plate and $\langle V_2^2 \rangle$ is the mean square velocity of the outer surface of the decoupling layer).

Figure 2.18 shows the radiated sound power calculated with the locally reacting model and with the 3D model with three different coating densities[1] (ρ_2 = 10 kg/m^3, ρ_2 = 300 kg/m^3, ρ_2 = 600 kg/m^3, all other parameters are identical to the case of Figure 2.17). When a small density is considered (10 kg/m^3) the 3D model shows small damping in high frequency (> 1000 Hz) and higher damping in low frequency. In high frequency VIBRO and VIBRO3D give very consistent results except that the sound power level calculated with VIBRO3D (ρ_2 = 10 kg/m^3) is larger than with VIBRO. When the density of the coating is increased to ρ_2 = 300 kg/m^3 and ρ_2 = 600 kg/m^3 the results obtained with VIBRO3D show a much larger damping. This example shows that the density of the coating is an important parameter in the damping behaviour of the plate/coating/fluid system. Because of its inherent massless behaviour of the coating material, the locally reacting model is unable to adequately predict the energy dissipation associated with the thickness deformation of the coating material.

On the other hand, despite its limitations for highly damped coatings, the locally reacting model is however able to adequately predict the mean square velocity ratio (i.e. the vibration isolation), Figure 2.19.

[1] A zero density is impossible in the 3D model because it corresponds to infinite wave velocity.

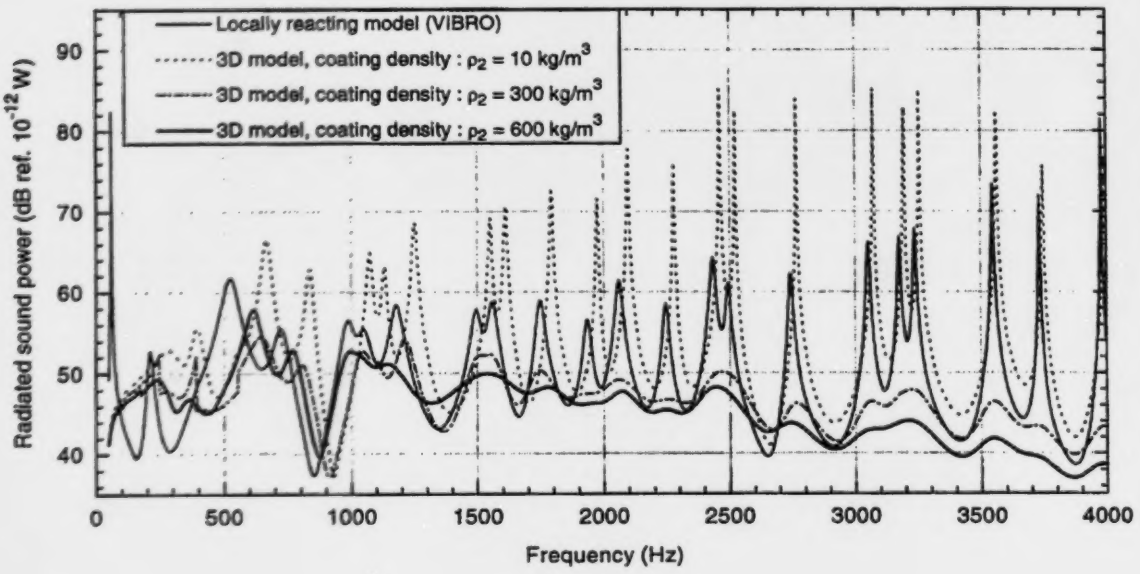
Locally reacting model (VIBRO)
3D model, coating density : ρ_2 = 10 kg/m^3
3D model, coating density : ρ_2 = 300 kg/m^3
3D model, coating density : ρ_2 = 600 kg/m^3
Radiated sound power (dB ref. 10^{-12} W)
Frequency (Hz)

Figure 2.18 : Influence of the coating density on the acoustic response of the system.

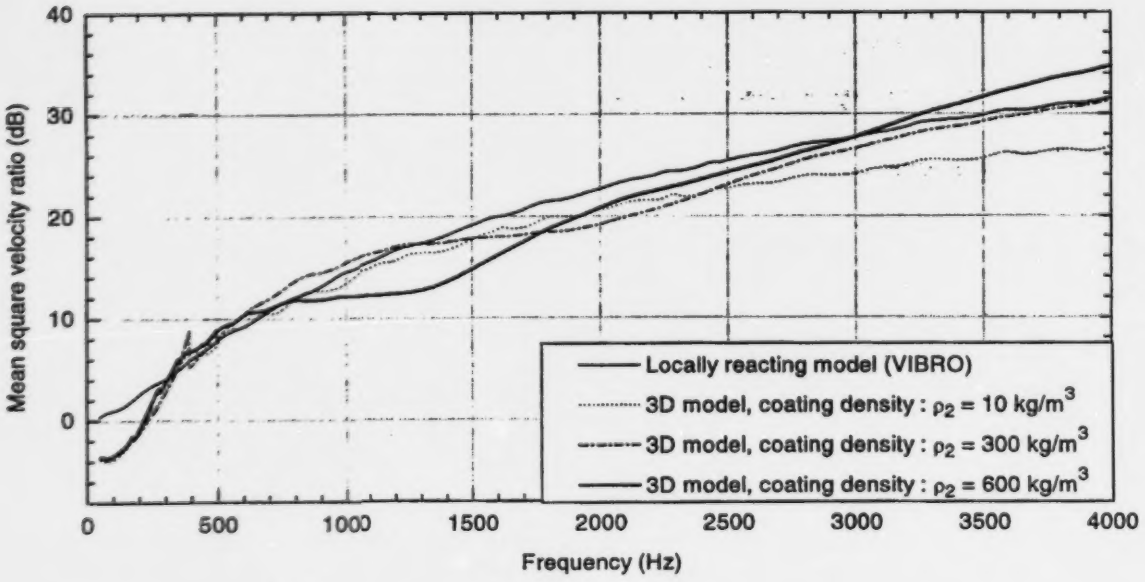
Locally reacting model (VIBRO)
3D model, coating density : ρ_2 = 10 kg/m^3
3D model, coating density : ρ_2 = 300 kg/m^3
3D model, coating density : ρ_2 = 600 kg/m^3
Mean square velocity ratio (dB)
Frequency (Hz)

Figure 2.19 : Influence of the coating density on the vibration isolation of the system.

2.4 Comparison between the model of Ko and VIBRO3D

Ko (1997) proposed a model to predict the response of an *infinite* plate covered by a decoupling coating and immersed in water. Both the base plate and the coating were modelled using the three-dimensional theory of elasticity. There are two main differences between VIBRO3D and the model of Ko: (1) Ko considered only an *infinite*, fluid-loaded plane structure while the present model applies to a finite, baffled plane structure; (2) Ko used the three-dimensional theory of elasticity to describe wave propagation in both the base structure and the coating, while our 3D model uses the three-dimensional theory of elasticity for the coating and assumes a plate theory for the base structure. The pure bending assumption in VIBRO3D should reasonably apply to the relatively large plates involved in marine structures, low-frequency sound radiation and transverse excitation.

Figure 2.20 and Figure 2.21 show comparisons of Ko's results with VIBRO3D. The data used for these simulations are those reported in Ko (1997), and are as follows:

ρ_0 (water density)	1000 kg/m^3
c_0 (sound speed in water)	1500 m/s
h_1 (steel plate thickness)	5.08 cm
ρ_1 (steel density)	7800 kg/m^3
c_{T1} (shear wave speed in steel)	3100 m/s
c_{L1} (longitudinal wave speed in steel)	5790 m/s
η_{T1} (shear loss factor of steel)	0.005
η_{L1} (longitudinal loss factor of steel)	0.001
h_2 (coating thickness)	7.62 cm (Figure 2.20), 2.54 cm (Figure 2.21)
ρ_2 (coating density)	600 kg/m^3
c_{T2} (shear wave speed in coating)	50 m/s
c_{L2} (longitudinal wave speed in coating)	500 m/s
η_{T2} (shear loss factor of coating)	0.3
η_{L2} (longitudinal loss factor of coating)	0.05

The excitation in the model of Ko is a line force acting on the base structure. In addition, it is necessary to define the plate dimensions in VIBRO3D. The plate dimensions used are $a = b = 1$ m and the excitation in VIBRO3D is a point force located at $x = 0.0375$ m, $y = 0.0792$ m from a corner of the plate). The indicator used by Ko is the noise reduction (Ko 1997, equation 49), defined by :

$$NR = 10\log_{10}\left[\frac{Q_b(\omega)}{Q_0(\omega)}\right], \tag{2.5}$$

where $Q_b(\omega)$ represents the acoustic pressure at a point in contact with the free surface of the decoupling layer and $Q_0(\omega)$ is the acoustic pressure at the same location in the absence of a decoupling layer (to be coherent with the indicators defined in VIBRO3D, *-NR* was used in the following comparisons). This ratio is compared to the mean square velocity ratio and to the insertion loss calculated with VIBRO3D. The mean square velocity ratio is defined by:

$$V_R = 10\log_{10}\left(\frac{\langle V_1^2\rangle}{\langle V_2^2\rangle}\right), \tag{2.6}$$

where $\langle V_1^2\rangle$ and $\langle V_2^2\rangle$ are the mean square velocity of the base plate with coating and the mean square velocity of the outer surface of the coating respectively. The definition of the insertion loss is :

$$IL = 10\log_{10}\left(\frac{W_{without}}{W_{with}}\right), \tag{2.7}$$

where $W_{without}$ is the sound power of the plate without coating and W_{with} is the sound power with the coating.

Figure 2.20 and Figure 2.21 show that the mean square velocity ratio calculated with the 3D model gives results closer to Ko's results than the insertion loss. The reason is that the base plate considered by Ko is very thick (5.08 cm) and therefore has a very low modal density when dimensions $a = b = 1$m are used (about only 15 modes between 0 and 5000 Hz). The ratio of the radiated sound power without decoupling treatment to the sound power with a decoupling treatment (*IL*) has very strong variations with the frequency (due to mode shifts with and without the coating). The insertion loss was therefore plotted in 1/3 octave band to smooth out these variations. It should be noted that the *IL* takes negative values at some frequencies (corresponding to more sound radiation with the coating than without the coating), but again this phenomenon is directly related to mode shifts when the coating is added, and is not intrinsic to the coating material; the noise reduction for an infinite plate and the mean square velocity ratio do not take such negative values.

The following section presents the relation between the mean square velocity ratio and the insertion loss, and justifies the use of the mean square velocity ratio as a valuable indicator to be compared to the noise reduction of Ko. As already noted (DREA report CR/96/427 and Foin *et al* 1998), the mean square

velocity ratio is an interesting decoupling indicator because it is approximately independent of the plate dimensions and is a smooth, non-modal indicator (with the exception of coating thickness modes). It is thus of interest to compare the mean square velocity ratio for a finite plate to the noise reduction for an infinite plate.

The relation between the mean square velocity and the radiated sound power is :

$$W = \rho_0 c_0 ab \left\langle V^2 \right\rangle \sigma , \tag{2.8}$$

where W is the radiated sound power, ρ_0 and c_0 are respectively the density and the sound speed in the fluid, a and b are the plate dimensions, $\langle V^2 \rangle$ is the mean square velocity and σ is the radiation efficiency. Assuming that the radiation efficiency is unchanged when the coating is added (this assumption was verified in the DREA report CR/96/427, p. 42-44), the insertion loss (equation 2.7) can be written :

$$IL = 10 \log_{10} \left(\frac{\left\langle V^2_{without} \right\rangle}{\left\langle V^2_{with} \right\rangle} \right), \tag{2.9}$$

where $\langle V^2_{without} \rangle$ and $\langle V^2_{with} \rangle$ are the mean square velocity of the bare plate and the mean square velocity of the outer surface of the coating, respectively ($\langle V^2_{with} \rangle$ in equation 2.9 is similar to $\langle V_2^2 \rangle$ in equation 2.6). Thus, the mean square velocity ratio is almost equal to the insertion loss except that $\langle V^2_{without} \rangle$ is replaced by $\langle V_1^2 \rangle$. It can be concluded that the difference between the insertion loss and the mean square velocity ratio is the difference between the mean square velocity of the base plate without coating and the mean square velocity of the base plate with coating. A previous DREA report (CR/96/427, p. 38), showed that the vibration behaviour of the base plate when covered by a coating is comprised between two limiting cases of the uncoated base plate in water, and the uncoated base plate *in-vacuo*. For a soft coating, the results are closer to the uncoated base plate *in-vacuo*, whereas for a stiff coating, the results are closer to the uncoated base plate in water. The vibration level of the *in-vacuo* plate being larger than the vibration level of a plate in water, the mean square velocity ratio overestimates the insertion loss when soft coatings are considered and it is approximately equal to the insertion loss when stiff coatings are considered.

The cases presented in Figure 2.20 and Figure 2.21 effectively show that the mean square velocity ratio overestimates the noise reduction indicator of Ko (except in low frequency and around the coating mode on the Figure 2.21).

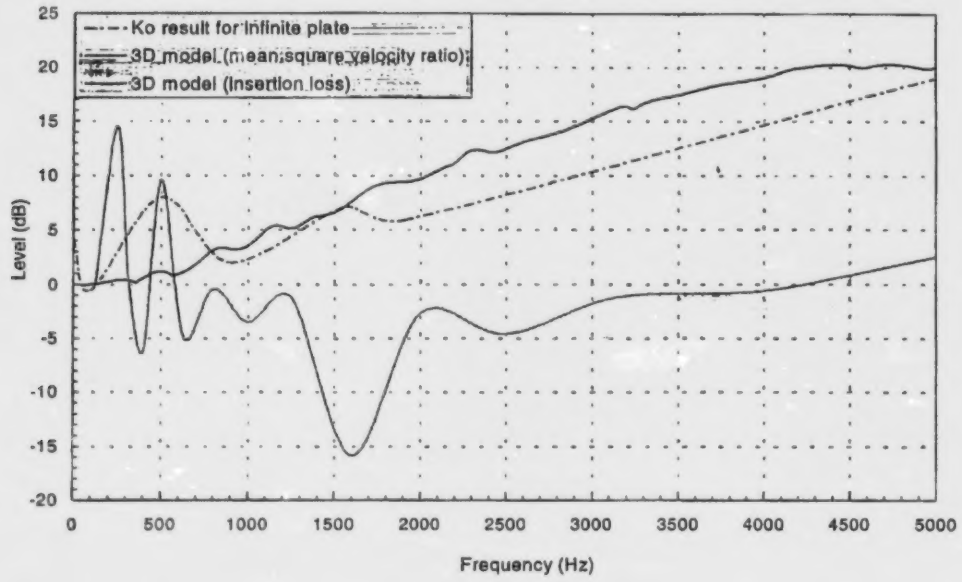

Figure 2.20 : Comparison of the noise reduction calculated by Ko (1997), and the mean square velocity ratio and the insertion loss calculated by VIBRO3D (coating thickness : $h_2 = 7.62$ cm).

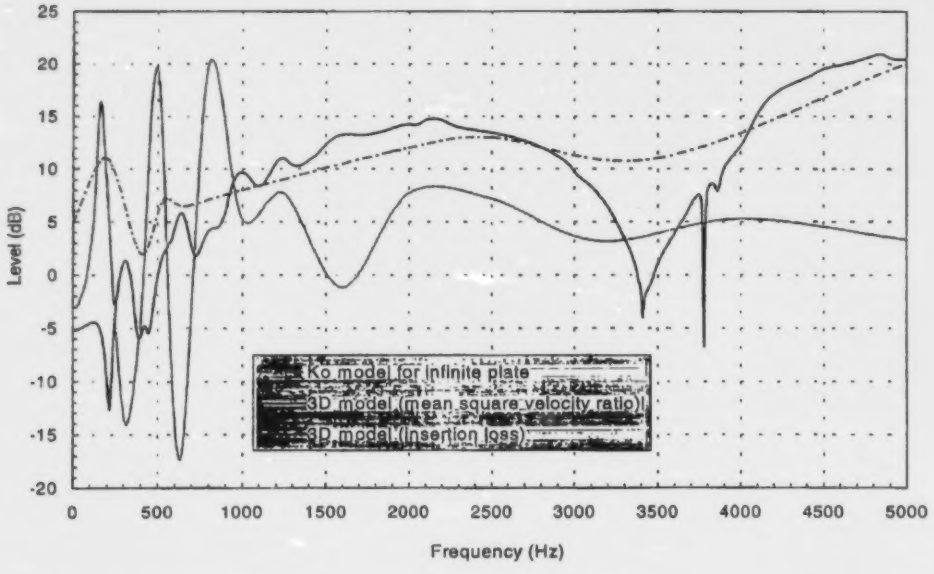

Figure 2.21 : Comparison of the noise reduction calculated by Ko (1997), and the mean square velocity ratio and the insertion loss calculated by VIBRO3D (coating thickness : $h_2 = 2.54$ cm).

2.5 Comparison between the model of House and VIBRO3D

House (1991) developed a very simple model to describe the sound radiation of an infinite base structure immersed in air on one side and covered by a decoupling coating which radiates sound in water on the other side. The excitation in his model is a normal acoustic plane wave acting on the base structure (air side). Each component (i.e. the base plate and the coating) are described by an equivalent fluid model and is characterised by its density and wave velocity. House calculated the transmission loss of this system, defined by :

$$TL = 10\log_{10}\left(\frac{A_1}{A_4}\right), \tag{2.10}$$

where A_1 is the magnitude of the incident plane wave and A_4 is the magnitude of the transmitted wave in water. House gives the following expression of the transmission loss :

$$\begin{aligned} TL_4 = 20\log_{10}\Bigg[\Bigg[&\cos(k_2 l_2)\cos(k_3 l_3)\left(1+\frac{z_1}{z_4}\right) - \sin(k_2 l_2)\sin(k_3 l_3)\left(\frac{z_2}{z_3}+\frac{z_1 z_3}{z_2 z_4}\right) \\ &+ j\cos(k_2 l_2)\sin(k_3 l_3)\left(\frac{z_1}{z_3}+\frac{z_3}{z_4}\right) + j\sin(k_2 l_2)\cos(k_3 l_3)\left(\frac{z_1}{z_2}+\frac{z_2}{z_4}\right)\Bigg]\Bigg] \end{aligned} \tag{2.11}$$

The notations of House are used in equation 2.11 and throughout this section. Subscripts 1, 2, 3 and 4 are devoted to air, the base structure, the coating and water, respectively. Also, z_i is the acoustic impedance ($z_i = \rho_i c_i$) of the medium i (i = 1,...4), ρ_i is the density, c_i is the wave velocity, k_i is the acoustic wavenumber $k_i = \omega / c_i$, l_2 and l_3 are the thicknesses of the base plate and the coating respectively. The indicator used by House to express the decoupling effect is the insertion loss defined by the difference between the transmission loss without coating and the transmission loss with the coating :

$$IL = TL_3 - TL_4, \tag{2.12}$$

where TL_3 is the transmission loss without coating (it can be obtained from equation 2.11 by taking l_3 =0).

Figure 2.22, Figure 2.23 and Figure 2.24 show comparisons between the model of House and VIBRO3D. The base plate is described in Table 2.1 (page 28) (h_2 = 0.009 m, c_2 = 6000 m/s, ρ_2 = 7850 kg/m^3). The decoupling layer has a thickness of 0.01 m, with ν_3 = 0.45, ρ_3 = 100 kg/m^3 , η_3 = 0.01. In Figure 2.22 and Figure 2.23 the Young's modulus of the coating is $E_3 = 10^5$ Pa (c_3 = 61.6 m/s) and in Figure 2.24, $E_3 = 10^3$ Pa (c_3 = 6.16 m/s). The parameters for air and water are : c_1 = 340 m/s, ρ_1 = 1.2

kg/m^3 and c_4 = 1460 m/s, ρ_4 = 1000 kg/m^3 , respectively. In Figure 2.22 and Figure 2.24, the excitation is a normal acoustic plane wave propagating on the air side of the system while in Figure 2.23 the excitation is a point force located at $x = y = 0.06$ m from a corner of the plate.

The first dip in the model of House and in the insertion loss curve of VIBRO3D corresponds to the mass-spring mode of the base structure / coating system. If the base plate is approximated by a lumped mass (with surface mass $\rho_2 h_2$) and the coating by a spring (characterised by a surface stiffness L_3 / h_3), the natural frequency of the mass-spring mode is given by the following formula :

$$F_r = \frac{1}{2\pi}\sqrt{\frac{L_3}{\rho_2 h_2 h_3}}, \tag{2.13}$$

where L_3 is the plate modulus of the coating (expressed in terms of Lamé constant by : $L_3 = \lambda_3 + \mu_3$). In the case of Figure 2.22, equation 2.13 gives a value of 116 Hz, whereas the dip in the model of House is found to be around 120 Hz. Figure 2.22 obviously shows that **VIBRO3D accurately predicts the first dip observed in the model of House**. Figure 2.23 (point force excitation) shows that the model of House is still in good agreement with VIBRO3D even if the excitation is not a normal plane wave. However it should be kept in mind that in theory, the model of House applies only to normal acoustic plane wave excitation.

All subsequent dips observed in the model of House correspond to coating modes, i.e., standing waves in the thickness of the coating. Figure 2.24 shows that the model of House gives results in good agreement with the 3D model. It is noted that the 1/3 octave band results do not reveal the coating modes because the frequency bands of integration are too large.

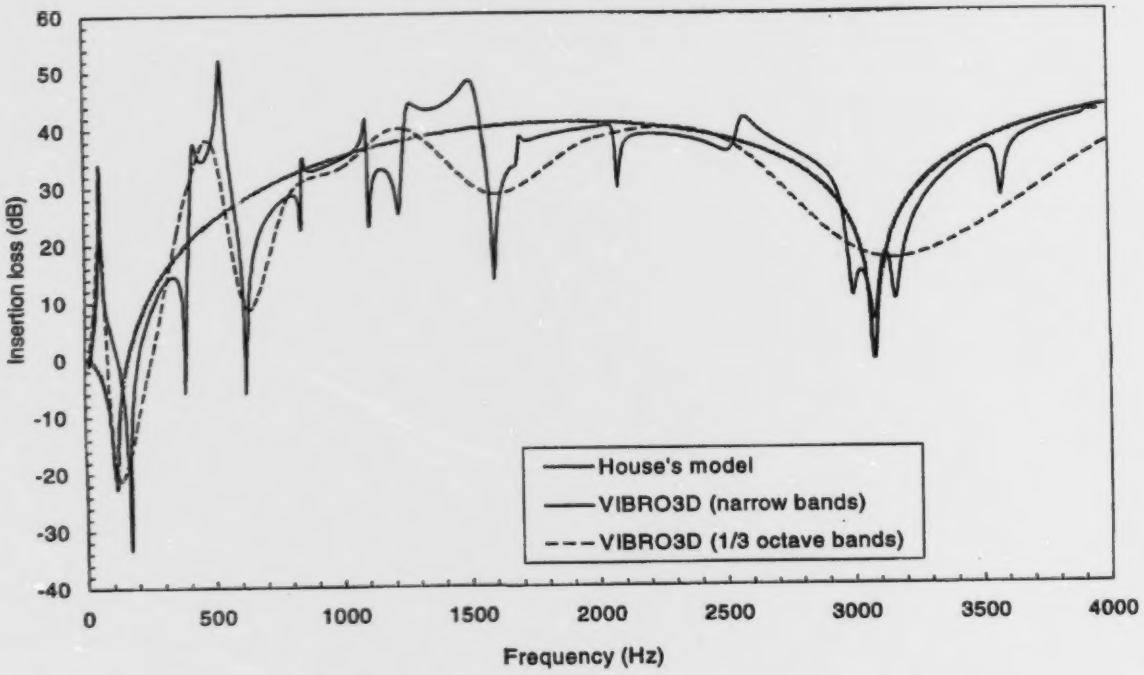

Figure 2.22 : Comparison of the insertion loss obtained by the model of House and by VIBRO3D (excitation : normal plane wave, coating Young's modulus : $E_3 = 10^5$ Pa, coating wave velocity : $c_3 = 61.6$ m/s).

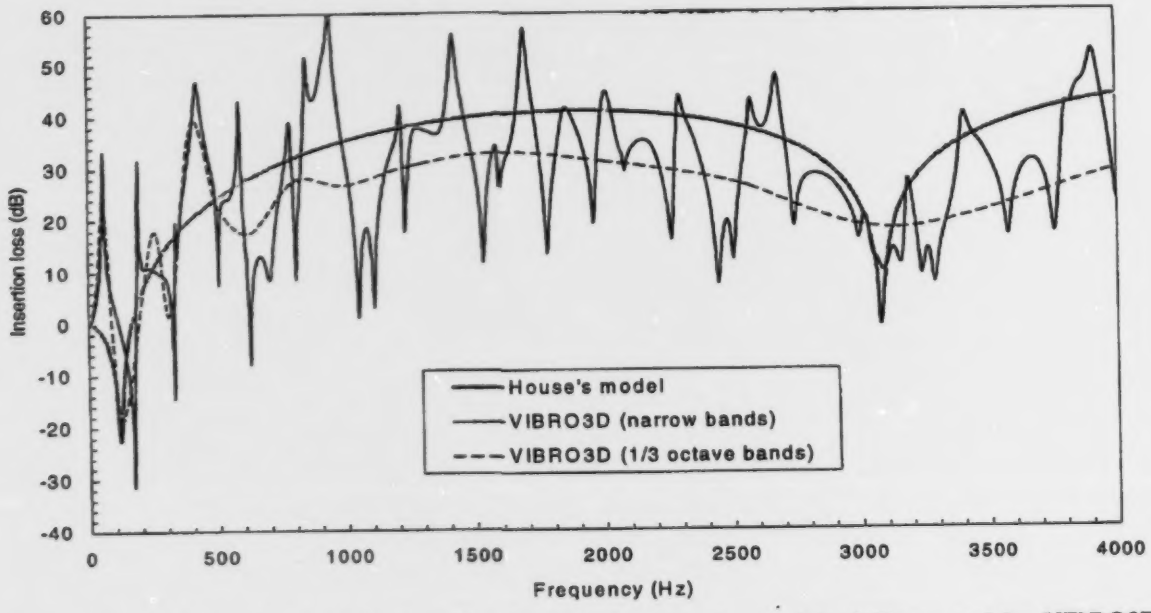

Figure 2.23 : Comparison of the insertion loss obtained by the model of House and by VIBRO3D (excitation : point force, coating Young's modulus : $E_3 = 10^5$ Pa, coating wave velocity : $c_3 = 61.6$ m/s).

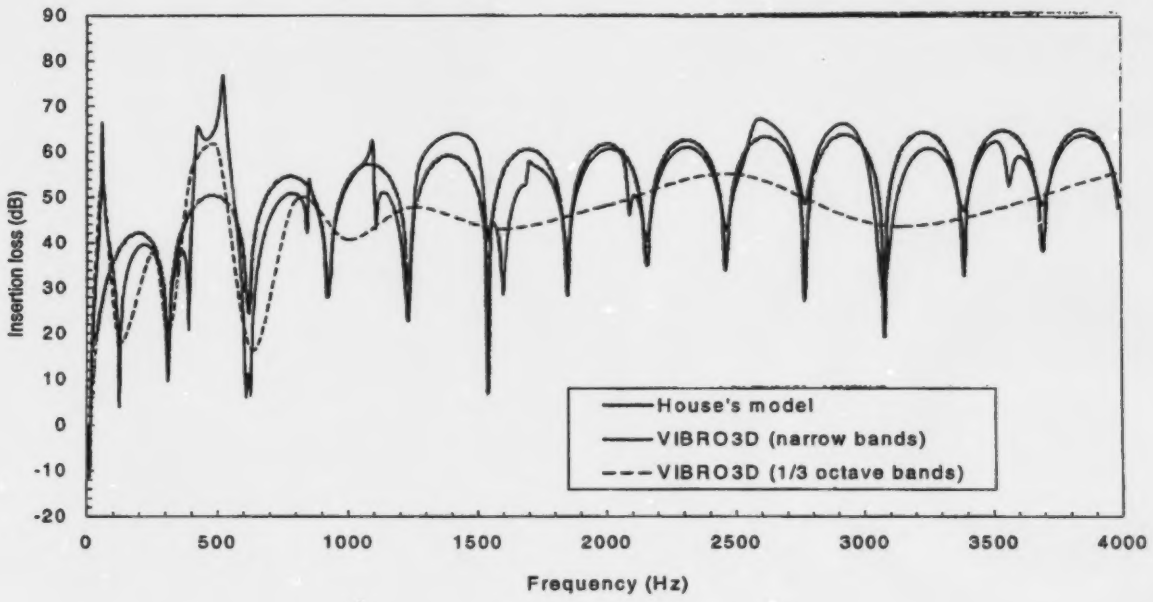

Figure 2.24 : Comparison of the insertion loss obtained by the model of House and by VIBRO3D (excitation : normal plane wave, coating Young's modulus : $E_3 = 10^3$ Pa, coating wave velocity : $c_3 = 6.16$ m/s).

2.6 *"Near-field" acoustic power*

In this section, "near-field" acoustic power calculations (see section 1.4.2) are compared to results obtained with the exact calculation of the acoustic power (equation 1.83). The "near-field" acoustic power is used to evaluate the insertion loss of the structure and it is compared to the exact calculation of the insertion loss (based on the exact sound power). The first example is a bare steel plate immersed in water (the geometry and material data are listed in Table 2.1, page 28) The excitation is a point force located at $x = y = 0.06$ m from a corner of the plate and the water characteristics are : $\rho_0 = 1000$ kg/m^3 and $c_0 = 1460$ m/s. The "near-field" power is calculated by integration over a mapping plane parallel to the plate surface and with dimensions equal to the plate. Figure 2.25 shows comparisons between the exact sound power and the "near-field" power for various distances d between the plate and mapping plane. When d is small (1 cm) the "near-field" power overestimates the exact sound power because the sign fluctuations of near-field active sound intensity are not taken into account in the "near-field" power calculation. On the other hand, the sign fluctuations in the sound intensity tend to decrease at increasing distances from the radiator, such that integrating the active sound intensity or integrating the absolute value of the active sound intensity should be equivalent at increasing distances from the plate (sign

fluctuations in active intensity are generally noticeable at distances up to half an acoustic wavelength from the radiator). However the results of Figure 2.25 show that when d increases the "near-field" power decreases and eventually becomes smaller than the exact sound power. This is due to the limited aperture of the mapping plane as d increases.

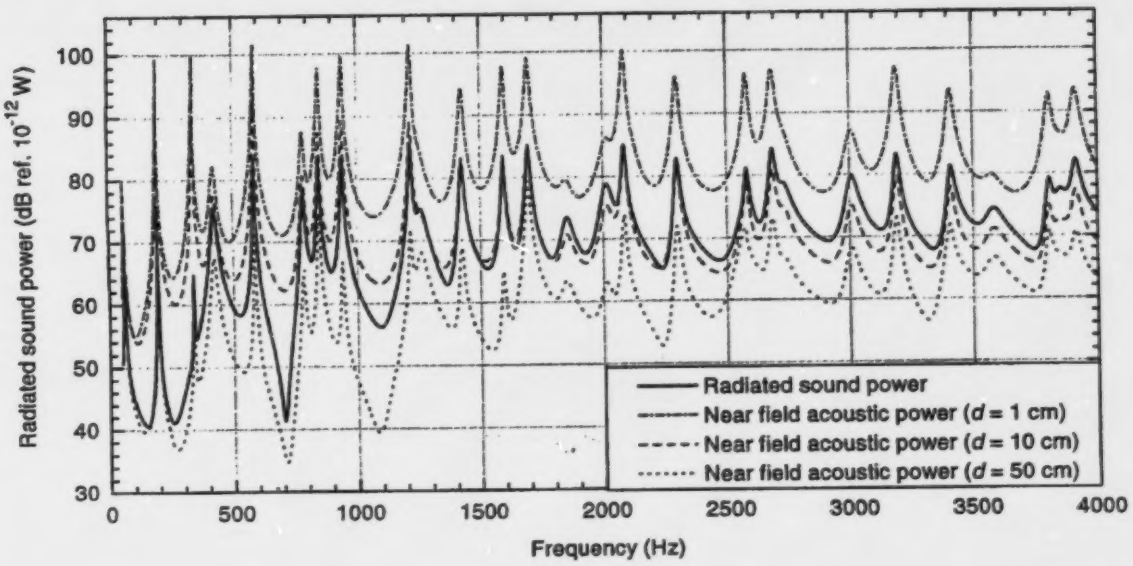

Figure 2.25 : Comparison between the radiated sound power and the "near-field" acoustic power for a steel base plate (d is the distance between the plate and the mapping plane).

The second example is the same steel plate of Figure 2.25 (with the acoustic medium and excitation), covered by a decoupling coating (its characteristics are listed in Table 2.4, page 41). Figure 2.26 shows comparisons between the exact sound power and the "near-field" sound power for this example. The same observations as in Figure 2.25 can be made on this figure.

Figure 2.27 shows the insertion loss calculated with the exact sound power and with the "near-field" sound power (the results are presented in 1/3 octave band). These results are relative to the base plate and coating of Figure 2.25 and Figure 2.26. The insertion loss calculated from the "near-field" power is defined by:

$$IL = 10\log_{10}\left(\frac{N_{F0}}{N_F}\right), \tag{2.14}$$

where N_{F0} is the "near-field" power calculated at a distance d for the base plate alone and N_F is the "near-field" power calculated at the same distance for the plate / coating system. Figure 2.27 shows that the

insertion loss calculated from the "near-field" power gives results very similar when compared to the exact calculation of the insertion loss. Therefore, the "near-field" sound power seems to be a valuable indicator to estimate the insertion loss of a plate-coating system, even though it is not an appropriate indicator of the sound power radiated by the system.

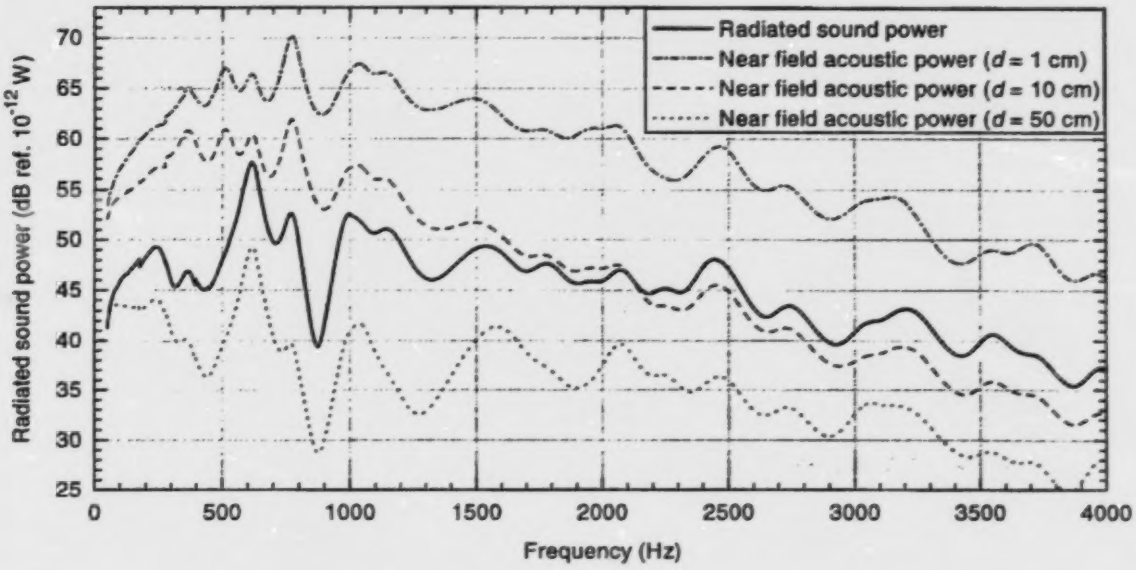

Figure 2.26 : Comparison between the radiated sound power and the near field power for a steel base plate covered by a decoupling coating (*d* is the distance between the plate and the mapping plane).

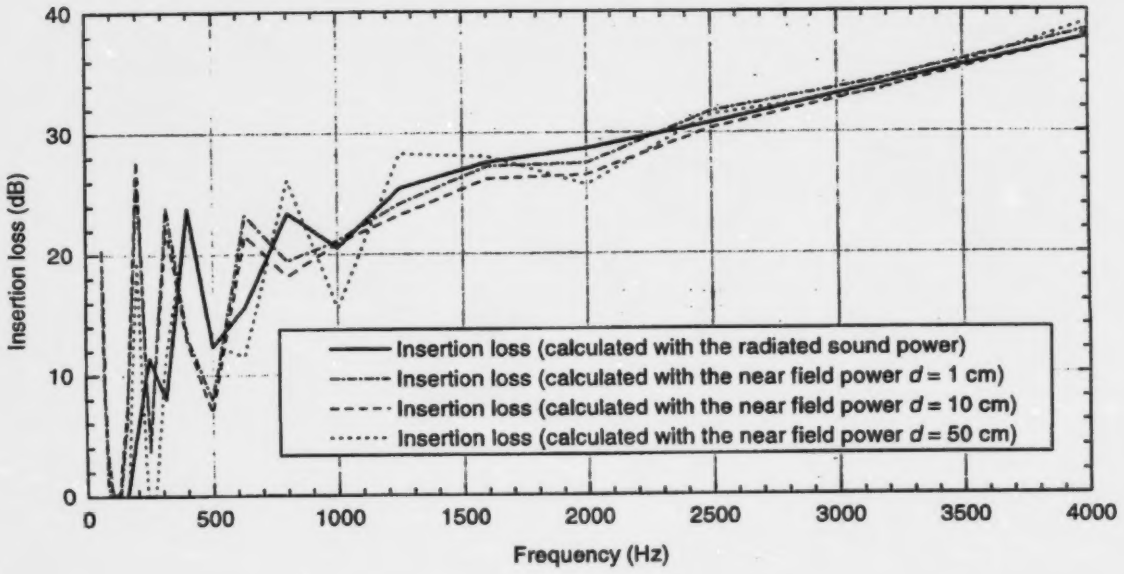

Figure 2.27 : Comparison of the insertion loss calculated from the exact sound power and from the "near-field" sound power.

3 Partial coverage for decoupling coating

In this section the partial coverage of a base structure by a decoupling coating is investigated. For many reasons it is possible that the coating only covers a part of the ship hull, hence it is interesting to study the influence of such partial coating on the global noise reduction. The case of a base structure partially covered by a coating and immersed in water is really too complex to be solved by an exact analytical model. Thus, an approximate method was used to evaluate the effect of partial coverage on the noise reduction. An "hybrid method" implemented in a computer code called "HYMNE (Foin 1999) was developed. The following section briefly explains the theoretical background and the interest of this method.

3.1 Presentation of the hybrid method

The goal of the hybrid method is to predict the sound power radiated by a complex structure from its measured displacement field (Figure 3.shows the method schematically). This method is devoted to structures with a complex vibration response that cannot be accurately evaluated by analytical methods. The first step of the method is to measure the displacement field of the structure. This can be done using accelerometers or a laser vibrometer at several locations on the structure. Frequency response functions (FRF) are measured between the displacement of a point on the mesh of the structure and a reference accelerometer (or force transducer in case of a point force excitation). The measured FRFs are then read by a computer code called "HYMNE" that evaluates the radiated sound power of the measured structure. The radiated sound power is calculated with the integral formulation. In this method there is no available information of the mechanical or acoustic behaviour of the structure outside the measured section, hence,

for the calculation of the sound power, it is necessary to make some assumptions regarding the areas outside the measured section. In the hybrid method two hypotheses are considered to take into account the areas outside the measured surface : (1) the case where the structure is inserted into an infinite rigid baffled, and (2) the case where it is unbaffled (i.e. the measured area is surrounded by the acoustic medium). In this document we only consider the case where the structure is inserted in an infinite rigid baffle because it is more realistic for a ship hull.

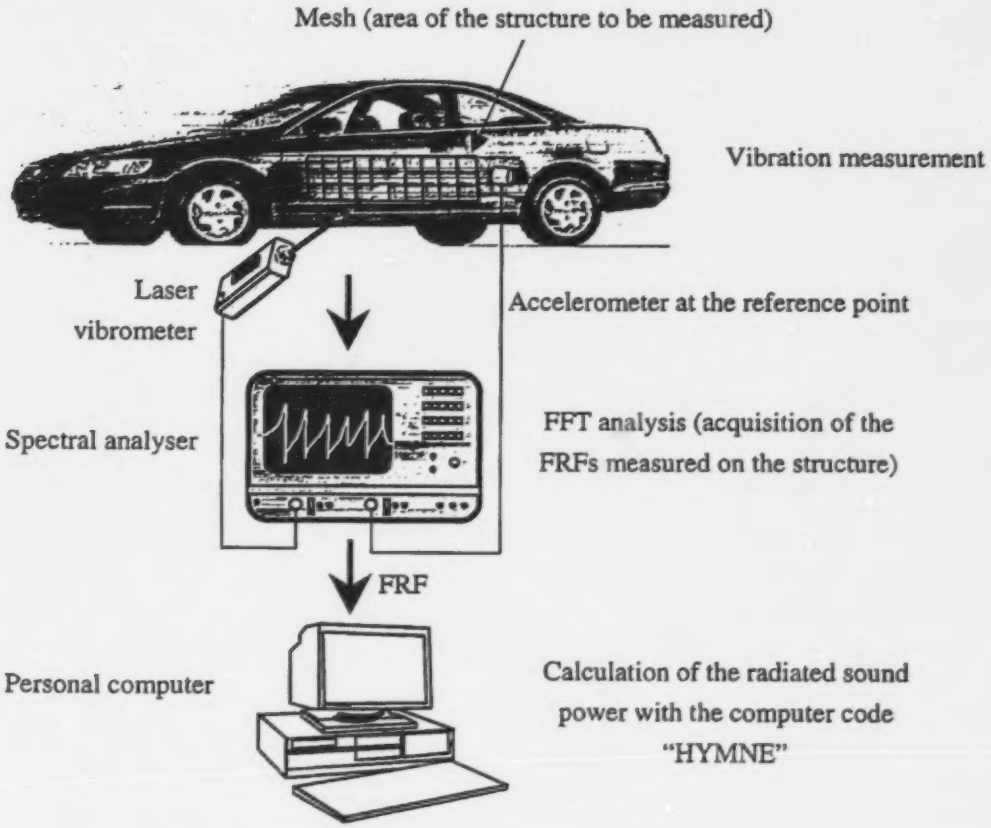

Figure 3.1 : Presentation of the hybrid method. In this document the measurement of the FRF is replaced by calculation with the modified version of VIBRO3D.

3.2 Partial coating with the hybrid method

In the present situation, the hybrid method is based on some analytical approximations of the surface vibration instead of measurements. The approximate method to evaluate the vibration behaviour of a

partially covered plate is as follows: The vibration response of three different plates with or without coating is calculated and these plates are then assembled to form only one structure (Figure 3.2); it is assumed that the three plates are simply supported on their boundaries. The global structure is thus composed of three plates which can be covered or not by a decoupling coating. A computer code was developed to calculate the FRFs on the meshing of the plate: this code calls VIBRO3D to compute the necessary information. The excitation being a point force, each FRF is the ratio of the displacement of a point on the structure to the input force :

$$\begin{cases} FRF(\omega) = \dfrac{u_z(x, y, -h_2, \omega)}{F(\omega)} & \text{when a coating is added} \\ FRF(\omega) = \dfrac{w(x, y, \omega)}{F(\omega)} & \text{for a bare plate} \end{cases} \tag{3.15}$$

where $u_z(x,y,-h_2,\omega)$ is the displacement at the surface of the coating and $w(x,y,\omega)$ is the displacement of the base plate and $F(\omega)$ is the force exerted on the base structure.

In the following numerical results, a 10 by 10 meshing is used for each plate so that there are 280 points for the whole structure (20 points are shared by 2 adjacent plates). Each plate was excited by a point force located at $x = y = 0.06$ m from the lower-left corner of each plate (Figure 3.2).

The three plates in these tests have different dimensions in order to avoid mode coincidences between the various sub-plates. Figure 3.3 shows the 8 possible cases of partial coating coverage for a 3-plates assembly.

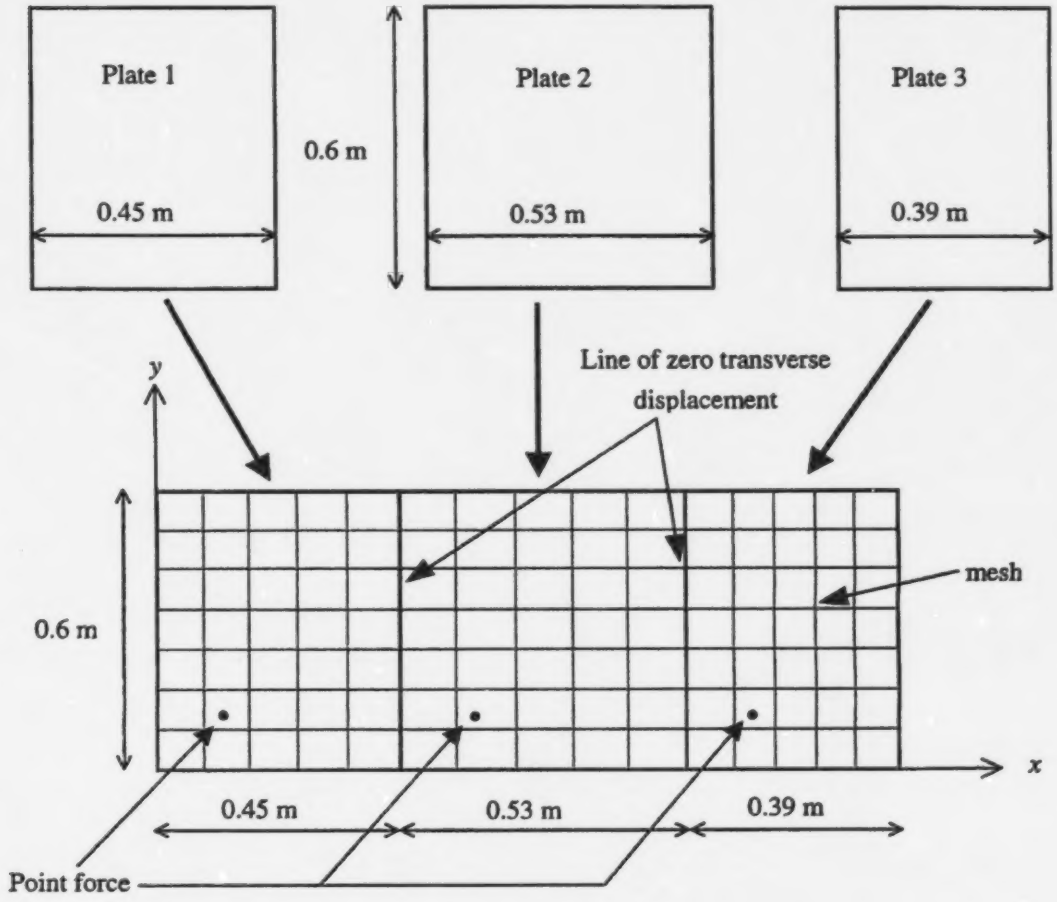

Figure 3.2 : Presentation of the assembly of the three simply supported plates to form a unique structure (in the calculation a 10 by 10 mesh is used for each plate). In this assembly the boundary conditions of each plate are simply supported.

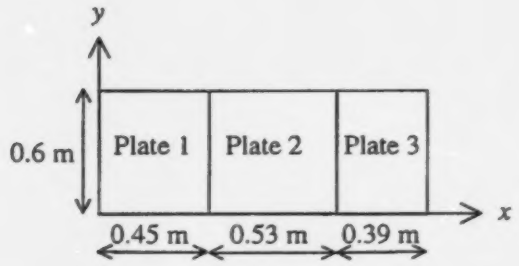

Case 1 : uncovered plate

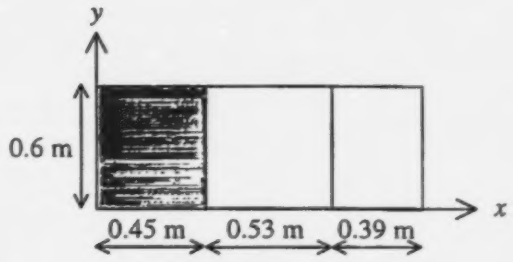

Case 2

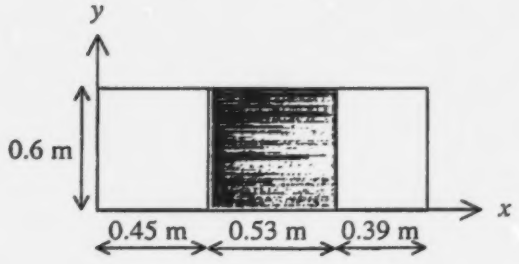

Case 3

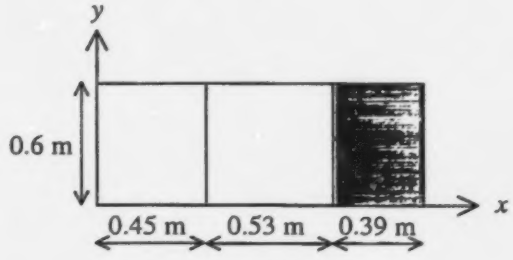

Case 4

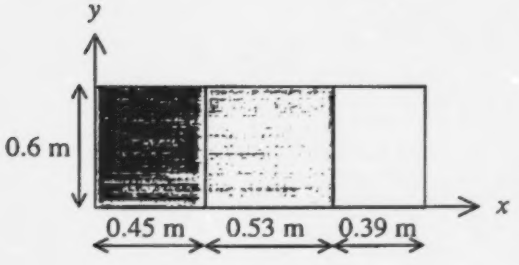

Case 5

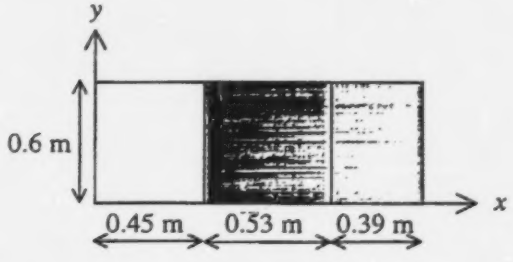

Case 6

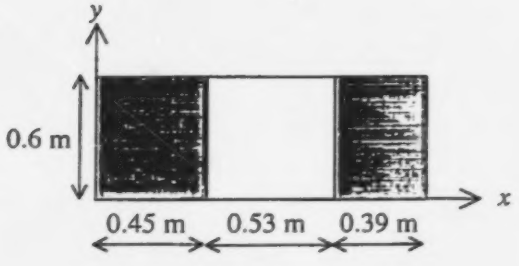

Case 7

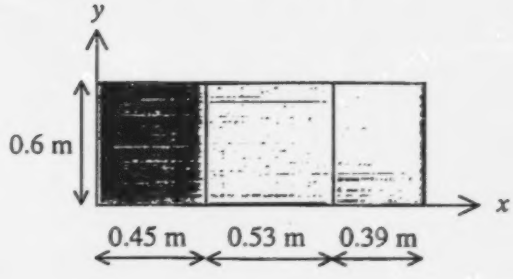

Case 8 (full coverage)

Figure 3.3 : The possible configurations for the partial coverage study (the grey area represents the structure covered by the coating).

3.3 Validation of the hybrid method

In this section results given by the hybrid method are compared to the direct results calculated by VIBRO3D. In order to perform such a comparison the FRFs (ratio of the displacement of a point on the structure to the input force) have to be calculated by the modified version of VIBRO3D and read by HYMNE. In the case of a single plate both VIBRO3D and HYMNE can evaluate the radiated sound in an exact manner. This comparison is possible only for a steel bare plate or a plate with full coating coverage.

Two cases are considered in the present test : (1) the case of a steel plate immersed in water, and (2) the case of a steel plate covered by a decoupling coating and immersed in water. The characteristics of the steel plate are given in Table 2.1 (page 28) except that the dimensions of the plate are : $a = 0.53$ m and $b = 0.6$ m. This base plate is used for both cases 1 and 2. The coating characteristics are given in Table 3.1. The excitation is a point force applied at $x = y = 0.06$ m. The surrounding fluid is water ($\rho_0 = 1000$ kg/m^3, $c_0 = 1460$ m/s).

Figure 3.4 presents the comparison between VIBRO3D and HYMNE (the base plate + coating is calculated with the 3D model with compressional wave only). This figure shows that the hybrid method is able to give the tendencies of the acoustic response of a plate with or without a decoupling coating and immersed in water. The accuracy of the hybrid method strongly depends on the number of measurement points, thus, a refined mesh would probably gives more precise results (100 points calculated by VIBRO3D are used for the tests).

Table 3.1 : Characteristics of the coating used for the partial coverage study.

Thickness (mm)	Density (kg/m^3)	Young's modulus (Pa)	Loss factor	Poisson's ratio
h_2	ρ_2	E_2	η_2	ν_2
50	600	5×10^6	0.65	0.38

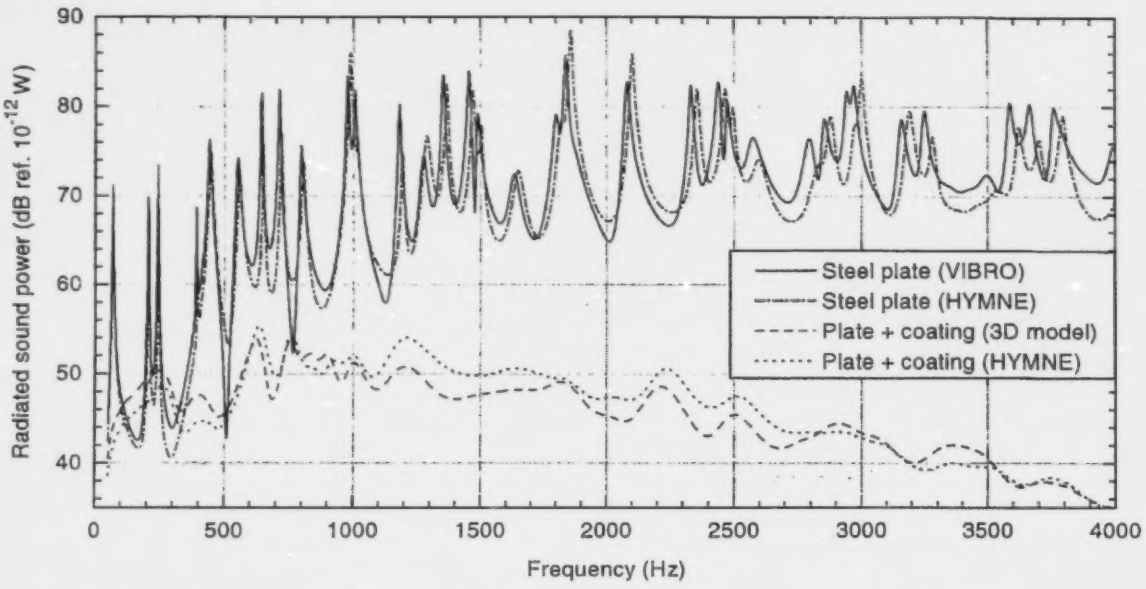
Radiated sound power (dB ref. 10^{-12} W)
Frequency (Hz)
Steel plate (VIBRO)
Steel plate (HYMNE)
Plate + coating (3D model)
Plate + coating (HYMNE)

Figure 3.4: Comparison between the direct calculation (VIBRO/VIBRO3D) and the hybrid method (HYMNE) to predict the acoustic response of a plate with or without a coating and immersed in water.

3.4 Partial coverage analysis

The 8 configurations presented in section 3.2 (Figure 3.) are computed with HYMNE, and results are analysed in this section. Case 1 represents the uncovered case, while case 8 is the full coverage case; these limiting situations serve as a comparison basis for the intermediate, partial coverage cases. The base plate characteristics are presented in Table 2.1 and the dimensions of the plate are presented in Figure 3.. The coating characteristics are listed in Table 3..

Cases 2, 3, 4 (Figure 3.5, Figure 3.6, Figure 3.7) are for a one-element coating. In these situations, adding a partial coating does not significantly reduce the total noise radiation; the decoupling material will however significantly damp the modes of the plate area on which it is applied. Partial coating of the third plate element (case 4) is the most efficient in terms of noise reduction, while partial coating of the central element (case 3) gives almost no noise reduction. Such a result can be explained by corner or edge radiation mechanisms of the structure at low frequency (see Beranek 1988 p. 290-293 and Figure 3.11); therefore, vibration reduction in the central area of the structure has almost no impact on the radiated sound.

Cases 5, 6, 7 (Figure 3.8, Figure 3.9, Figure 3.10) are for a two-element coating. Again, the main effect of partial coating in cases 5 and 6 is to damp many structural modes; however, the total noise radiation is not significantly reduced by the partial coating. Case 7 shows a much more effective noise reduction: the justification is again related to the edge and corner-mode radiation of the structure in the frequency range of interest. In low frequency (below the critical frequency), the areas mainly responsible for the noise radiated by a baffled simply-supported plate are the four corners or the edges of the plate, because there is no acoustic cancellation of the structural waves in these regions (see Figure 3.11). In case 7, the four corners are covered by a decoupling material, thus only the centre of the structure radiate noise and the acoustic cancellation ("short-circuit effect") leads to a large noise reduction.

As a conclusion, there is no simple relation between the percentage of covered area on the structure and the amount of noise reduction, and the spatial configuration of the coating has a large influence on the sound radiation. In our view, these conclusions should however apply to situations where the uncovered area is "fairly large"; in cases where the uncovered area is much smaller than the structural and acoustic wavelengths, the problem remains open. Also, it should be kept in mind that the hybrid method neglects the structural coupling between adjacent plate elements and assumes that each element is driven by an external force: these are important simplifications with respect to a real situation, and more work is needed to address these aspects.

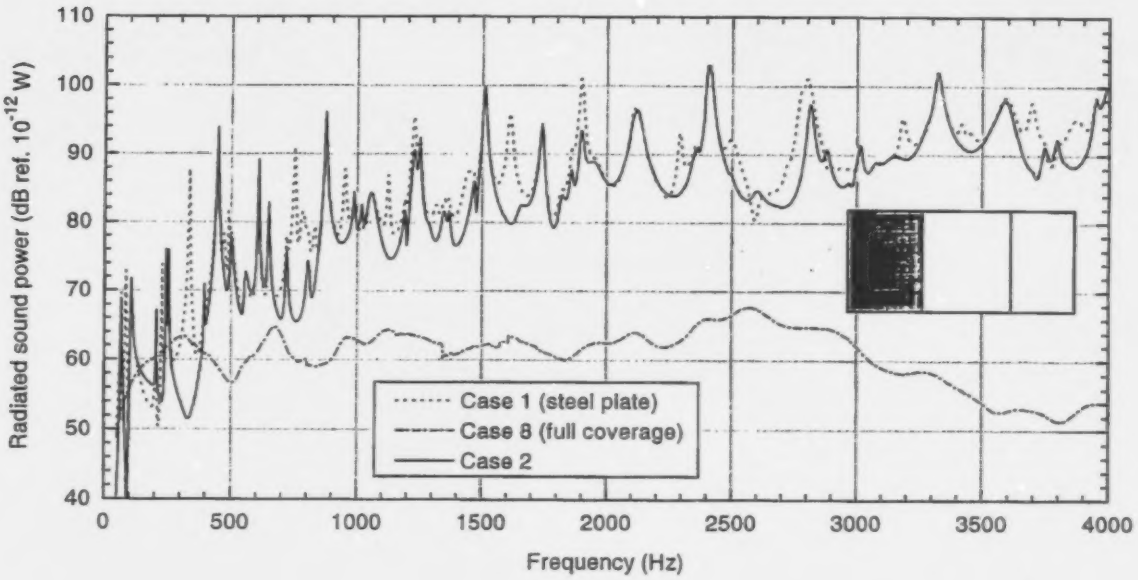

Figure 3.5 : Partial coverage study, comparison between the steel bare plate, the fully covered plate and the case 2.

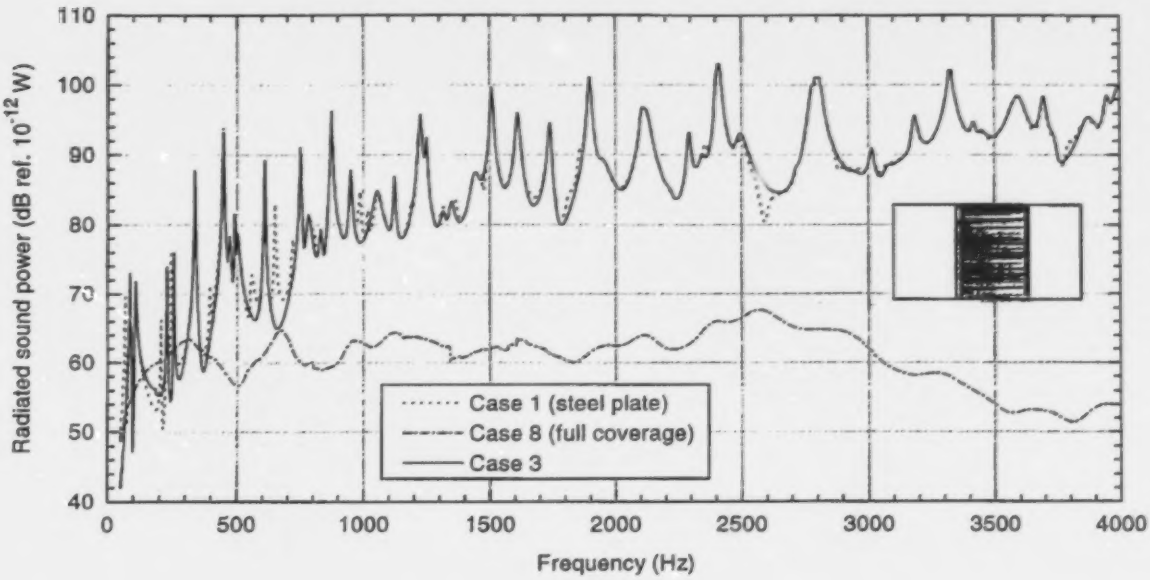

Figure 3.6 : Partial coverage study, comparison between the steel bare plate, the fully covered plate and the case 3.

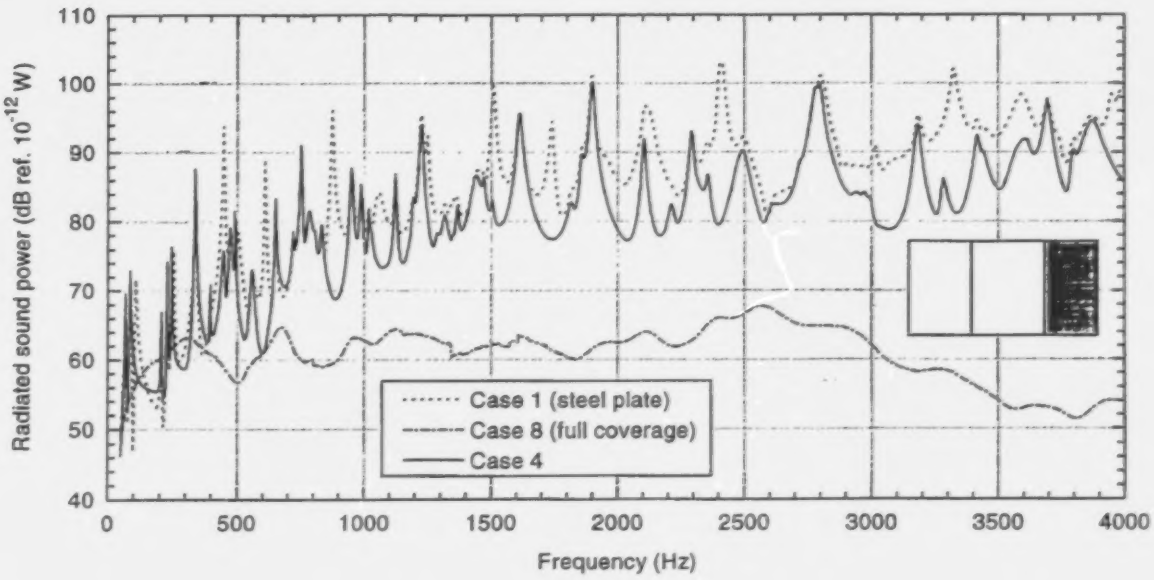

Figure 3.7 : Partial coverage study, comparison between the steel bare plate, the fully covered plate and the case 4.

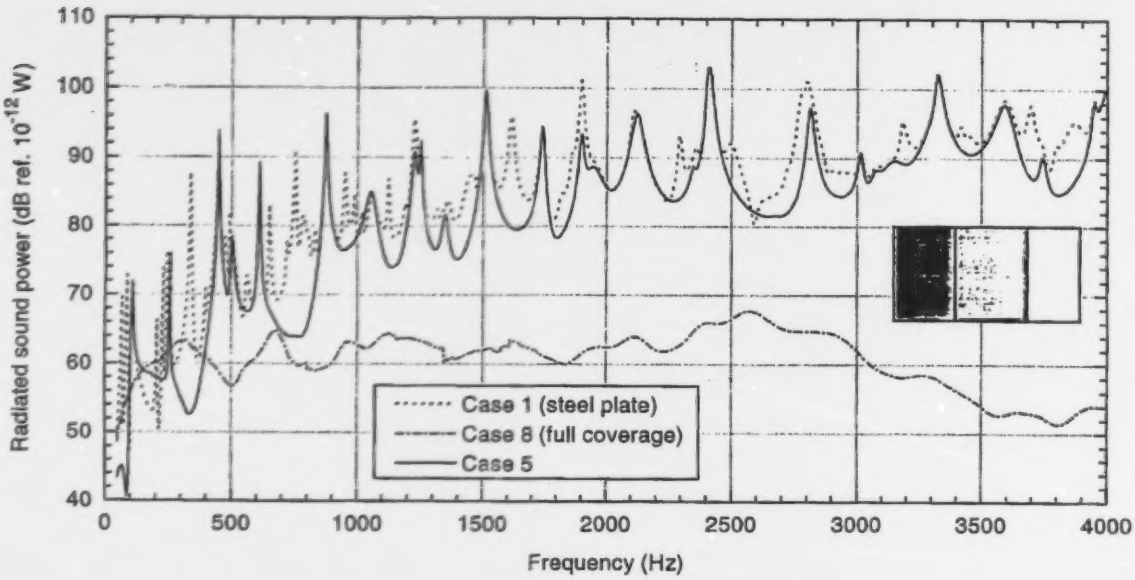

Figure 3.8 : Partial coverage study, comparison between the steel bare plate, the fully covered plate and the case 5.

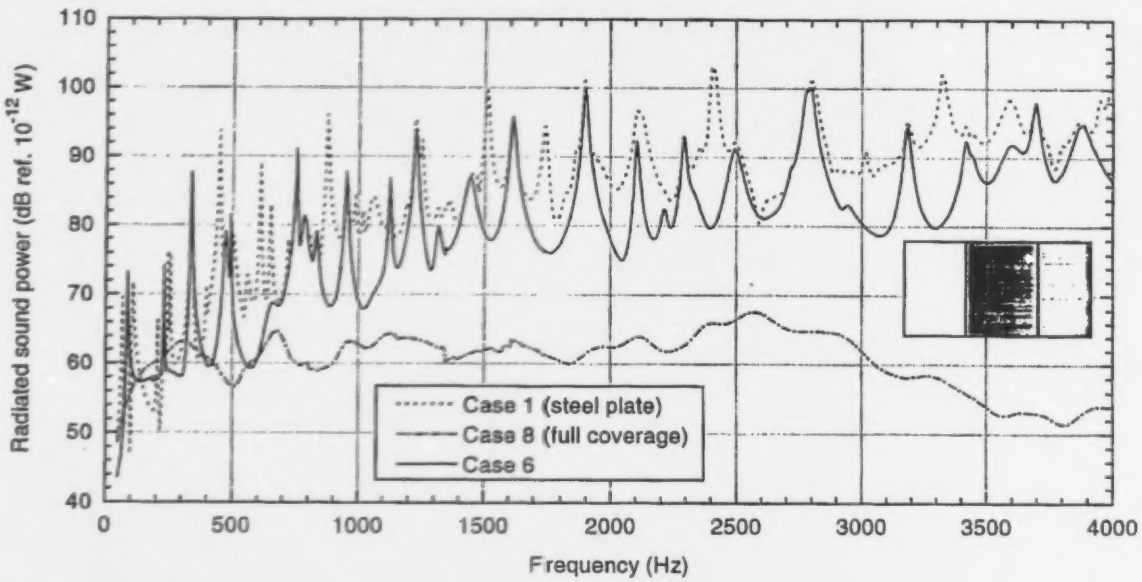

Figure 3.9 : Partial coverage study, comparison between the steel bare plate, the fully covered plate and the case 6.

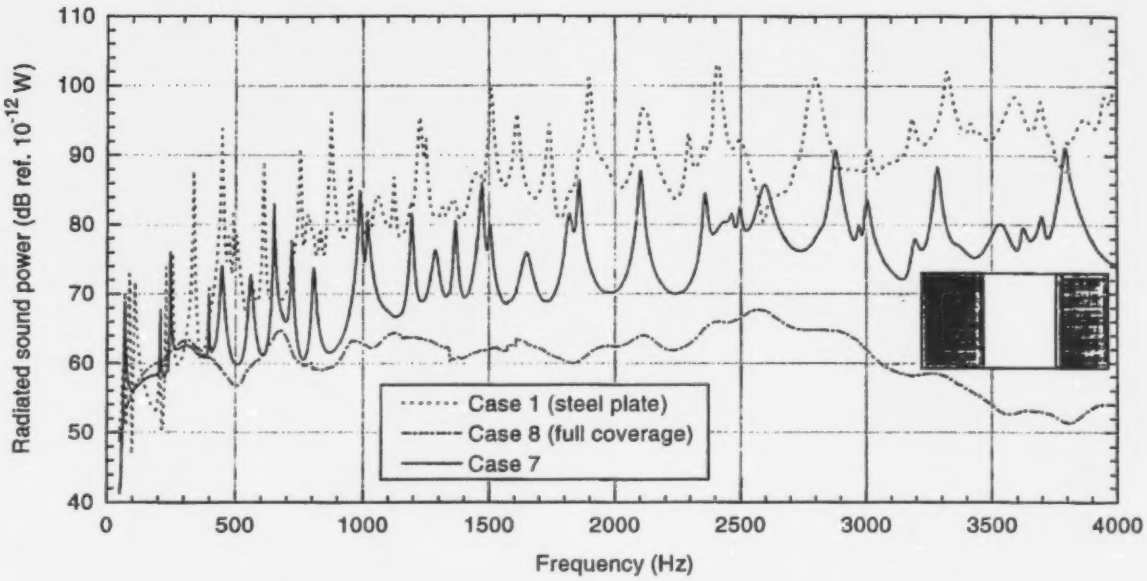

Figure 3.10 : Partial coverage study, comparison between the steel bare plate, the fully covered plate and the case 7.

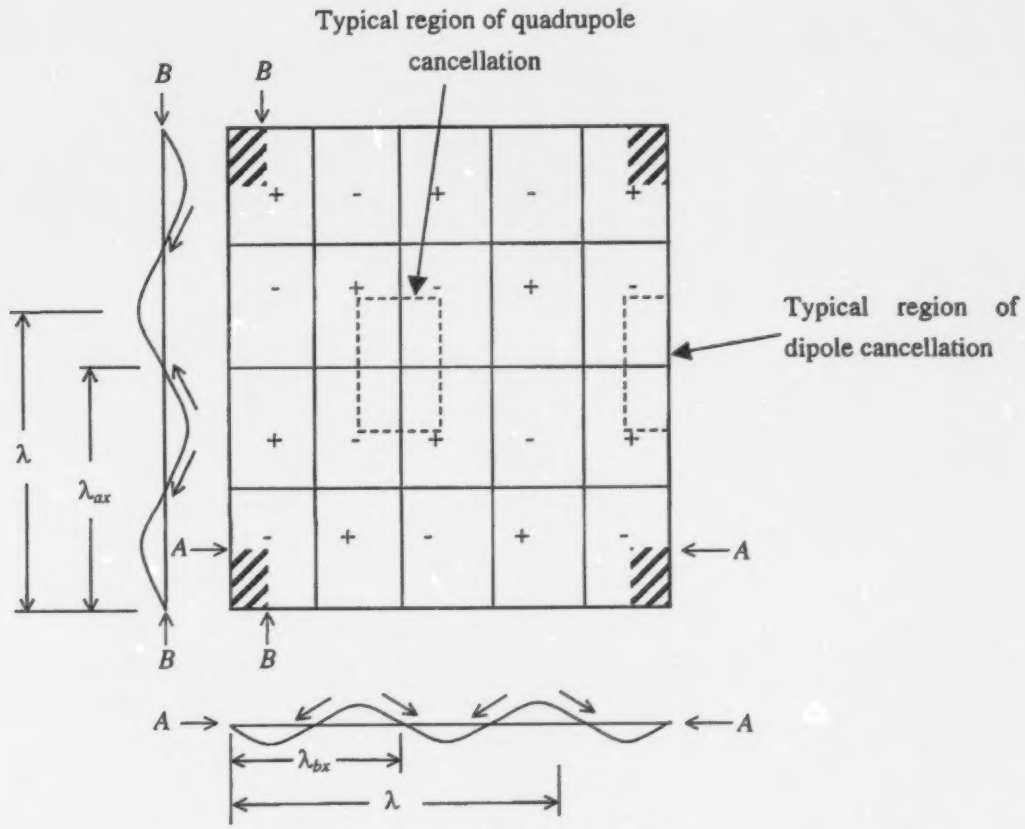

Figure 3.11 : Displacement pattern for the $m = 5$, $n = 4$ mode on a panel with simply supported edges. The relative phases of the plate regions are indicated by + and -. Arrows indicates fluid motion during the corresponding half-period of vibration. The uncancelled corner areas are widely separated compared to a wavelength in air and do not cancel each other. This mode is called a *corner mode* (from Beranek 1988, p. 291).

4 Analysis of driving point mobility

This section addresses the possibility of evaluating the mechanical properties of a coating layer by measuring the vibration response on the air side of the base structure with and without the coating layer. In effect, the presence of a coating layer modifies the response of the global system. Measuring this response under carefully controlled conditions may be useful to characterise the properties of the coating material. The global system (plate/coating/fluid) is complex and several parameters play an important role in the vibroacoustic response : the size, the thickness, the material properties and the boundary condition of the base plate, the mechanical properties of the decoupling/damping coating, the excitation, the fluid, etc... As mentioned earlier (section 2.4), when a coating is added, the response of the base plate will vary between two limiting cases: the base plate in water (for a stiff coating), and the base plate *in-vacuo* (for a soft coating). For the base plate, adding the coating is thus equivalent to (partially) removing the fluid effect. The fluid has two distinct effects on the base structure : (1) an added mass effect due to the density of the fluid and (2) a damping effect due to the sound radiation into the fluid. The added mass has the effect of shifting the modes of the system to lower frequencies, and the damping effect reduces the vibration amplitudes at resonance. When relatively soft decoupling materials are considered, the response of the base plate rapidly tends to an *in-vacuo* plate so that it is difficult to differentiate the coating characteristics by only measuring the air side of the base plate.

An example is used to illustrate the difficulty of deriving the decoupling coating characteristics by only measuring the driving point mobility on the base plate. The base plate used in the test is described in Table 2.1 (page 28), the decoupling layers are described in Table 4.1. The excitation is a point force applied at $x = 0.06$ m, $y = 0.06$ m. The fluid is water ($\rho_0 = 1000$ kg/m^3, $c_0 = 1460$ m/s). The driving point mobility is expressed by :

$$Dr = 10\log\left(\left|\frac{V_{excitation}}{F}\right|^2\right), \tag{2.16}$$

where $V_{excitation}$ is the velocity at the excitation point on the base plate and F is the force injected (in the present case the force magnitude is 1 N so that the mobility is equal to the velocity squared).

Table 4.1 : Characteristics of the decoupling coatings used for the driving point mobility tests (case 1 corresponds to the realistic material properties supplied by DREA, see section 2.3.3).

	Thickness (mm)	Density (kg/m^3)	Young's modulus (Pa)	Loss factor	Poisson's ratio
	h_2	ρ_2	E_2	η_2	ν_2
Case 1	50	600	5×10^6	0.65	0.38
Case 2	50	600	5×10^5	0.65	0.38
Case 3	50	600	5×10^4	0.65	0.38

Figure 4.1 shows the mean square velocity ratio for the three cases of the Table 4.1. It is seen that cases 1, 2, 3 correspond to increasing decoupling effectiveness.

Figure 4.2 presents the driving point mobility for the case 1, the case 3 and the case 1 when the loss factor of the decoupling coating is 0.01 instead of 0.65. Case 1 shows a very damped response due to the large loss factor of the decoupling layer and because the decoupling is not very large (when the decoupling between the base plate and the fluid is low the base plate and the coating layer have a coupled motion. In this case the coating response is damped because of its high loss factor; therefore the motion of the base plate is also damped). Case 3 shows little damping, since when the decoupling is large the base plate response tends to the *in-vacuo* base plate. The case 1 calculated with a low loss factor of the coating shows an lightly damped response which is very similar to case 3 (despite very different properties of the decoupling material). This example shows the difficulty to predict the decoupling/damping behaviour of a plate/coating/fluid system by only interpreting the driving point mobility response.

Figure 4.3 presents the driving point mobility when the velocity at *the coating surface* is used instead of the velocity on the base plate. It is expressed by :

$$Dr_{coating} = 10\log\left(\left|\frac{V_{coating}}{F}\right|^2\right), \tag{2.17}$$

where $V_{coating}$ is the velocity on the coating surface at a position corresponding to the excitation point and F is the force injected to the base plate. It is clear in Figure 4. that the velocity on the coating is much more representative of the decoupling effect due to the coating, and more sensitive to the properties of the decoupling material. It is also apparent that the velocity on the coating surface is close to the mean square velocity of the coating surface. This means that only one measurement at the driving point location on the coating surface is able to give indications on the global response at the surface of the decoupling layer.

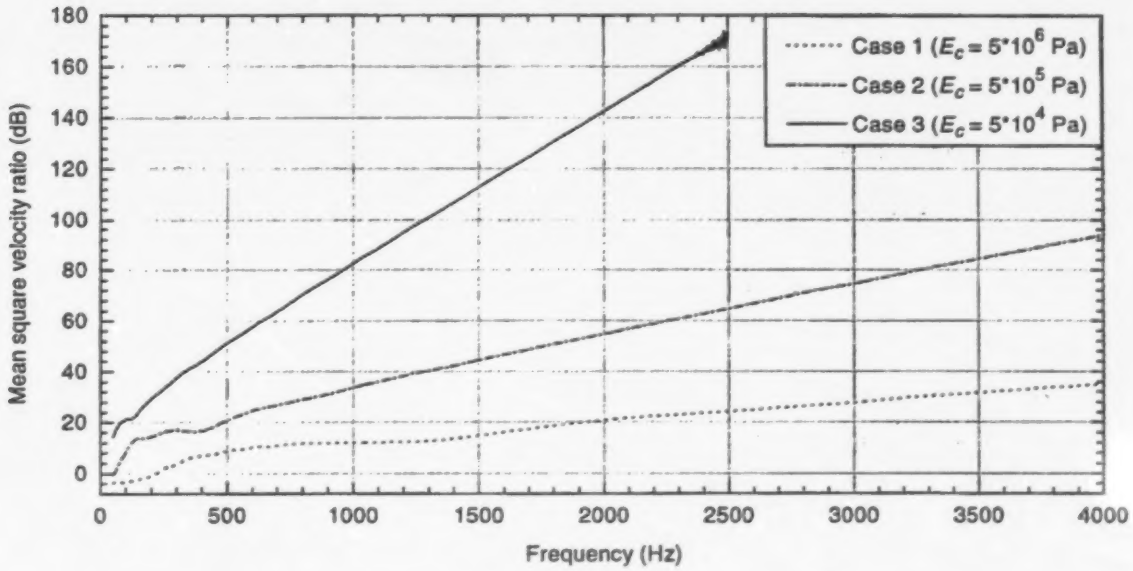

Figure 4.1 : Mean square velocity ratio for the three cases of the Table 4.1.

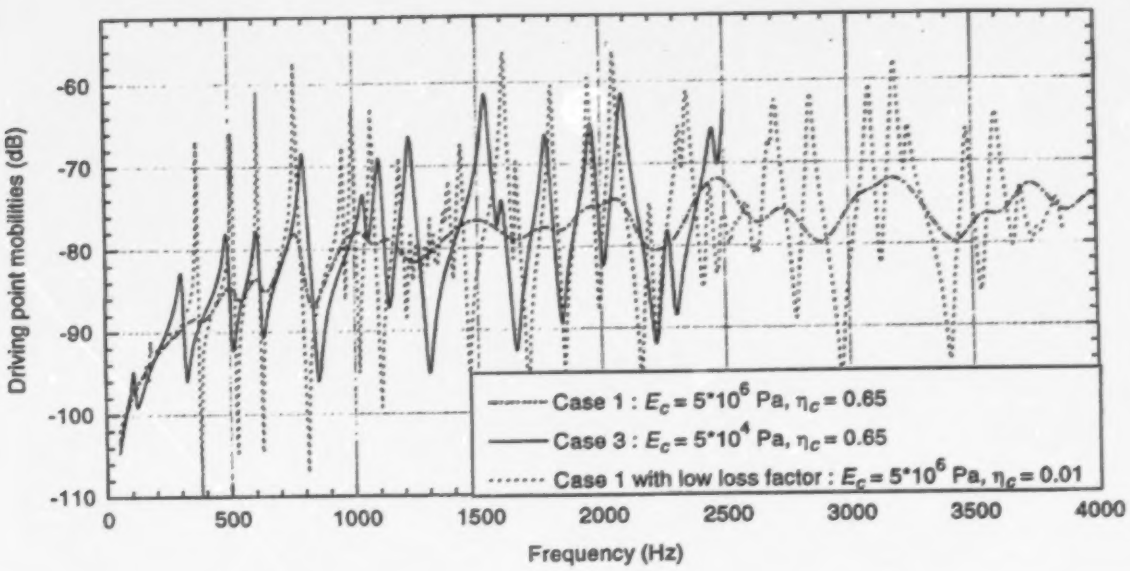

Figure 4.2 : Driving point mobility for the cases 1 and 3 of the Table 4.1, along with the case 1 with a low loss factor of the coating layer (0.01 instead of 0.65).

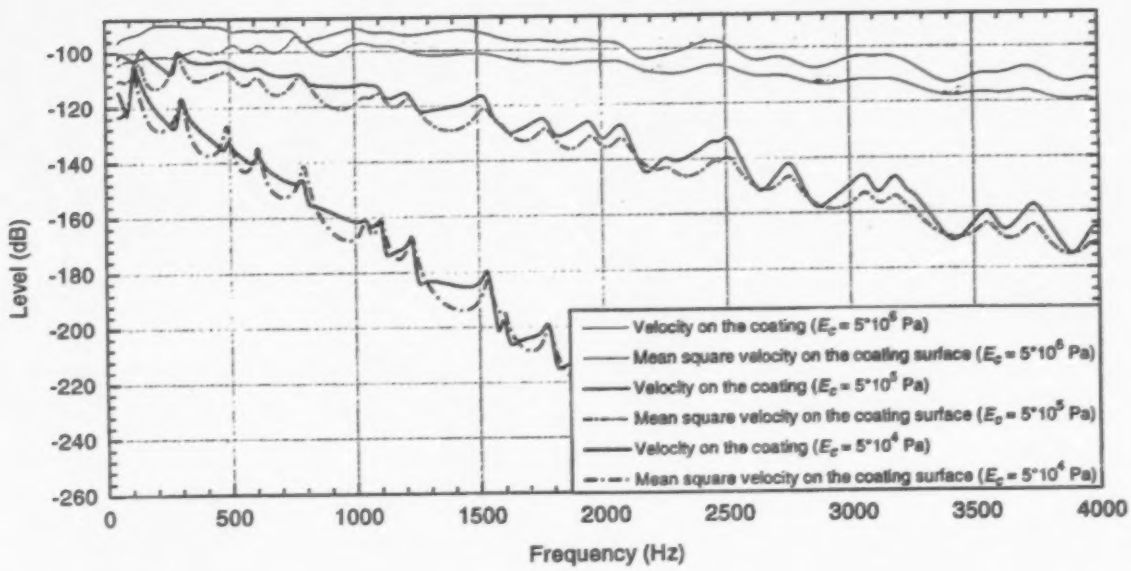

Figure 4.3 : Velocity on the coating surface at the excitation point and mean square velocity on the coating surface for the three cases of the Table 4.1.

5 Partial coverage for damping material

5.1 Introduction

This section presents the theoretical model and the numerical results for the vibration and acoustic response of a plate partially covered by a constrained viscoelastic layer (Figure 5.1). It is based on the model presented in chapter 5 of the DREA report CR/96/427 ("Exact model for sandwich plate" p. 66-78). The "Simple model for sandwich plate" presented at pages 79-93 of the DREA report CR/96/427 was not used here because it is not able to account for partial coverage. The calculation of the kinetic and strain energy of the viscoelastic and constraining layers are now performed over the partial coverage area and not on the base plate area. Furthermore, the boundary conditions of the partial coverage have to be modified to account for the free displacement at its boundary. The partial coverage consists of a rectangular surface of viscoelastic layer covered by a constraining layer (Figure 5.1). The viscoelastic layer and the constraining layer have the same surface and location.

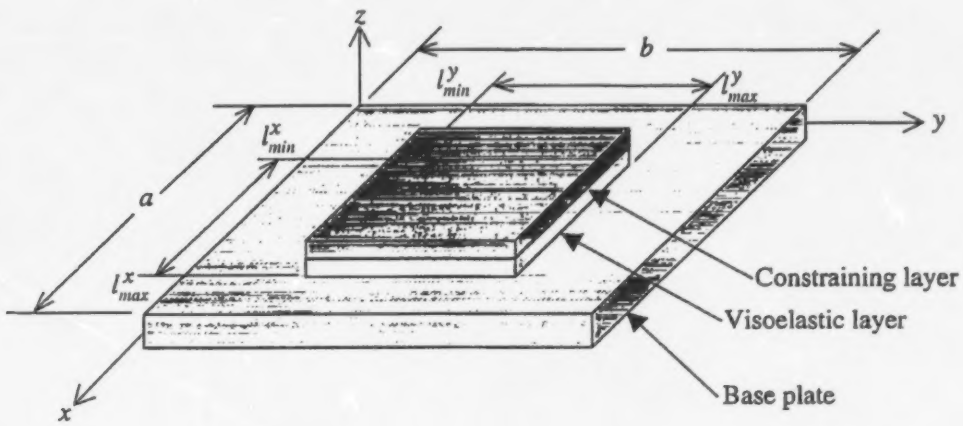

Figure 5.1 : Base plate covered by a partial constrained damping treatment.

5.2 Theoretical model

5.2.1 Hypotheses

The model presented below describes the vibro-acoustic behavior of a baffled, simply supported, sandwich plate. It uses the following hypotheses :

1. A linear displacement field is defined for each layer (as in discrete layer models), and the continuity of the displacement is assumed at each layer interface.
2. Normal strain is neglected (plane stress hypothesis).
3. Torsional motion is neglected in the whole plate.
4. Shear motion is only accounted for in the viscoelastic layer.
5. Excitation is either a point force on the base plate or an acoustic plane wave (propagating in the $z < 0$ side).
6. Fluid loading is taken into account on the $z > 0$ side.
7. The acoustic radiation is investigated only in the heavy fluid ($z > 0$).

5.2.2 *Displacement field*

The first step in the variational approach is to define the displacement field of the system. In the present model, a displacement field is defined for each layer. The outer elastic layers only account for traction-compression effect (in-plane motion) and the bending effect (out-of-plane motion). Thus, the displacement field of these layers is :

$$\begin{cases} u^{(i)}(x,y,z,t) = u_0^{(i)}(x,y,t) - z_i \dfrac{\partial w(x,y,t)}{\partial x} \\ v^{(i)}(x,y,z,t) = v_0^{(i)}(x,y,t) - z_i \dfrac{\partial w(x,y,t)}{\partial y} \\ w^{(i)}(x,y,z,t) = w(x,y,t) \end{cases} \tag{5.3}$$

with $i = 1$ or 3. Subscripts 1, 2, 3 are respectively devoted to the base plate, the viscoelastic layer and the constraining layer. The origin of the z coordinate is taken in the mid-plane of each layer. $u_0^{(i)}$ and $v_0^{(i)}$ represent the traction-compression displacements in the x and y directions, w is the transverse displacement of the plate. $-z_i\,\partial w/\partial x$ and $-z_i\,\partial w/\partial y$ represent the bending rotation in the x and y directions (Love-Kirchhoff theory).

The displacement of the viscoelastic layer takes into account the traction-compression, the shear and the bending effects. This leads to the following displacement field :

$$\begin{cases} u^{(2)}(x,y,z,t) = u_0^{(2)}(x,y,t) + z_2 \Psi_x^{(2)}(x,y,t) \\ v^{(2)}(x,y,z,t) = v_0^{(2)}(x,y,t) + z_2 \Psi_y^{(2)}(x,y,t) \\ w^{(2)}(x,y,z,t) = w(x,y,t) \end{cases} \tag{5.4}$$

$u_0^{(2)}$ and $v_0^{(2)}$ are traction-compression displacements and $\Psi_x^{(2)}$ and $\Psi_y^{(2)}$ represent the rotational displacements of a cross section of the viscoelastic layer, that includes bending and shear motion (Reissner-Mindlin theory). Imposing the continuity of the u, v displacements at the viscoelastic layer interfaces, one can write the displacement field of the viscoelastic layer as a function of the two elastic layers:

$$\begin{cases} u^{(2)}(x,y,z,t) = \dfrac{1}{h_2}\left[u_0^{(3)} + \dfrac{1}{2}\dfrac{\partial w}{\partial x}(h_3 + h_1) - u_0^{(1)}\right] z_2 + \dfrac{1}{2}\left[u_0^{(3)} + \dfrac{1}{2}\dfrac{\partial w}{\partial x}((h_3 - h_1)) + u_0^{(1)}\right] \\ v^{(2)}(x,y,z,t) = \dfrac{1}{h_2}\left[v_0^{(3)} + \dfrac{1}{2}\dfrac{\partial w}{\partial y}(h_3 + h_1) - v_0^{(1)}\right] z_2 + \dfrac{1}{2}\left[v_0^{(3)} + \dfrac{1}{2}\dfrac{\partial w}{\partial y}((h_3 - h_1 -)) + v_0^{(1)}\right] \\ w^{(2)}(x,y,z,t) = w(x,y,t) \end{cases} \tag{5.5}$$

where h_1, h_2, h_3, are the thickness of layer 1, 2, 3, respectively.
The displacement field of each layer of the plate is now expressed in terms of the motion of the outer layers : $u_0^{(1)}(x,y,t), v_0^{(1)}(x,y,t), w(x,y,t), u_0^{(3)}(x,y,t), v_0^{(3)}(x,y,t)$, which represent the five unknown displacements of the plate.

5.2.3 *Strain field*

In linear elasticity, the strain field is deduced from the displacement field using the following strain-displacement equations :

$$\varepsilon_{kl}^{(i)} = \frac{1}{2}\left(\frac{\partial u_k^{(i)}}{\partial x_l} + \frac{\partial u_l^{(i)}}{\partial x_k}\right) \tag{5.6}$$

where $k, l = x, y, z$.
For the outer elastic layers this gives :

$$\begin{cases} \varepsilon_x^{(i)} = \dfrac{\partial u_0^{(i)}}{\partial x} - z_i \dfrac{\partial^2 w}{\partial x^2} \\ \varepsilon_y^{(i)} = \dfrac{\partial v_0^{(i)}}{\partial y} - z_i \dfrac{\partial^2 w}{\partial y^2} \\ \varepsilon_z^{(i)} = 0 \\ \gamma_{xy}^{(i)} = 2\varepsilon_{xy}^{(i)} = \dfrac{\partial u_0^{(i)}}{\partial y} + \dfrac{\partial v_0^{(i)}}{\partial x} - 2z_i \dfrac{\partial^2 w}{\partial x \partial y} \\ \gamma_{xz}^{(i)} = 0 \\ \gamma_{yz}^{(i)} = 0 \end{cases} \tag{5.7}$$

where $i = 1, 3$.
and for the viscoelastic layer :

$$\begin{cases} \varepsilon_x^{(2)} = \dfrac{\partial u_0^{(2)}}{\partial x} + z_2 \dfrac{\partial \Psi_x^{(2)}}{\partial x} \\ \varepsilon_y^{(2)} = \dfrac{\partial v_0^{(2)}}{\partial y} + z_2 \dfrac{\partial \Psi_y^{(2)}}{\partial y} \\ \varepsilon_z^{(2)} = 0 \\ \gamma_{xy}^{(2)} = 2\varepsilon_{xy}^{(2)} = \dfrac{\partial u_0^{(2)}}{\partial y} + \dfrac{\partial v_0^{(2)}}{\partial x} + z_2 \left(\dfrac{\partial \Psi_x^{(2)}}{\partial y} + \dfrac{\partial \Psi_y^{(2)}}{\partial x} \right) \\ \gamma_{xz}^{(2)} = 2\varepsilon_{xz}^{(2)} = \Psi_x^{(2)} + \dfrac{\partial w}{\partial x} \\ \gamma_{yz}^{(2)} = 2\varepsilon_{yz}^{(2)} = \Psi_y^{(2)} + \dfrac{\partial w}{\partial y} \end{cases} \tag{5.8}$$

The ε_x , ε_y and γ_{xy} strains are linear functions of z, and there is continuity of these strains at each layer interface. The transverse strain ε_z is zero in the whole plate. Shear strains γ_{xz} , γ_{yz} are constant and non zero in the viscoelastic layer but are equal to zero in the outer layers. Thus, there is no continuity of the shear strains at the layer interfaces.

5.2.4 Stress field

The stress field of each layer is calculated from the strain field using an elasticity matrix that satisfies the Hooke's law. The two-dimensional theory of elasticity is used (plane stress hypothesis). This theory is based on the fact that the normal stress σ_z is negligible in comparison to the other stresses. It leads to a 5×5 matrix of elasticity instead of the 6×6 matrix. The following relations are obtained :

$$\begin{Bmatrix} \sigma_x \\ \sigma_y \\ \sigma_{xy} \end{Bmatrix} = \begin{bmatrix} Q_{11} & Q_{12} & 0 \\ Q_{21} & Q_{22} & 0 \\ 0 & 0 & Q_{44} \end{bmatrix} \begin{Bmatrix} \varepsilon_x \\ \varepsilon_y \\ \gamma_{xy} \end{Bmatrix} \tag{5.9}$$

$$\begin{Bmatrix} \sigma_{xz} \\ \sigma_{yz} \end{Bmatrix} = \begin{bmatrix} Q_{55} & 0 \\ 0 & Q_{66} \end{bmatrix} \begin{Bmatrix} \gamma_{xz} \\ \gamma_{yz} \end{Bmatrix} \tag{5.10}$$

In the outer layers the shear strains and stresses (γ_{xz}, γ_{yz}, σ_{xz}, σ_{yz}) are not taken into account : thus, only the equation 5.9 is used for these layers. For an isotropic material the coefficients of the matrices are :

$$Q_{11} = Q_{22} = \frac{E}{1-\nu^2},\ Q_{12} = Q_{21} = \frac{E\nu}{1-\nu^2},\ Q_{44} = Q_{55} = Q_{66} = G = \frac{E}{2(1+\nu)},$$

where E is the Young's modulus of the material, ν is the Poisson ratio and G is the shear modulus.

5.2.5 *Rayleigh-Ritz method*

Once the displacement field of the plate is defined, the five unknown displacements have to be expressed in terms of an admissible functional basis that satisfies the boundary condition of the structure. For the base plate, the boundary conditions are :

$$\begin{aligned} &\text{for } x=0 \text{ and } x=a: \ w(x,y)=v_0^{(1)}(x,y)=0 \\ &\text{for } y=0 \text{ and } y=b: \ w(x,y)=u_0^{(1)}(x,y)=0 \end{aligned} \tag{5.11}$$

If the boundary conditions previously defined for the base plate are also used for the partial coverage, this implies that the four corners of the damping material are constrained. To avoid this non-physical constraint, the hypothesis of Lall *et al* (1987) is used. It consists of adding a rigid body motion to the constraining layer displacement field; this leads to the following boundary condition for the in-plane motion of the constraining layer:

$$\begin{aligned} &\text{for } x=l_{\min}^x \text{ and } x=l_{\max}^x : u_0^{(3)}(x,y)=C_1 \text{ and } v_0^{(3)}(x,y)=C_2 \\ &\text{for } y=l_{\min}^y \text{ and } y=l_{\max}^y : u_0^{(3)}(x,y)=C_1 \text{ and } v_0^{(3)}(x,y)=C_2 \end{aligned} \tag{5.12}$$

Under these conditions, an admissible set of functions consists of a combination of sine and cosine functions :

$$\begin{cases} w(x,y) = \sum_{m=1}^{N}\sum_{n=1}^{N} A_{mn} \sin\left(m\pi\frac{x}{a}\right)\sin\left(n\pi\frac{y}{b}\right) \\ u_0^{(1)}(x,y) = \sum_{m=1}^{N}\sum_{n=1}^{N} B_{mn} \cos\left(m\pi\frac{x}{a}\right)\sin\left(n\pi\frac{y}{b}\right) \\ v_0^{(1)}(x,y) = \sum_{m=1}^{N}\sum_{n=1}^{N} C_{mn} \sin\left(m\pi\frac{x}{a}\right)\cos\left(n\pi\frac{y}{b}\right) \\ u_0^{(3)}(x,y) = C_1 + \sum_{m=1}^{N}\sum_{n=1}^{N} D_{mn} \cos\left(\frac{m\pi\left(x-l_{\min}^{x}\right)}{l_{\max}^{x}-l_{\min}^{x}}\right)\sin\left(\frac{n\pi\left(y-l_{\min}^{y}\right)}{l_{\max}^{y}-l_{\min}^{y}}\right) \\ v_0^{(3)}(x,y) = C_2 + \sum_{m=1}^{N}\sum_{n=1}^{N} E_{mn} \sin\left(\frac{m\pi\left(x-l_{\min}^{x}\right)}{l_{\max}^{x}-l_{\min}^{x}}\right)\cos\left(\frac{n\pi\left(y-l_{\min}^{y}\right)}{l_{\max}^{y}-l_{\min}^{y}}\right) \end{cases} \tag{5.13}$$

In effect, the various displacements of equation 5.13 satisfy the boundary conditions 5.11 and 5.12.

5.2.6 *Hamilton functional*

The Hamilton functional, expressed in terms of the seven unknown displacements of the plate is :

$$H\left(u_0^{(1)}, v_0^{(1)}, w, u_0^{(3)}, v_0^{(3)}, C_1, C_2\right) = \int_{t_0}^{t_1} (T - V + W)\,dt\,, \tag{5.13}$$

where T is the kinetic energy of the plate, V is the strain energy of the plate and W is the work of external forces. The condition $\delta H = 0$ furnishes the equation of motion of the plate. In the following paragraph the energies of the system are detailed in order to construct the Hamilton functional of the problem.

5.2.7 *Kinetic energy*

The kinetic energy of an elastic solid with displacements u, v, w, a volume v and density ρ, is given by :

$$T = \frac{1}{2}\rho \iiint_{v} \left[\left(\frac{\partial u}{\partial t}\right)^2 + \left(\frac{\partial v}{\partial t}\right)^2 + \left(\frac{\partial w}{\partial t}\right)^2\right] dv\,. \tag{5.14}$$

In this study only the transverse displacement is considered, the traction-compression displacements and the rotational inertia are neglected in the kinetic energy of the structure. The total kinetic energy of the plate is the sum of the kinetic energies of each layer. The kinetic energy of the base plate is :

$$T^{(1)} = \frac{1}{2}\rho_1 h_1 \int_0^a \int_0^b \left(\frac{\partial w}{\partial t}\right)^2 dxdy , \tag{5.15}$$

where a and b are the dimensions of the plate. For the viscoelastic layer and the constraining layer the kinetic energies are :

$$T^{(i)} = \frac{1}{2}\rho_i h_i \int_{l_{\min}^x}^{l_{\max}^x} \int_{l_{\min}^y}^{l_{\max}^y} \left(\frac{\partial w}{\partial t}\right)^2 dxdy , \tag{5.16}$$

where $i = 2, 3$. The integration is performed over the coverage surface of the constrained viscoelastic layer.

5.2.8 Strain energy

The strain energy of a plane structure (assuming plane stress) is given by :

$$V = \frac{1}{2}\iiint_V \left(\sigma_x \varepsilon_x + \sigma_y \varepsilon_y + \sigma_{xy}\gamma_{xy} + \sigma_{xz}\gamma_{xz} + \sigma_{yz}\gamma_{yz}\right) dxdydz , \tag{5.17}$$

In the present case, the total strain energy of the structure is the sum of the strain energies of each layer.

Base plate

The strain energy of the base plate is the sum of the following two terms :

$$V_1^{(1)} = \frac{h_1 E_1}{2\left(1-\nu_1^2\right)} \int_0^a \int_0^b \left[\left(\frac{\partial u_0^{(1)}}{\partial x}\right)^2 + \left(\frac{\partial v_0^{(1)}}{\partial y}\right)^2 + 2\nu_1 \frac{\partial u_0^{(1)}}{\partial x}\frac{\partial v_0^{(1)}}{\partial y} + \frac{1-\nu_1}{2}\left(\frac{\partial u_0^{(1)}}{\partial y} + \frac{\partial v_0^{(1)}}{\partial x}\right)^2 \right] dxdy , \tag{5.18}$$

$$V_2^{(1)} = \frac{(h_1)^3}{24}\frac{E_1}{1-\nu_1^2}\int_0^a\int_0^b\left[\left(\frac{\partial^2 w}{\partial x^2}\right)^2 + \left(\frac{\partial^2 w}{\partial y^2}\right)^2 + 2\nu_1\frac{\partial^2 w}{\partial x^2}\frac{\partial^2 w}{\partial y^2} + 2(1-\nu_1)\left(\frac{\partial^2 w}{\partial x \partial y}\right)^2\right]dxdy, \qquad (5.19)$$

where $V_1^{(1)}$ represents the traction-compression energy and $V_2^{(1)}$ represents the bending energy.

Viscoelastic layer

For the viscoelastic layer and the constraining layer, the integration is performed over the surface of the partial coverage instead of the surface of the plate. The strain energy of the viscoelastic layer is given by the sum of the following three terms :

$$V_1^{(2)} = \frac{h_2 E_2}{2(1-\nu_2^2)}\int_{l_{\min}^x}^{l_{\max}^x}\int_{l_{\min}^y}^{l_{\max}^y}\left[\left(\frac{\partial u_0^{(2)}}{\partial x}\right)^2 + \left(\frac{\partial v_0^{(2)}}{\partial y}\right)^2 + 2\nu_2\frac{\partial u_0^{(2)}}{\partial x}\frac{\partial v_0^{(2)}}{\partial y} + \frac{1-\nu_2}{2}\left(\frac{\partial u_0^{(2)}}{\partial y} + \frac{\partial v_0^{(2)}}{\partial x}\right)^2\right]dxdy, \qquad (5.20)$$

$$V_2^{(2)} = \frac{(h_2)^3}{24}\frac{E_2}{1-\nu_2^2}\int_{l_{\min}^x}^{l_{\max}^x}\int_{l_{\min}^y}^{l_{\max}^y}\left[\left(\frac{\partial \Psi_x^{(2)}}{\partial x}\right)^2 + \left(\frac{\partial \Psi_y^{(2)}}{\partial y}\right)^2 + 2\nu_2\frac{\partial \Psi_x^{(2)}}{\partial x}\frac{\partial \Psi_y^{(2)}}{\partial y} + \frac{1-\nu_2}{2}\left(\frac{\partial \Psi_x^{(2)}}{\partial y} + \frac{\partial \Psi_y^{(2)}}{\partial x}\right)^2\right]dxdy \qquad (5.21)$$

$$V_3^{(2)} = \frac{h_2 E_2}{4(1+\nu_2)}\int_{l_{\min}^x}^{l_{\max}^x}\int_{l_{\min}^y}^{l_{\max}^y}\left[\left(\Psi_x^{(2)} + \frac{\partial w}{\partial x}\right)^2 + \left(\Psi_y^{(2)} + \frac{\partial w}{\partial y}\right)^2\right]dxdy, \qquad (5.22)$$

where $V_1^{(2)}$ represents the traction-compression energy, $V_2^{(2)}$ represents the rotational energy (coupling between bending and shear), $V_3^{(2)}$ represents the shear energy.

Constraining layer

The strain energy of the constraining layer is given by the sum of the following two terms:

$$V_1^{(3)} = \frac{h_3 E_3}{2\left(1-\nu_3^2\right)} \int_{l_{\min}^x}^{l_{\max}^x} \int_{l_{\min}^y}^{l_{\max}^y} \left[\left(\frac{\partial u_0^{(3)}}{\partial x} \right)^2 + \left(\frac{\partial v_0^{(3)}}{\partial y} \right)^2 + 2\nu_3 \frac{\partial u_0^{(3)}}{\partial x} \frac{\partial v_0^{(3)}}{\partial y} + \frac{1-\nu_3}{2} \left(\frac{\partial u_0^{(3)}}{\partial y} + \frac{\partial v_0^{(3)}}{\partial x} \right)^2 \right] dxdy \,, \quad (5.23)$$

$$V_2^{(3)} = \frac{(h_3)^3}{24} \frac{E_3}{1-\nu_3^2} \int_{l_{\min}^x}^{l_{\max}^x} \int_{l_{\min}^y}^{l_{\max}^y} \left[\left(\frac{\partial^2 w}{\partial x^2} \right)^2 + \left(\frac{\partial^2 w}{\partial y^2} \right)^2 + 2\nu_3 \frac{\partial^2 w}{\partial x^2} \frac{\partial^2 w}{\partial y^2} + 2(1-\nu_3) \left(\frac{\partial^2 w}{\partial x \partial y} \right)^2 \right] dxdy \,, \quad (5.24)$$

where $V_1^{(3)}$ represents the traction-compression energy and $V_2^{(3)}$ represents the bending energy.

5.2.9 *Work of external forces*

Two types of external forces have to be considered : the excitation forces (point force or plane wave) and the sound pressure exerted by the fluid medium. In this study, only the sound pressure exerted by the heavy fluid ($z > 0$) is considered, the effect of the light fluid ($z < 0$) is neglected. The work of the excitation forces is:

$$W_{excitation} = \int_0^a \int_0^b f(x,y,0) w(x,y) dxdy \,. \quad (5.25)$$

If the excitation is a point force :

$$W_{excitation} = F_0 w(x_0, y_0), \quad (5.26)$$

where F_0 is the magnitude of the force located at (x_0 , y_0). When the excitation is a plane wave, the expression of $W_{excitation}$ is given in the appendix 1 of the DREA report CR/96/427. The work of the acoustic pressure in the heavy fluid is :

$$W_{fluid} = \int_0^a \int_0^b p(x,y,0) w(x,y) dxdy \,, \quad (5.27)$$

where $p(x,y,0)$ is the acoustic pressure exerted by the heavy fluid on the plate. In order to calculate this pressure, the integral formulation has to be used.

5.2.10 *Integral formulation*

In this section, the main results of the integral method are recalled. The acoustic pressure radiated by the baffled plate, immersed in a heavy fluid is governed by the Helmholtz equation and the boundary conditions (in the plane $z = 0$). The Helmholtz equation, expressed in the frequency domain, is :

$$\Delta p(M) + k_0^2 p(M) = 0 , \tag{5.28}$$

where $p(M)$ is the acoustic pressure at point M in the fluid, k_0 is the acoustic wavenumber : $k_0 = \omega/c_0$, c_0 is the speed of sound in the heavy fluid.
The boundary condition expresses the continuity of the acoustic and mechanical normal velocities on the plate :

$$\frac{\partial p(M)}{\partial \underline{n}_M} = \rho_0 \omega^2 w(M), \tag{5.29}$$

where ρ_0 is the density of the heavy fluid and $\underline{n}_M$ is the direction normal to the plate oriented into the heavy fluid.

In order to solve the problem, the integral method is used. This method allows the acoustic pressure to be expressed at any point in the fluid space, in terms of the acoustic pressure on the plate and in terms of a Green's function of the problem. The present case is an external problem, the integral formulation takes the form :

$$p(Q) = \iint_S \left[\frac{\partial G(Q,M)}{\partial \underline{n}_M} p(M) - \frac{\partial p(M)}{\partial \underline{n}_M} G(Q,M) \right] dS_M . \tag{5.30}$$

The Green's function for an infinite half-space is used. This function satisfies the Sommerfeld radiation condition and the Helmholtz equation. Furthermore, the normal derivative of this function is zero on the plate. Using this property, a simpler form of the integral formulation, called the Rayleigh integral, is obtained. The continuity of the mechanical and acoustical velocities on the plate allows the Rayleigh integral to be written in terms of the transverse displacement of the plate w , and in terms of the Green's function :

$$p(Q) = -\omega^2 \rho_0 \iint_S w(M) G(M,Q) dS_M . \tag{5.31}$$

Using the previous equation, the work of the acoustic pressure on the plate is given by:

$$W_{fluid} = \int_0^a \int_0^b p(x,y,0)w(x,y)dxdy = j\omega \sum_{m=1}^{\infty}\sum_{n=1}^{\infty}\sum_{p=1}^{\infty}\sum_{q=1}^{\infty} A_{mn}Z_{mnpq}A_{pq}\,, \tag{5.32}$$

where Z_{mnpq} are the coefficients of the radiation impedance matrix :

$$Z_{mnpq} = j\rho_0\omega \int_S\int_S w_{pq}(M)G(M,Q)w_{mn}(Q)dS_M dS_Q \tag{5.33}$$

The numerical calculation of the radiation impedance matrix is presented in the appendix 2 of the DREA report CR/96/427. In brief, this calculation is performed using a Gauss numerical integration method.

5.2.11 *Equation of motion of the plate*

Using the previous expressions of the kinetic energy, strain energy and work of the exterior forces, the Hamilton functional can be evaluated. The stationarity of the Hamilton functional leads to the equation of motion of the plate. It is expressed by the Lagrange equations, in terms of the generalized coordinates of the system : $A_{mn}, B_{mn}, C_{mn}, D_{mn}, E_{mn}, C_1, C_2 \;\forall(m,n)\in[1,..N]^2$. The Lagrange equations are :

$$\begin{cases} \dfrac{d}{dt}\dfrac{\partial T}{\partial \dot{A}_{mn}} + \dfrac{\partial V}{\partial A_{mn}} = \dfrac{\partial W_{excitation}}{\partial A_{mn}} + \dfrac{\partial W_{fluid}}{\partial A_{mn}} \\ \dfrac{d}{dt}\dfrac{\partial T}{\partial \dot{B}_{mn}} + \dfrac{\partial V}{\partial B_{mn}} = 0 \\ \dfrac{d}{dt}\dfrac{\partial T}{\partial \dot{C}_{mn}} + \dfrac{\partial V}{\partial C_{mn}} = 0 \\ \dfrac{d}{dt}\dfrac{\partial T}{\partial \dot{D}_{mn}} + \dfrac{\partial V}{\partial D_{mn}} = 0 \\ \dfrac{d}{dt}\dfrac{\partial T}{\partial \dot{E}_{mn}} + \dfrac{\partial V}{\partial E_{mn}} = 0 \\ \dfrac{d}{dt}\dfrac{\partial T}{\partial \dot{C}_1} + \dfrac{\partial V}{\partial C_1} = 0 \\ \dfrac{d}{dt}\dfrac{\partial T}{\partial \dot{C}_2} + \dfrac{\partial V}{\partial C_2} = 0 \end{cases} \tag{5.34}$$

In a reduced matrix form :

$$[M]\{\ddot{X}\} + [K]\{X\} = \{f\} - \{P\}, \tag{5.35}$$

where $\langle X \rangle = \{A_{mn}\ B_{mn}\ C_{mn}\ D_{mn}\ E_{mn}\ C_1\ C_2\}$, $[M]$ is the mass matrix of the multilayered plate, $[K]$ is the stiffness matrix, $\{f\}$ is the generalized vector of external forces (excitation) and $\{P\}$ is the vector of fluid loading.

Assuming a time-harmonic dependence in $e^{j\omega t}$ (angular frequency ω), and taking the finite Fourier transform of equation (5.35), the following equation of motion of the multilayered plate is obtained in the frequency domain :

$$\left(-\omega^2[M]+[K]\right)\{X\} = \{f\} - j\omega[Z]\{X\}, \tag{3.36}$$

where $[Z]$ is the radiation impedance matrix :

$$[Z] = \begin{bmatrix} Z_{mnpq} & 0 & 0 & 0 & 0 \\ 0 & 0 & 0 & 0 & 0 \\ 0 & 0 & 0 & 0 & 0 \\ 0 & 0 & 0 & 0 & 0 \\ 0 & 0 & 0 & 0 & 0 \end{bmatrix} \tag{3.37}$$

Solving the linear system 3.36 allows the displacement field of the base plate covered by a partial constrained viscoelastic treatment to be evaluated. The calculation of the various vibroacoustic indicators is not presented since their derivation is identical to what was detailed in the DREA report CR/96/427.

5.3 Numerical results

In this section numerical results obtained with the model for partial constrained damping coverage of a simply-supported plate in water is analysed. The influence of the coverage percentage on the overall acoustic response of the structure is investigated. The cases of 25 %, 50 % and 75 % coverage are compared to the full coverage case and to the bare plate case. The characteristics of the base plate are presented in Table 2.1, the constraining layer has the same characteristics as the base plate except the thickness which is 0.5 mm. The characteristics of the viscoelastic layer are listed in Table 5.1. The excitation is a point force acting at $x = y = 0.06$ m from a corner of the plate. The fluid is water (ρ_0 = 1000 kg/m^3, c_0 = 1460 m/s). Figure 5.3 presents the vibration response of the partial coverage cases in low frequency (0-1500 Hz) and Figure 5.4 presents the vibration response in high frequency (1500-4000 Hz). Figure 5.5 presents the acoustic response in low frequency (0-1500 Hz) and Figure 5.6 presents the acoustic response in high frequency (1500-4000 Hz). For better clarity, the case of 75 % coverage is removed in Figure 5.5 and Figure 5.6.

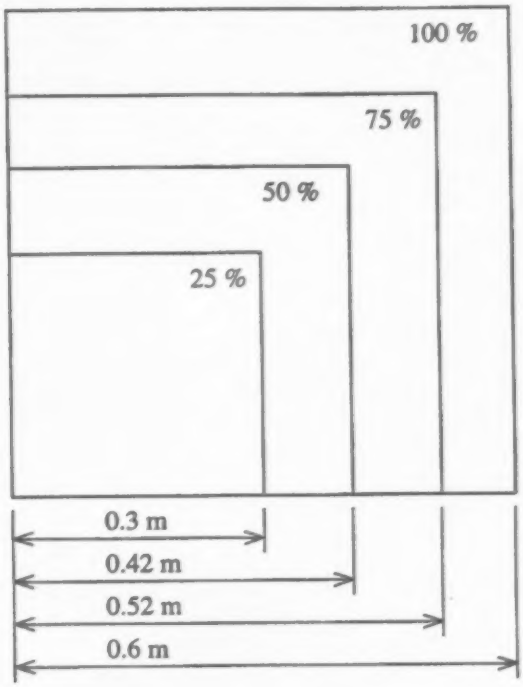

Figure 5.2 : Presentation of the four cases tested with the partial damping coverage.

Table 5.1 : Characteristics of the viscoelastic layer used for the partial constrained damping coverage.

Thickness (mm)	Density (kg/m^3)	Young's modulus (Pa)	Loss factor	Poisson's ratio
h_2	ρ_2	E_2	η_2	ν_2
0.5	1000	10^8	1	0.3

The partial coverage results show that increasing the surface of the damping treatment always increases the overall damping of the system. This effect is fairly uniform in frequency, except for the first three modes where the damping is not very efficient in all cases. However, there is no linear relation between the damping and the coverage percentage. As a matter of fact adding only 25 % of constrained damping gives a global acoustic attenuation of 2.7 dB, while the difference between 75 % and 100 % coverage is almost negligible (75 % : 5.3 dB of global acoustic attenuation and 100 % : 5.6 dB of global acoustic attenuation). Covering only 50 % of the plate gives 4.1 dB of global acoustic attenuation. Many similar simulations performed in air or in water reveal the same tendencies. When partial constrained

damping treatment is considered, it is not very important to cover the whole plate, usually 75 % of coverage gives almost the same attenuation as full coverage.

Two cases should be considered when optimising the location of the partial coverage : (1) in low frequency where the structural wavelength in the base plate is larger than the dimensions of the coverage and (2) in high frequency where the structural wavelength in the base plate is smaller than the dimensions of the coverage. In order to be effective, the viscoelastic layer should be subject to transverse shear deformation. The maximum shear deformation of the viscoelastic layer occurs when the viscoelastic layer is located at the maximum bending strain of the base plate. In low frequency the structural wavelength is large and the coverage is smaller than the structural wavelength. In such a case the location of the coverage is important, because if it is located in a low bending strain area it will be subject to small shear strain and will provide small damping. However, in high frequency the coverage is larger than the structural wavelength, and the location of the coverage does not significantly affect the overall attenuation. Foin *et al* (1999 (a) and (b)) have presented results on the influence of the location of partial damping coverage for various plane structures radiating in air. They found that when the coverage percentage is 50 % or more, the damping is found to be almost independent of the viscoelastic location.

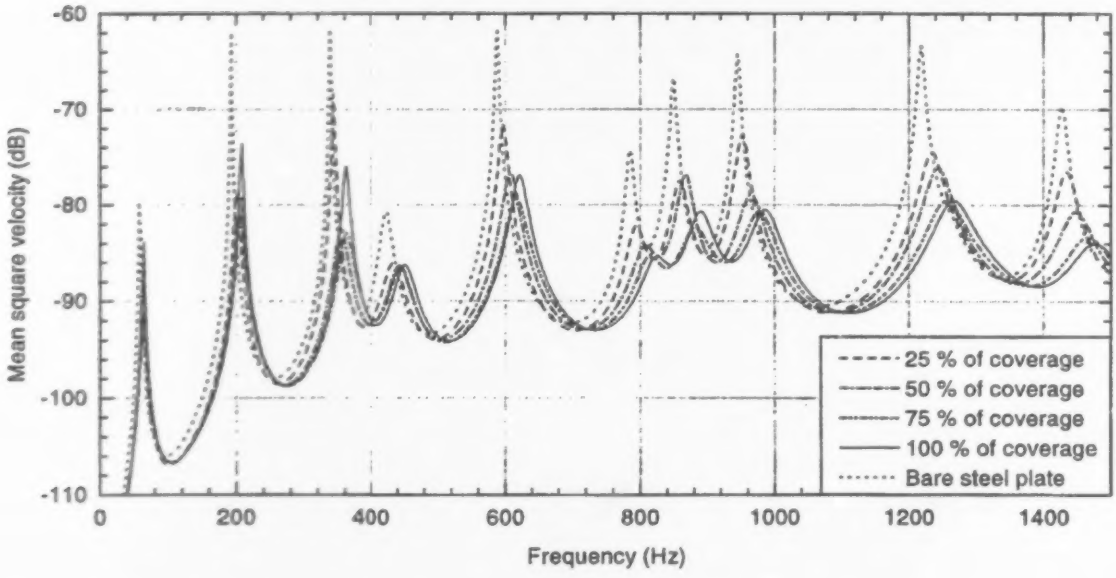

Figure 5.3 : Influence of the surface of the partial constrained damping coverage on the vibration response in low frequency.

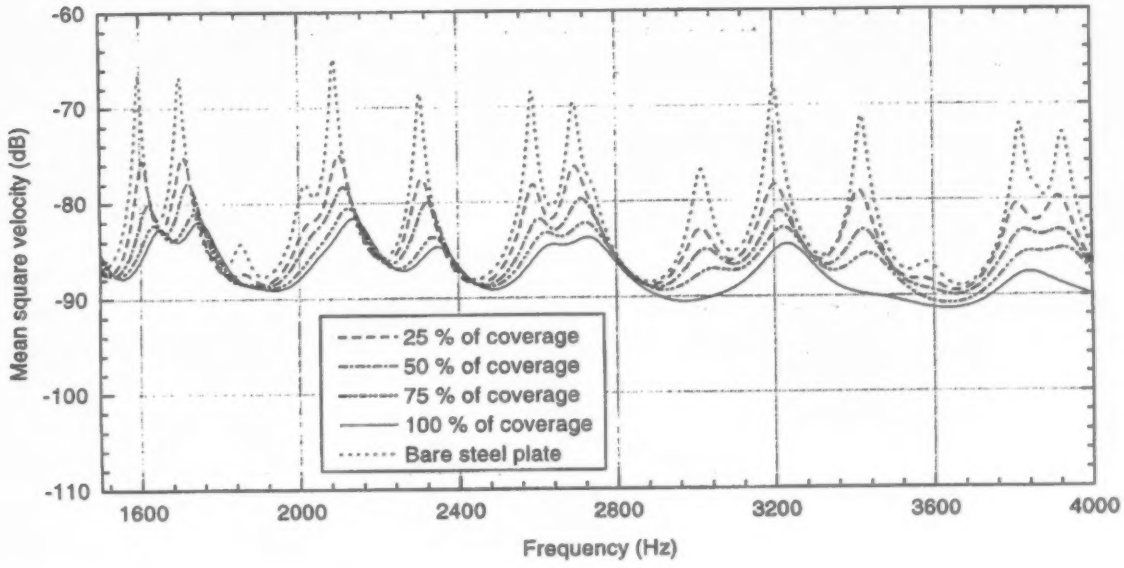

Figure 5.4 : Influence of the surface of the partial constrained damping coverage on the vibration response in high frequency.

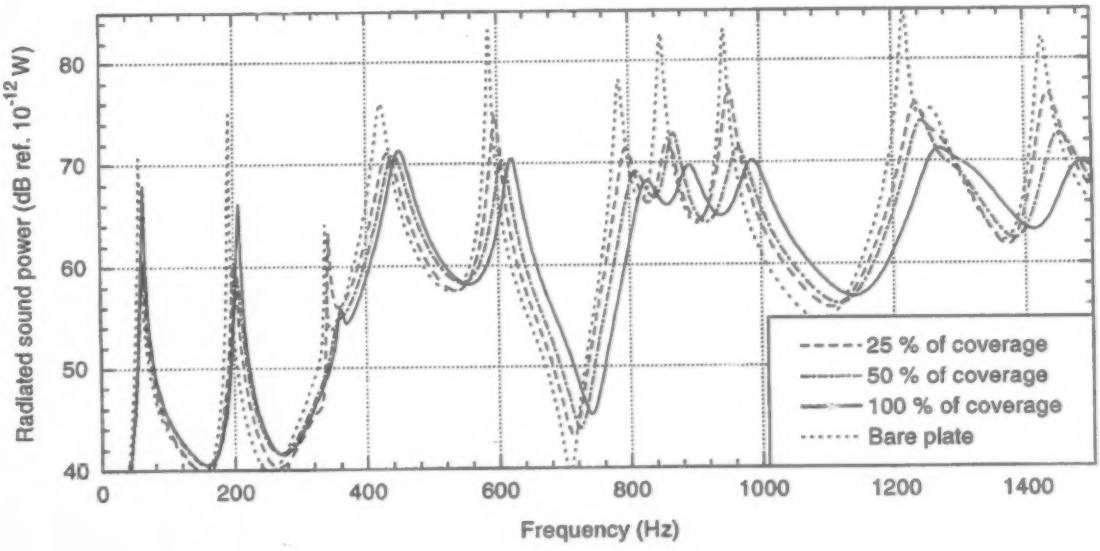

Figure 5.5 : Influence of the surface of the partial constrained damping coverage on the acoustic response in low frequency.

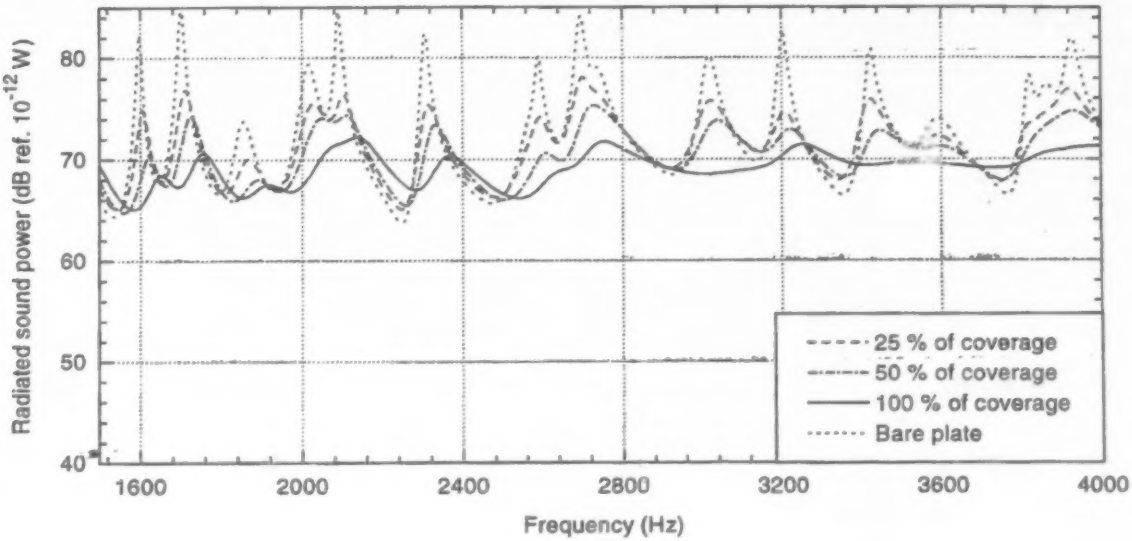

Figure 5.6 : Influence of the surface of the partial constrained damping coverage on the acoustic response in high frequency.

6 Conclusion

This report has presented the theoretical formulation and numerical results of a new 3D model to describe the vibroacoustic behaviour of an elastic plate covered by a decoupling coating and immersed in water. This 3D model (VIBRO3D) uses the three-dimensional theory of elasticity to describe stress and strain within the decoupling material, and is therefore more complete than the locally-reacting model implemented in a previous version of the software (VIBRO). The following general conclusions can be drawn from this study:

- It was found that shear wave components in the 3D model are usually much less important than longitudinal wave components, and can generally be neglected in order to reduce the calculation time of the 3D model.
- A good agreement was found between the locally reacting model and the 3D model in the case of relatively stiff , lightly damped and low mass density coating materials. In the other cases the locally reacting model overestimates the decoupling effectiveness in comparison to the 3D model.
- The model of House was found to be in good agreement with the 3D model in terms of the insertion loss of a plate covered by a decoupling coating. An attractive aspect in the model of House is its simplicity.
- Good agreement was observed between the model of Ko for infinite plates and the 3D model in terms of the mean square velocity ratio.
- The calculation of the absolute intensity through a mapping plane at a distance d (called *near field acoustic power* in this report) was found to be a valuable indicator to evaluate the transmission loss of a plate/coating system.
- The driving point mobility (defined as the ratio of the velocity at the excitation point to the input force) was investigated as a potential experimental parameter to characterise the coating material.

However, the driving point mobility was found to vary in a complex way with the coating properties, and is sometimes not very sensitive to the coating properties. On the other hand, the velocity ratio (velocity at the coating surface / velocity at driving point) was found to be a more appropriate indicator to measure the properties of the coating material

- The approximate (hybrid) method proposed to evaluate the influence of partial decoupling on the acoustic response shows that small uncovered areas rapidly reduce the global decoupling effectivess.
- Finally, a model that considers a simply supported base plate partially covered by a constrained damping treatment was proposed. The parametric study shows that efficient global damping can be achieved without covering the whole structure. In general, a 50% coverage is sufficient to obtain significant vibration / sound attenuation, and additional coverage above this value has a low impact on the attenuation obtained.

7 Appendix A Some useful vectorial analysis definitions

The nabla operator is defined by :

$$\nabla = \vec{i}\frac{\partial}{\partial x} + \vec{j}\frac{\partial}{\partial y} + \vec{k}\frac{\partial}{\partial z},$$

where $\vec{i}$, $\vec{j}$ and $\vec{k}$ are unitary vectors in the x, y, and z direction, respectively.
The gradient is defined by :

$$\nabla U = \frac{\partial U}{\partial x}\vec{i} + \frac{\partial U}{\partial y}\vec{j} + \frac{\partial U}{\partial x}\vec{k}\,.$$

The divergence is defined by :

$$\nabla \cdot \vec{A} = \frac{\partial A_x}{\partial x} + \frac{\partial A_y}{\partial y} + \frac{\partial A_z}{\partial x},$$

where A_x, A_y, A_z, are the components of the vector $\vec{A}$ in the x, y, and z direction, respectively.
The curl is defined by :

$$\nabla \times \vec{A} = \left(\frac{\partial A_z}{\partial y} - \frac{\partial A_y}{\partial z}\right)\vec{i} + \left(\frac{\partial A_x}{\partial z} - \frac{\partial A_z}{\partial x}\right)\vec{j} + \left(\frac{\partial A_y}{\partial x} - \frac{\partial A_x}{\partial y}\right)\vec{k},$$

where $\times$ is the vector product.

The Laplacien is defined by :

$$\nabla^2 \bar{A} = \frac{\partial^2 \bar{A}}{\partial x^2} + \frac{\partial^2 \bar{A}}{\partial y^2} + \frac{\partial^2 \bar{A}}{\partial x^2}.$$

8 Bibliography

Achenbach, 1973, **Wave propagation in elastic solids**, ed. North Holland.

Batoz, J. L., Dhatt, G., 1990, **Modélisation des structures par éléments finis**, ed. Hermes, vol. 1.

Beslin, O., Foin, O., Nicolas, J., *Hybrid tool for quickly estimating the radiated acoustic power from a vibrating structure in a multi-sources environment*, submitted in The Journal of the Acoustical Society of America.

Corsaro, R. D., Sperling, L. H., 1990, **Sound and vibration attenuation with polymers**, ed. the American Chemical Society.

Davies, J. L., 1988, **Wave propagation in solids and fluids**, ed. Springer Verlag.

Ferry, J. D., 1980, **Viscoelastic properties of polymers**, John Wiley and Sons, Toronto.

Foin, O., Berry, A., Szabo, J.P., 1998, *Underwater acoustic radiation of an elastic rectangular plate covered by a decoupling coating*, submitted in The Journal of the Acoustical Society of America.

Foin, O. 1999 (a), *Outils de prédiction numérique pour l'optimisation des stratégies de contrôle du bruit à la source*, Ph.D. thesis, University of Sherbrooke.

Foin., O., Berry, A., Nicolas, J., 1999 (b), *Optimization of viscoelastic treatment to maximize the plates damping*, to be submitted.

House, J. R. C., *Consideration for underwater decoupling treatment*, Proceeding of the Institute of Acoustics, vol. 13, Part 3.

Ko, S. H., 1997, *Reduction of structure-borne noise using an air-voided elastomer*, J. Acoust. Soc. Am., vol. 101, No 6.

Kolsky, H., 1963, **Stress waves in solids**, ed. Dover.

Miklowitz, J., 1969, **Wave propagation in solids**, ed. The American Society of Mechanical Engineers.

Read, B., Dean, G. D., 1978, **The determination of dynamic properties of polymers and composites**, Adam Hilger Ltd, England.